

5-2019

# Plasma-assisted liquid phase epitaxy of gallium nitride using molten gallium.

Daniel Felipe Jaramillo-Cabanzo  
*University of Louisville*

Follow this and additional works at: <https://ir.library.louisville.edu/etd>

 Part of the [Other Chemical Engineering Commons](#)

---

## Recommended Citation

Jaramillo-Cabanzo, Daniel Felipe, "Plasma-assisted liquid phase epitaxy of gallium nitride using molten gallium." (2019). *Electronic Theses and Dissertations*. Paper 3146.  
<https://doi.org/10.18297/etd/3146>

This Doctoral Dissertation is brought to you for free and open access by ThinkIR: The University of Louisville's Institutional Repository. It has been accepted for inclusion in Electronic Theses and Dissertations by an authorized administrator of ThinkIR: The University of Louisville's Institutional Repository. This title appears here courtesy of the author, who has retained all other copyrights. For more information, please contact [thinkir@louisville.edu](mailto:thinkir@louisville.edu).

PLASMA-ASSISTED LIQUID PHASE EPITAXY OF GALLIUM NITRIDE USING  
MOLTEN GALLIUM

By

Daniel Felipe Jaramillo-Cabanzo

Bachelor of Engineering, Universidad de los Andes, Bogotá, Colombia, 2011

Master of Engineering, Universidad de los Andes, Bogotá, Colombia, 2012

A Dissertation

Submitted to the Faculty of the

J.B. Speed School Engineering of the University of Louisville

in Partial Fulfillment of the Requirements

for the Degree of

Doctor of Philosophy in Chemical Engineering

Department of Chemical Engineering

University of Louisville

Louisville, Kentucky

May 2019

© Copyright 2019 by Daniel Felipe Jaramillo-Cabanzo

All rights reserved



PLASMA-ASSISTED LIQUID PHASE EPITAXY OF GALLIUM NITRIDE USING  
MOLTEN GALLIUM

By

Daniel Felipe Jaramillo-Cabanzo

Bachelor of Engineering, Universidad de los Andes, Bogotá, Colombia, 2011

Master of Engineering, Universidad de los Andes, Bogotá, Colombia, 2012

A Dissertation Approved on

April 24, 2019

By the following Dissertation Committee:

---

Dr. Mahendra K. Sunkara, Dissertation Director

---

Dr. Gamini Sumanasekera

---

Dr. Thomas Starr

---

Dr. Gerold A. Willing

---

Dr. Bruce Alphenaar

DEDICATION

*A mi familia*

## ACKNOWLEDGMENTS

First, I would like to thank Dr. Mahendra Sunkara for his mentorship and continuous support throughout my doctoral studies. I would like to acknowledge the University of Louisville, the Conn Center for Renewable Energy Research, and the National Science Foundation (NSF EPSCoR) for financial support. I would also like to acknowledge the dissertation committee members: Dr. Gamini Sumanasekera, Dr. Gerold A. Willing, Dr. Bruce Alphenaar, and Dr. Thomas Starr for their valuable insights.

I would like to acknowledge the staff at the Conn Center for Renewable Energy Research and the Chemical Engineering department. A special acknowledgment is made to Dr. William Paxton who always was willing to help me. I would also like to thank all my lab mates from whom I never stopped learning. My experience at the University of Louisville would not have been the same without them.

I am very grateful to my friends for always letting me know that they are there for me. Specially, I would like to thank Alejandro Martinez for looking out for me, and Lisa Michelson for making my life easier. Lastly, I would like to express my deepest gratitude to my family for their unconditional love and for supporting me in whatever I do.

Go Cards!

ABSTRACT

PLASMA-ASSISTED LIQUID PHASE EPITAXY OF GALLIUM NITRIDE USING  
MOLTEN GALLIUM

Daniel Felipe Jaramillo-Cabanzo

April 24, 2019

Next generation semiconductor materials such as Gallium Nitride (GaN) and Silicon Carbide (SiC) are rapidly replacing Silicon (Si) for high power and high frequency applications due to Si's inherent limitations. Despite the advantages of GaN over SiC, adoption of GaN has been hindered due to the lack of a cost-effective bulk production technique. Thus, the inability to procure native substrates requires GaN-based architectures to be heteroepitaxially synthesized on non-native substrates, such as sapphire and even SiC. This research seeks to develop a cost effective and scalable method to produce low defect, bulk GaN encouraging the adoption of GaN based devices which ultimately will allow reduction of energy losses in the grid. Specifically, two conceptual methods for the growth of bulk GaN will be explored. The first one is a film-based method, which is based on self-oriented growth of GaN films on a melt gallium layer. In this process, a highly oriented GaN film, made by exposing Ga to plasma-activated nitrogen atoms, is epitaxially thickened into a millimeter-thick GaN film via metalorganic chemical vapor deposition (MOCVD) or halide vapor phase epitaxy (HVPE). The second proposed concept is a crystal-based method. In this process, single crystalline GaN crystals are obtained by



nucleation of GaN out of a Ga melt when exposed to nitrogen plasma. Later, those crystals are enlarged via plasma-assisted liquid phase epitaxy.

As a first step to develop a plasma-assisted liquid phase epitaxy technique the wetting properties of Ga, as well as the interaction between molten Ga and plasma were studied. It was found that both an increment in temperature and the addition of other elements can improve the wettability of Ga by reducing the surface tension of the molten metal. However, these variables were not as effective as the dissolution of nitrogen radicals into the melt. Adsorption/desorption experiments indicated a rapid adsorption/dissolution of the gas into the molten metal when gallium was exposed to plasma. The overall interaction between Ga and plasmas is composed of five processes: (1) surface adsorption, (2) diffusion into the bulk, (3) recombination inside the bulk, (4) surface recombination, and (5) desorption of species from the bulk. The concentration of radicals inside the metal is determined by the rate in which each process is completed.

The self-oriented growth of GaN crystals on molten Ga was found to be dependent of the ability of Ga to spread. XRD characterization showed that flat GaN films only presented reflections of the (0002) and (0004) planes of the hexagonal GaN, whereas the non-flattened GaN films showed the presence of all the characteristic planes of the wurtzite GaN. On the other hand, micron-sized wurtzite and zincblende GaN crystals were obtained by exposing a mixture of Ga and LiCl to nitrogen plasma. It is believed that GaN crystals crystallized from a Li-Ga-N melt that was formed by the interaction between  $\text{Li}_3\text{N}$ , Li and Ga.

In a typical plasma nitridation experiment, spontaneous nucleation of GaN out of molten Ga leads to the formation of a thick GaN crust on top of the surface of the metal.

Similarly, the regrowth experiments using GaN seeds or GaN-on-sapphire substrates failed because of such spontaneous nucleation. The formation of the GaN crust can be explained by the spinodal decomposition mechanism when the concentration of nitrogen inside the Ga reaches a limit. To control the concentration of nitrogen inside the melt, a unique concept of pulsed plasma was introduced. Results showed that pulsed plasma-assisted liquid phase epitaxy allowed a delay in spontaneous nucleation while promoting the growth of additional layers on the pre-existing seeds. A mass transport model was developed to discuss the effect of bulk recombination, diffusion, and pulsing in the concentration of nitrogen into the molten Ga. Results indicated that in the pulsing experiments both the recombination of radicals in the bulk and the diffusion of species into the metal are favored compared to the dissolution of radicals. As a result, the concentration of nitrogen at the surface of the metal is decreased, while the concentration of nitrogen at the surface of the substrate is increased.

The results presented in this work provide insights into low-pressure, metastable crystal growth processes that include both nitrogen dissolution and crystallization of GaN out of a Ga melt. Specifically, the roles of plasma and alkali or semi alkali metals in the dissolution of nitrogen into Ga and the understanding of the mechanism in which GaN crystals nucleate are elucidated. Furthermore, the results obtained in this work could be extended to several other compound semiconductor systems that decompose before melting and are unsuitable for traditional crystal growth techniques.

## TABLE OF CONTENTS

	PAGE
ACKNOWLEDGMENTS .....	iv
ABSTRACT.....	v
LIST OF TABLES .....	xi
LIST OF FIGURES .....	xiii
CHAPTER	
1. INTRODUCTION.....	1
2. BACKGROUND.....	8
2.1. Gallium nitride.....	8
2.2. Growth of GaN films .....	12
2.2.1. Substrate consideration .....	13
2.2.2. Metal organic chemical vapor deposition .....	17
2.2.3. MBE.....	19
2.2.4. HVPE .....	20
2.3. Growth of bulk GaN .....	21
2.3.1. High pressure solution .....	22
2.3.2. Ammonothermal .....	26
2.3.3. Na flux .....	28
2.4. Low pressure liquid phase epitaxy of GaN.....	32
2.4.1. Nitride flux.....	33
2.4.2. Low pressure growth of GaN under ammonia atmosphere .....	38

2.4.3.	Plasma-assisted growth of GaN .....	46
2.4.4.	Challenges.....	50
2.4.4.1.	Wetting properties .....	50
2.4.4.2.	Homogeneous nucleation .....	53
3.	EXPERIMENTAL METHODS .....	58
3.1.	Nitridation experiments .....	58
3.1.1.	RF-plasma reactor.....	58
3.1.2.	ECR-plasma reactor .....	60
3.1.3.	Typical nitridation experiment.....	62
3.2.	Contact angle experiments.....	63
3.3.	Characterization techniques .....	64
3.3.1.	X-ray diffraction .....	64
3.3.2.	Scanning electron microscopy .....	65
4.	FUNDAMENTAL PROPERTIES OF GA IN THE PRESCENCE OF PLASMA ..	67
4.1.	Introduction.....	67
4.2.	Wetting properties.....	68
4.3.	Interaction radicals into molten Ga.....	76
4.4.	Growth of Si NWs on Cu foils.....	85
4.5.	Summary .....	95
5.	PLASMA-ASSISTED LIQUID PHASE EPITAXY OF GAN .....	97
5.1.	Introduction.....	97
5.2.	Highly oriented GaN films .....	98
5.3.	GaN seeds for growth of GaN .....	100
5.3.1.	Regrowth of GaN seeds .....	104
5.4.	Plasma-assisted liquid phase epitaxy of GaN.....	105
5.5.	Parametric analysis of pulsed plasma-assisted liquid-phase epitaxy of GaN.	116
5.6.	Summary .....	127
6.	CONCLUSIONS .....	128

7. RECOMMENDATIONS .....	132
REFERENCES .....	135
APPENDIX I .....	148
CURRICULUM VITAE.....	149

## LIST OF TABLES

Table 1-1. Material properties of Si and GaN <sup>1</sup> .....	2
Table 2-1. Physical and optical properties of wurtzite (hexagonal) and zincblende (cubic) GaN. Adapted from Levinshtein <i>et al.</i> <sup>21</sup> .....	9
Table 2-2. Electronical properties of wurtzite (hexagonal) and zincblende (cubic) GaN. Adapted from Levinshtein <i>et al.</i> <sup>21</sup> .....	10
Table 2-3. Problems commonly faced with heteroepitaxy. Adapted from Liu and Edgar. <sup>24</sup> .....	14
Table 2-4. Crystallographic information and thermal expansion coefficient of sapphire, Si, and 6H-SiC .....	15
Table 2-5. Lateral lattice mismatch and the difference in the thermal expansion coefficient of sapphire, Si, and 6H-SiC with respect to GaN. ....	15
Table 2-6. Relationship between the experimental conditions and the type of outcome in a Li <sub>3</sub> N flux process for GaN growth. Adapted from Song <i>et al.</i> <sup>114</sup> .....	34
Table 2-7. Equilibrium pressures of N <sub>2</sub> over GaN and the N equivalent. Adapted from J.S. Dyck. <sup>140</sup> .....	48
Table 4-1. Contact angle experiments results. Ambient setup.....	70
Table 4-2. Contact angle experiments results. Vacuum setup. ....	71

Table 4-3. Estimated surface tension of different Ga alloys at the temperatures that the contact angle experiments were performed.....	73
Table 4-4. Chemical reactions and their enthalpy of formation for the Ga - N <sub>2</sub> and Ga - H <sub>2</sub> plasma systems.....	83

## LIST OF FIGURES

Figure 1.1 (a) Film-based and (b) crystal-based methods proposed for the growth of bulk GaN.....	4
Figure 2.1. Graphical representation of (a) hexagonal and (b) cubic GaN, and the stacking sequence in (c) wurtzite GaN along the [0001] direction and in (d) zincblende GaN along the [111] direction. Ga and nitrogen atoms are represented in gray and purple, respectively.....	12
Figure 2.2. Atomic arrangements of the sapphire (0001) surface and the (0001) surface of GaN. Aluminum and oxygen atoms in sapphire are shown in blue and red, respectively while gallium and nitrogen atoms in GaN are shown in gray and purple, respectively.....	16
Figure 2.3. Atomic arrangements of the Si (111) surface and the (0001) surface of GaN. Silicon atoms are shown in green while gallium and nitrogen atoms in GaN are shown in gray and purple, respectively. ....	16
Figure 2.4 (a) Temperature dependence of the solubility of N in liquid Al, Ga, and In. Adapted from S. Porowski. <sup>52</sup> (b) Gibbs free energy of GaN and its constituents (reaction 2.8) in terms of pressure and temperature. Adapted from I. Grzegory. <sup>55</sup> .....	23



Figure 2.5 Li-Ga-N ternary phase diagram at 800°C and 1 bar. Data taken by Chen <i>et al.</i> <sup>115</sup> .....	36
Figure 2.6. (a) Partial pressure of N <sub>2</sub> in equilibrium with GaN when formed from Ga and N <sub>2</sub> , ( <i>PN<sub>2</sub> vs. 104T</i> ). (b) Partial pressure of NH <sub>3</sub> in equilibrium with GaN when formed from Ga and NH <sub>3</sub> , ( <i>logPNH<sub>3</sub> vs. 104T</i> ). <i>PH<sub>2</sub></i> is 1 atm. Dashed lines represent a ±1 kcal uncertainty in the free energy of formation of GaN. Adapted from Thurmond and Logan. <sup>129</sup> .....	41
Figure 2.7. Diagram for the LP-LPE growth of GaN using ammonia. Ammonia partial pressure versus temperature with regions of dissociation of GaN (checkered), homogeneous nucleation and GaN growth (striped), and the Ostwald-Miers region (gray). Hydrogen and nitrogen were used as carrier gases and the total pressure was 1 atm. Adapted from Hussy <i>et al.</i> <sup>136</sup> .....	45
Figure 2.8. (a) Self-oriented growth of GaN. Adapted from Chandrasekaran <i>et al.</i> <sup>14</sup> . (b) Self alignment of the platelets due to the movement. Adapted from Chandrasekaran <i>et al.</i> <sup>14</sup> . (c) Cross-sectional SEM image of oriented GaN film. Adapted from Li <i>et al.</i> <sup>15</sup> .....	49
Figure 2.9. Interaction between liquid, solid, and gas in a liquid-solid-gas system. ....	52
Figure 2.10 Synthesis of Ge nanowires from a Ga melt. The region between the liquidus and the spinodal line depicts the condition in which the growth of nanowires is promoted. ....	55
Figure 3.1 RF-plasma reactor P&ID. ....	59
Figure 3.2 ECR-plasma reactor P&ID. ....	61

Figure 3.3 ASTeX AX4500 source configuration. Adapted from the operation manual of the ASTeX AX4500 ECR Plasma Source. <sup>156</sup> .....	62
Figure 4.1 Process that explains the wetting behavior of Ga under hydrogen plasma. (a) A solid Ga film is transformed into a (b) liquid Ga film by increasing the temperature of the system. Hydrogen plasma exposure removes the oxide layer of the melt, which causes (c) agglomeration of the film. Finally, after the oxide layer has been completely removed a (d) Ga droplet is formed. ....	74
Figure 4.2 Ga film after being exposed to nitrogen plasma at 800 °C. (b) Ga droplet contained in a reservoir made of GaN-on-sapphire. (c) Same Ga/reservoir arrangement after pulse experiment. ....	76
Figure 4.3 Schematic of the system used for the absorption/desorption experiments. ....	79
Figure 4.4. On/off experiments. Change in pressure when uncoated (top) and Ga-coated (bottom) supports are exposed intermittently to nitrogen plasma. Experiments were performed at 400 °C and a power of 100 W. ....	79
Figure 4.5. On/off experiments. Change in pressure when uncoated (top) and Ga-coated (bottom) supports are exposed intermittently to hydrogen plasma. Experiments were performed at 400 °C and a power of 100 W. ....	80
Figure 4.6. Proposed mechanism: (a) creation of atomic species, (b) surface adsorption, (c) diffusion into the bulk, (d) recombination inside the bulk, (e) surface recombination, (f) desorption of molecular species, and (g) molecular species in the gas phase. ....	81

Figure 4.7 Growth of Si NWs on Al <sub>2</sub> O <sub>3</sub> -coated Cu substrates. Densely packed (a) Si NWs (d~100 nm) were grown (b) uniformly all over the surface of the alumina-coated substrates. (c) Formation of silicides was not observed. ....	89
Figure 4.8 Flexible anode for Li-ion batteries. Anode is composed Si NWs arrays grown on Al <sub>2</sub> O <sub>3</sub> -coated Cu. ....	91
Figure 4.9 Charge/discharge cycle performance of Si NWs arrays grown on Al <sub>2</sub> O <sub>3</sub> -coated Cu as anode material in Li-ion batteries. ....	93
Figure 4.10 Growth of Si NWs on Si substrates at (a) 200, (b) 250, (c) 300, and (d) 350 °C. ....	94
Figure 4.11 Growth of Si NWs on UNCD-coated Si substrates. The temperature of the growth was 350 °C. ....	95
Figure 5.1. (a) Top morphology of flat GaN film, with the top right corner (b) showing the film as deposited. (c) X-ray spectra for the flat film. (d) Top morphology of non-flatten GaN film with the top right corner (e) showing the film as deposited. (f) X-ray spectra for the non-flatten film.....	100
Figure 5.2. Morphological analysis of the samples synthesized by exposing a Ga-LiCl melt to N <sub>2</sub> plasma. (a) Particle formed out of platelets. (b) Close-up of the platelets. (c) Agglomerates with pillars on their surface. (d) Close up of one of the pillar structures. (e) Agglomerates of hexagonal and cubic crystals. (f) Close up of a cubic crystal. ....	102
Figure 5.3. XRD spectrum of powders synthesized by exposing a Ga-LiCl melt to N <sub>2</sub> plasma. ....	103

Figure 5.4 (a) Formation of a GaN crust on top of Ga after continuous exposure to nitrogen plasma. Dashed circle indicates (b) the interface between Ga and the GaN crust.....	107
Figure 5.5. Growth of GaN via pulsed plasma-assisted liquid phase epitaxy was performed at 900 °C utilizing a five-minutes on, five-minutes off pulse. ....	107
Figure 5.6 Pulse experiment performed for a short period of time.....	108
Figure 5.7 Ga film formation during LPE experiments. A Ga film with varying thickness is formed on top of the substrate due to the incorporation of nitrogen into the melt. ....	108
Figure 5.8 Growth of GaN via pulsed plasma-assisted LPE utilizing a Ga film with varying thickness. (a) Polycrystalline GaN was obtained in the thinnest area of the film. (b) Epitaxial growth of GaN was obtained in a mid-point between the edge and the center of the film. (d)-(e) GaN crystals were obtained in the thickest area of the film. ....	110
Figure 5.9 TEM characterization of the GaN crystals obtained in the thickest area of the Ga film. (a) SEM image of the TEM lamella used during characterization. White outlined area indicates the (b) area that was analyzed using TEM. (c) High resolution TEM image of the crystal. White outlined area indicates the interface between the grown layer and the substrate. (d) High-resolution TEM image of the interface. The area between the dashed lines indicates where the interface is. (e) Electron diffraction pattern of the substrate. (f) Electron diffraction pattern of the grown crystal.....	111

Figure 5.10 Pulsed plasma-assisted LPE of GaN utilizing a modified pulse sequence. In this experiment a two minutes-on, five-minutes off pulse was used. ....	114
Figure 5.11 TEM characterization of the GaN film grown via the pulsed plasma-assisted LPE technique utilizing the modified pulse sequence. (a) SEM image of the TEM lamella used during characterization. White outlined area indicates the (b) area that was analyzed using TEM. (c) TEM image of the film. White outlined area indicates the interface between the grown layer and the substrate. (d) High-resolution TEM image of the interface. The area between the dashed lines indicates where the interface is. (e) Electron diffraction pattern of the substrate. (f) Electron diffraction pattern of the grown layer. ....	115
Figure 5.12. Time-dependent diffusion of nitrogen radicals from a plasma source into a molten Ga film. ....	116
Figure 5.13 Effect of bulk recombination in the concentration of nitrogen inside a 1mm thick Ga film. Concentration profiles were calculated using $DNGa = 5 \times 10^{-6} \text{ cm}^2 \text{ s}^{-1}$ , $pt = 1$ and $kBR =$ (a) 0, (b) $1 \times 10^{-1}$ , (c), 1, and (d) 10.....	120
Figure 5.14 Effect of diffusion in the concentration of nitrogen inside a 1mm thick Ga film. Concentration profiles were calculated using $kBR = 1 \times 10^{-1}$ , $pt = 1$ and $DNGa =$ (a) $5 \times 10^{-4}$ , (b) $5 \times 10^{-5}$ , (c) $5 \times 10^{-6}$ , and (d) $5 \times 10^{-7} \text{ cm}^2 \text{ s}^{-1}$ .....	121

Figure 5.15 Effect of pulsing in the concentration of nitrogen inside a 1mm thick Ga film. Concentration profiles were calculated using  $kBR = 1 \times 10^{-1}$   $DNGa = 5 \times 10^{-6} \text{ cm}^2 \text{ s}^{-1}$ , and  $pt =$  (a) 1, (b) 0.5 and (c) five to five minutes on/off pulse. Pulse wave is shown in (d)..... 124

Figure 5.16. Liquid phase epitaxy of GaN utilizing a diluted nitrogen plasma. Nitrogen was diluted in argon in a 1:9 ratio in order to reduce the concentration of nitrogen radicals in the system. (a) Resultant film is characterized by having two distinct growths i.e., epitaxial and polycrystalline. (b) Zoom into the epitaxial GaN layer. .... 125

Figure 5.17 Concentration profile of modified pulsing sequence. Concentration profiles were calculated using  $kBR = 1 \times 10^{-1}$   $DNGa = 5 \times 10^{-6} \text{ cm}^2 \text{ s}^{-1}$  and a modified pulse sequence. Concentration profile in (a) corresponds to pulse sequence presented in (b), while concentration profile in (c) corresponds to pulse sequence presented in (d) ..... 126

Figure 5.18 Pulsed plasma assisted LPE of GaN using a modified pulsing sequence. The sequence is described as five min on, then thirty min off, and then a one-to-thirty min on/off pulse, which is performed until the end of the experiment..... 127

## CHAPTER 1

### INTRODUCTION

As clean energy is being adopted around the globe, the role of power electronic devices, which convert and control the flow of electrical power, become even more relevant. Historically, these devices have been manufactured using silicon (Si). However, the operating limits of Si devices, which are set by the material's intrinsic properties, fail to perform with more demanding applications.<sup>1</sup> Gallium nitride (GaN), a direct bandgap semiconductor, has emerged as the prime material to be utilized in the new generation of power devices. With inherent high breakdown strength, high saturation electron velocity, and good thermal conductivity (see Table 1-1), GaN has the potential to revolutionize not only the fields of power conversion and transmission via power switches, amplifiers and transistors, but also the field of optoelectronics. In the case of power switching applications, GaN has the potential to reduce the consumption of energy in various commercial, industrial and military systems, namely smart grid, electric and hybrid vehicles and bulk energy storage, among others.<sup>2-3</sup> In fact, GaN Systems Inc., one of the most prominent global developers and distributors of GaN devices, claims that their power systems are already four times smaller, four times lighter and four times more efficient compared to its Si counterpart.<sup>4</sup> Furthermore, GaN microwave amplifiers can provide ten times more signal and power enhancement compared to Si and gallium arsenide (GaAs)

devices in cell phones.<sup>5</sup> Qorvo, a public company that specializes in radiofrequency (RF) solutions, argues GaN will overtake traditional semiconductor materials for fifth-generation (5G) network applications like small cells, which will require higher frequencies, tight integration, and minimal implementation cost.<sup>6</sup> In terms of transistors, GaN also offers the ability to form heterojunctions, making this material suitable for fabrication of high electron mobility transistors (HEMTs).<sup>7</sup> Finally, the blue and UV light emission of GaN is of great interest in optoelectronics, specifically in the light, display, and storage industries as it can make light bulbs last up to ten years, brighten flat panel displays, and quadruple the storage capacity of traditional optical storage devices such as CDs and DVDs.<sup>8-9</sup>

Table 1-1. Material properties of Si and GaN<sup>1</sup>

Material property	Si	GaN
Bandgap (eV)	1.12	3.4
Critical Field ( $10^6$ V/cm)	0.3	3.3
Carrier mobility (cm <sup>2</sup> /Vs)	1500	990,2000 <sup>a</sup>
Electron saturation velocity ( $10^6$ cm/s)	10	25
Thermal conductivity (W/cm <sup>2</sup> K)	1.5	1.3

<sup>a</sup>In bulk GaN/2D electron gas region of GaN/AlGaIn HEMT, respectively

The potential of GaN for semiconductor applications is substantial. According to a report by Transparency Market Research (TMR), the global GaN semiconductor devices market was estimated to be at US\$870.9 mn and is expected to grow to US\$3.438 bn by 2024. The military (i.e. aerospace and defense) sector dominates with 42% of the total market share. However, the relatively higher price of GaN-based devices compared to Si-



based devices has become the main obstacle for large-scale adoption. The reason for this price difference is attributed to the high cost of low defect density GaN wafers. Currently, there is no commercial technique for bulk GaN growth, which would alleviate the higher price of GaN-based devices.

Due to the lack of a commercial technique for bulk GaN, current GaN-based devices are being made through heteroepitaxial vapor deposition of GaN on sapphire, silicon carbide (SiC) or silicon (Si) substrates. However, these films suffer from a large dislocation density ( $\sim 10^6\text{--}10^9\text{ cm}^{-2}$ ) due to a mismatch of lattice parameters and thermal expansion coefficients between the GaN and the underlying substrate<sup>10</sup>. These values are significantly higher than those required for high-efficiency power devices ( $<10^6\text{ cm}^{-2}$ ). The use of native substrates for homoepitaxial growth, rather than heteroepitaxial growth, of GaN has been identified as the only existing way to overcome this problem. GaN crystals cannot be grown using typical Bridgman or Czochralski type of techniques because the decomposition occurs prior to the melting point. Bulk synthesis methods, i.e. high-pressure solution, ammonothermal, and alkali salt fluxes, have been used to obtain GaN crystals with low defect density.<sup>11</sup> Among these, the ammonothermal method has been the one that provides the best quality.<sup>12</sup> However, bulk synthesis methods are characterized for being performed under extreme temperatures and pressures for long periods of time (in the order of days)<sup>13</sup> making them cost prohibited and therefore noncompetitive for production.

In the development of this dissertation, two different approaches have been proposed for the growth of bulk GaN, which potentially would help to achieve the ultimate technological goal of producing large area single crystalline GaN with low defect density at low cost. The approaches are presented in Figure 1.1.

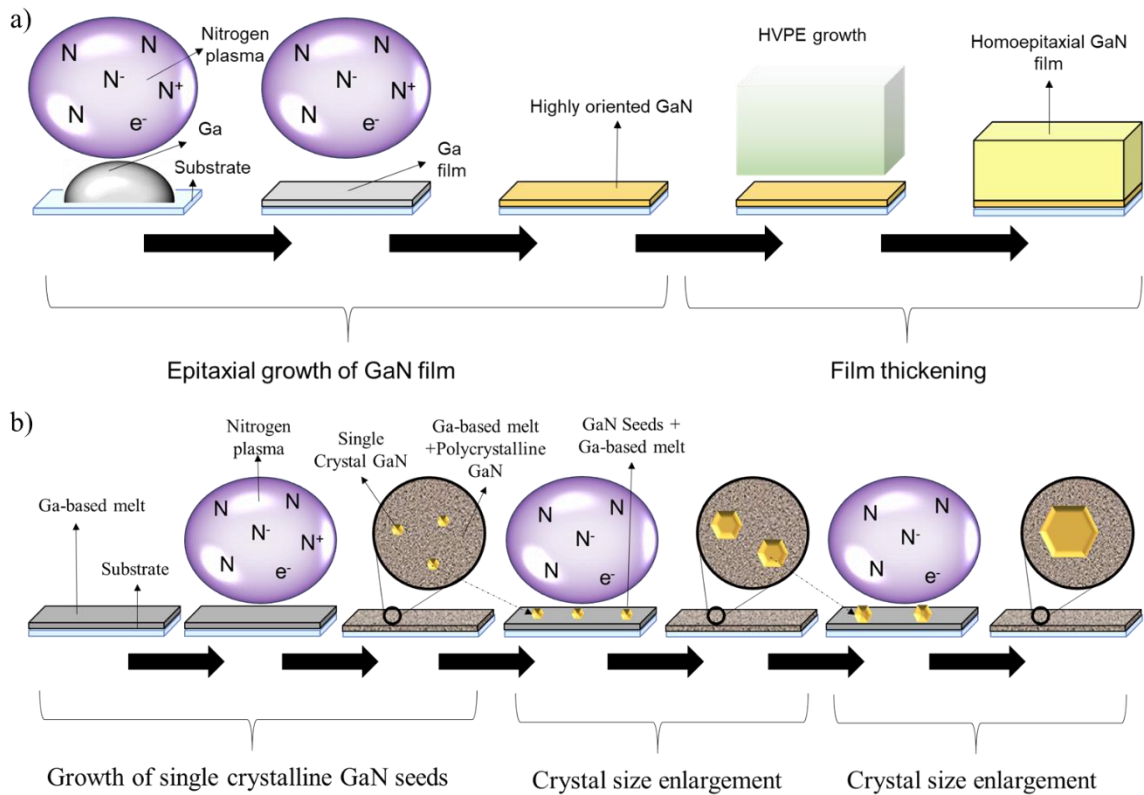


Figure 1.1 (a) Film-based and (b) crystal-based methods proposed for the growth of bulk GaN

The first one, Figure 1.1(a), corresponds to a film-based method, which is based on results obtained from Sunkara *et. al* on self-oriented growth of GaN films.<sup>14-16</sup> In this process, upon exposure of metallic Ga to plasma-activated nitrogen atoms, GaN platelets nucleate and coalesce on the surface of the molten Ga. During the process, these platelets self-orient and form an epitaxial layer. In a following step, hydride vapor phase epitaxy (HVPE), which is characterized by high growth rate and excellent crystal quality, is used for epitaxial thickening of these layers to obtain millimeter thick GaN wafers. When the process is performed on a foreign substrate, the epitaxial film grown in the first step acts as a buffer layer for the second step. Conversely, when the growth is performed on a native

substrate, the homoepitaxial GaN film obtained in the first step can reduce the dislocation density of the original substrate, which promotes the growth of higher quality GaN in the second step.<sup>17-18</sup> Alternatively, metal organic chemical vapor deposition (MOCVD) can be used in the second step. The second approach, Figure 1.1(b), is described as a crystal-based method. In this process, single crystalline GaN crystals are synthesized by exposing a Ga melt or a mixture of molten Ga and alkali metals, alkali salts, or alkali nitrides to nitrogen plasma. These crystals are then immersed in a new Ga-based melt and expose to nitrogen plasma. As a result, homoepitaxial layers of GaN are grown onto the crystals, which ultimately is reflected in crystal size enlargement. This step can be repeated successively until the desired final size of the crystal is achieved.

In contrast to other bulk growth techniques, these processes are performed at low pressures (sub-atmospheric), relatively low temperatures (~900°C) and are considerably faster (in the order of hours) making them easy to scale and, more importantly, cheaper than the current GaN bulk techniques. If successful, these techniques will enable wide spread applications of GaN in power electronics and optoelectronics, which can ultimately result in enormous energy savings.

Because the success of these two approaches is determined primarily by the step in which the epitaxial growth of GaN takes place, the main goal of this dissertation is to provide a reliable process that allows for the epitaxial growth of GaN. Specifically, this dissertation presents the utilization of a novel technique in which epitaxial layers of GaN are grown via plasma-assisted liquid phase epitaxy (LPE).

The proposed technique, which is based on the interaction of gallium and nitrogen plasma and are carried out at relatively low temperatures (~900°C) and subatomic

pressures, will provide insight into low-pressure, metastable crystal growth processes that include both nitrogen dissolution and crystallization of GaN out of a Ga melt. Specifically, the roles of plasma and alkali or semi alkali metals in the dissolution of nitrogen into Ga and the understanding of the mechanism in which GaN crystals nucleate will be elucidated. The experiments presented in this work will also provide information about the flowing and the wetting behavior of nitrogenated-Ga melts on various substrates. Additionally, the results obtained in this work could be extended to several other compound semiconductor systems that decompose before melting and are unsuitable for traditional crystal growth techniques.

This dissertation is divided into nine distinct chapters. Chapter one presents the motivation behind developing a process to produce bulk GaN. Within this chapter, an introduction to the challenges and the limitations of current techniques for growth of bulk GaN are presented. Two different approaches, which are based on the interaction of nitrogen plasma and molten gallium, are proposed as alternatives to growing bulk GaN. Furthermore, main challenge of these two approaches is identified, and therefore, the main objective of this work is to develop a reliable plasma-assisted liquid phase epitaxy technique for GaN growth. The impact of this dissertation is also stated in this chapter.

Chapter two assesses the structure and fundamental properties of GaN, introduces the GaN thin film technology, and presents a comprehensive review of the state of the art of techniques for growth of bulk GaN. There will be an emphasis in the low-pressure techniques. Additionally, the main challenges in low-pressure liquid phase epitaxy of GaN are discussed.

Chapter three presents an overview of the experimental methods and characterization techniques employed in this study.

Chapter four presents a set of fundamental studies in order to understand the influence of different variables on the wetting properties of Ga and gain insight into the interaction between nitrogen plasma and molten Ga. Additionally, this chapter presents the growth of Si NWs on Cu foils to elucidate the potential of the synergism between molten Ga and plasma in other applications different than the growth of GaN

Chapter five presents a novel low-pressure technique for liquid-phase epitaxy of GaN. A unique concept of pulsed plasma allows for the control of spontaneous nucleation and promotes the epitaxial growth of GaN during the process. A mathematical model is also presented to discuss the effect of bulk recombination, diffusion, and pulsing in the concentration of nitrogen into the molten Ga. Additionally, this chapter presents the results concerning the growth of seeds for both the film- and crystal-based approaches.

Chapter seven and chapter eight present the conclusions of this study and the recommendations for future work, respectively.

## CHAPTER 2

### BACKGROUND

#### 2.1. Gallium nitride

Gallium nitride (GaN) is a III-V semiconductor material mostly known by its pivotal role in the development of light-emitting diodes (LEDs) for illumination (white light). GaN has a direct band gap of 3.4 eV that can be tunable in the visible and ultraviolet (UV) range by alloying with InN or AlN. Even so, the potential of GaN goes beyond the LED technology. GaN's physical and electrical properties make this material suitable for utilization in the new generation of power devices. A review of the physical and electrical properties of GaN is presented in Table 2-1 and Table 2-2 respectively.

The unique properties of gallium nitride are closely related to its crystal structure. GaN exists in two different polymorphs: wurtzite (hexagonal) and zincblende (cubic). Although very similar in their crystallographic structure, i.e. the bonding to the next neighbor in both structures is tetrahedral, the wurtzite polymorph is more stable.<sup>19</sup> The wurtzite GaN consists of two interpenetrating hexagonal close-packed (hcp) lattices. The unit cell is formed by two Ga atoms and two nitrogen atoms.<sup>20</sup> The Ga atoms are located at (0,0,0) and at (2/3,1/3,1/2), while the nitrogen atoms are located at (0,0,u) and at (2/3,1/3,1/2+u), where u is approximately 3/8. The crystallographic structure of wurtzite GaN is presented in Figure 2.1 (a).

Table 2-1. Physical and optical properties of wurtzite (hexagonal) and zinblende (cubic) GaN. Adapted from Levinshtein *et al.*<sup>21</sup>

Property	Wurtzite GaN	Zinblende GaN
Band gap (eV)	3.39	3.2
Lattice constants (Å)		
a	3.189	4.52
c	5.186	-
Density (g/cm <sup>3</sup> )	6.15	6.15
Bulk modulus (dyn cm <sup>-2</sup> )	20.4 x 10 <sup>11</sup>	20.4 x 10 <sup>11</sup>
Melting point (°C)	2500	2500
Specific heat (J g <sup>-1</sup> °C <sup>-1</sup> )	0.49	0.49
Thermal conductivity (W cm <sup>-1</sup> °C <sup>-1</sup> )	1.3	1.3
Thermal diffusivity (cm <sup>2</sup> s <sup>-1</sup> )	0.43	0.43
Thermal expansion, linear (°C <sup>-1</sup> )		
$\alpha_a$	5.59 x 10 <sup>-6</sup>	-
$\alpha_c$	3.17 x 10 <sup>-6</sup>	-
Infrared refractive index	2.3	2.3
Radiative recombination coefficient (cm <sup>3</sup> s <sup>-1</sup> )	1x10 <sup>-8</sup>	1x10 <sup>-8</sup>

Table 2-2. Electrical properties of wurtzite (hexagonal) and zincblende (cubic) GaN.

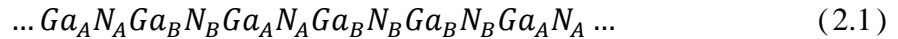
Adapted from Levinshtein et al.<sup>21</sup>

Property	Wurtzite	Zincblende
Dielectric constant		
Static	8.9	5.3
High-frequency	5.35	0.13
Electron affinity (eV)	4.1	4.1
Breakdown field (V cm <sup>-1</sup> )	~5 x 10 <sup>6</sup>	~5 x 10 <sup>6</sup>
Mobility (cm <sup>2</sup> V <sup>-1</sup> s <sup>-1</sup> )		
electrons	≤1000	≤1000
holes	≤200	≤350
Diffusion coefficient (cm <sup>2</sup> s <sup>-1</sup> )		
electrons	25	25
holes	5	9
Electron thermal velocity (m s <sup>-1</sup> )	2.6 x 10 <sup>5</sup>	3.2 x 10 <sup>5</sup>
Hole thermal velocity (m s <sup>-1</sup> )	9.4 x 10 <sup>4</sup>	9.5 x 10 <sup>4</sup>

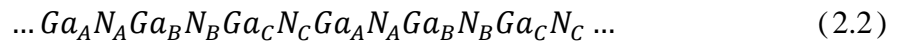


On the other hand, the zincblende GaN consists of two face center cubic (fcc) structures displaced along the cubic space diagonal by a vector  $(1/4, 1/4, 1/4)a_0$ , with  $a_0$  being the lattice constant. One of the fcc-substructures is occupied exclusively by Ga atoms and the other one is occupied exclusively by nitrogen atoms. As a result, the GaN zincblende unit cell is composed of 8 atoms: four gallium atoms and four nitrogen atoms.<sup>22</sup> The crystallographic structure of zincblende GaN is presented in Figure 2.1 (b)

Both the wurtzite and zincblende structures present a close packed arrangement in which the atoms on the (0001) planes of the wurtzite structure and the atoms on the (111) plane of the zincblende structure are arranged in a hexagonal pattern. The difference between the two structures is the stacking sequence along the axis perpendicular to the hexagons.<sup>19</sup> For the wurtzite structure, the stacking sequence along the [0001] direction is:



Whereas for the zincblende structure, the stacking sequence along the [111] direction is:



A graphical representation of both crystallographic structures as well as their respective stacking sequences is presented in Figure 2.1.

Due to its more stable nature, the wurtzite polymorph is easier to produce and therefore all commercial GaN applications are made out of hexagonal GaN. This work will focus on the growth of bulk hexagonal GaN. For the purposes of brevity and throughout this work, GaN will refer to hexagonal GaN unless specified otherwise.

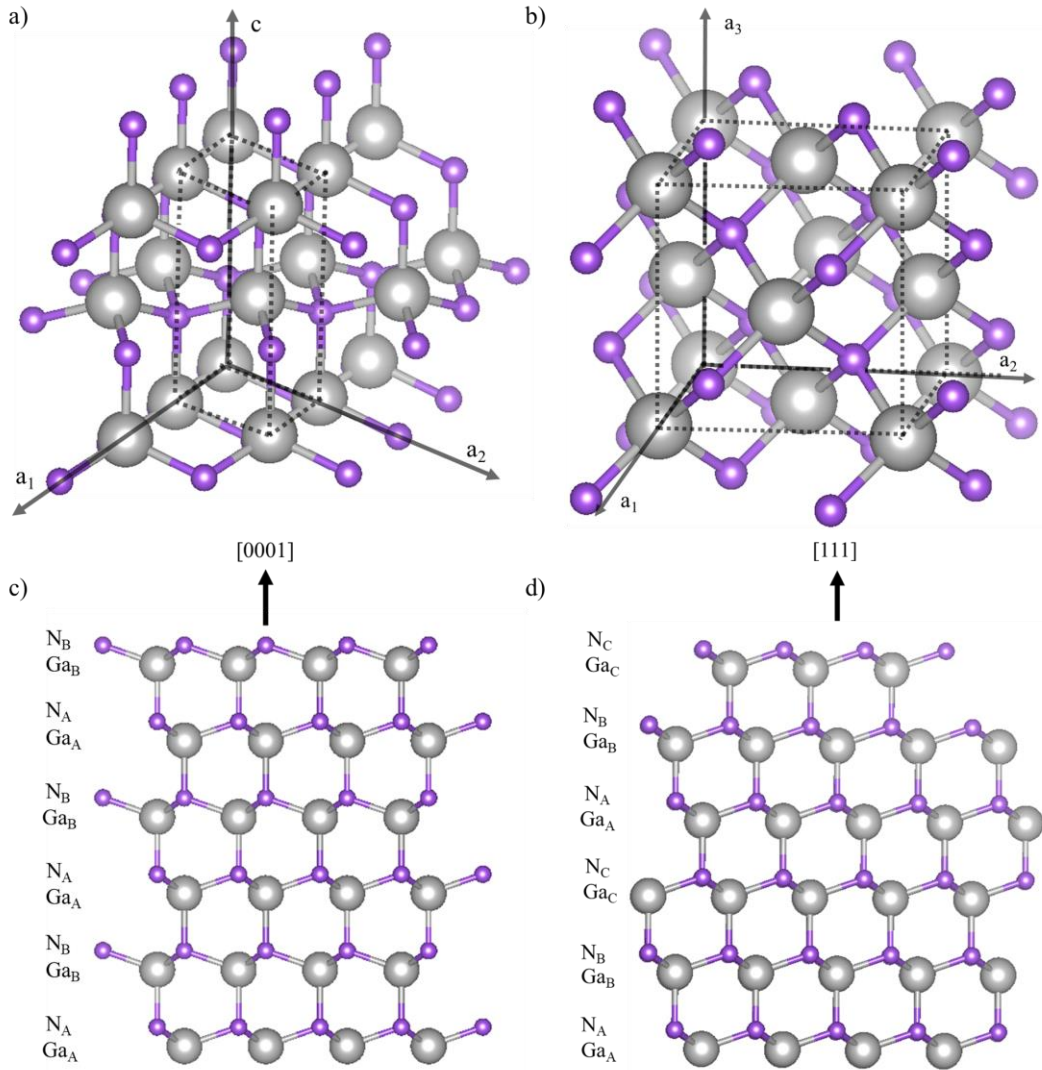


Figure 2.1. Graphical representation of (a) hexagonal and (b) cubic GaN, and the stacking sequence in (c) wurtzite GaN along the  $[0001]$  direction and in (d) zincblende GaN along the  $[111]$  direction. Ga and nitrogen atoms are represented in gray and purple, respectively.

## 2.2. Growth of GaN films

This section presents a brief review on the growth of GaN films. Specifically, this section elucidates the consequences of depositing GaN films on foreign substrates (materials other GaN) and introduces the most widely used vapor phase epitaxy methods for GaN growth.

### 2.2.1. Substrate consideration

GaN-based devices, in most cases, rely on the growth of high quality GaN layers. However, due to the lack of truly freestanding GaN wafers, the growth of GaN is performed on foreign substrates i.e. heteroepitaxial growth of GaN. As a result, the quality of the GaN films is conditioned by the properties of the substrate. A summary of the problems that arise from heteroepitaxy is presented in Table 2-3.

Commonly, the lateral lattice constant mismatch and the difference in thermal expansion coefficient have been the primary criteria for determining if a material is suitable as substrate for heteroepitaxial growth of GaN. Among the different materials that have been used as a substrate for GaN heteroepitaxy, sapphire ( $\text{Al}_2\text{O}_3$ ), Si, and SiC are the most widely utilized. The crystal structure, the lattice parameters, and the thermal expansion coefficient of these materials are presented in Table 2-4.

Because sapphire and Si have a completely different crystal structure than that of GaN, the lattice mismatch calculation cannot be performed using the difference between the lattice constants. Instead, the lattice spacing within the atoms on the planes where the atomic matching occurs should be used.<sup>23</sup> Among the different sapphire and silicon substrate orientations, sapphire (0001) and Si (111) are the ones that present the lowest lateral mismatch with respect to the c-oriented GaN. The lattice spacing in sapphire (1000) is  $2.75 \text{ \AA} \left(\frac{\sqrt{3}}{3}a\right)$  while in Si (111) is  $2.75 \text{ \AA} \left(\frac{\sqrt{2}}{2}a\right)$ . A comparison between the atomic arrangements of the sapphire c-plane (0001) surface and the Si (111) surface with respect to the c-plane (0001) surface of GaN is presented in Figure 2.2 and Figure 2.3, respectively. The lateral lattice mismatch and the difference in the thermal expansion coefficient,  $\alpha$ , of sapphire, Si, and SiC with respect to GaN are presented in Table 2-5.

Table 2-3. Problems commonly faced with heteroepitaxy. Adapted from Liu and Edgar.<sup>24</sup>

Substrate property	Consequence
Lateral ( <i>a</i> -lattice constant) mismatch	High misfit (primarily edge) dislocation densities which can cause: high device leakage currents, short minority carrier lifetimes, reduced thermal conductivity, and/or rapid impurity diffusion pathways
Vertical ( <i>c</i> -lattice constant) mismatch	Antiphase boundaries, inversion domain boundaries
Coefficient of thermal expansion mismatch	Thermally induced stress in the film and substrate which causes crack formation in film and substrate
Low thermal conductivity	Poor heat dissipation, unsuitability for high-power devices
Different chemical composition than the epitaxial film	Contamination of the film by elements from the substrate which can cause: electronic interface states created by dangling bonds and/or poor wetting of the substrate by the growing film
Non-polar surface	Mixed polarity in the epitaxial film, inversion domains
Surface steps in non-isomorphic substrates	Double positioning boundaries (stacking mismatch boundaries)

Table 2-4. Crystallographic information and thermal expansion coefficient of sapphire, Si, and 6H-SiC

Material	Structure	Lattice constants		$\alpha^a$		Ref.
		a	c	a	c	
Sapphire (Al <sub>2</sub> O <sub>3</sub> )	Rhombohedral	4.768	12.991	7.5	8.5	19
Si	Diamond	5.431	-	2.62		24
SiC	6H Hexagonal	3.081	15.117	4.46	4.16	24

<sup>a</sup>)Linear thermal expansion coefficient

Table 2-5. Lateral lattice mismatch and the difference in the thermal expansion coefficient of sapphire, Si, and 6H-SiC with respect to GaN.

Material	Structure	Lattice mismatch (%)	$\Delta\alpha^b$	
			a	c
Sapphire (Al <sub>2</sub> O <sub>3</sub> )	Rhombohedral	13.9	-1.91	-0.75
Si	Diamond	-20.41	2.97	-
SiC	6H Hexagonal	3.38	1.13	3.59

<sup>a</sup>)Mismatch = (GaN – Substrate) / GaN

<sup>b</sup>)Difference in thermal expansion coefficient = GaN - Substrate

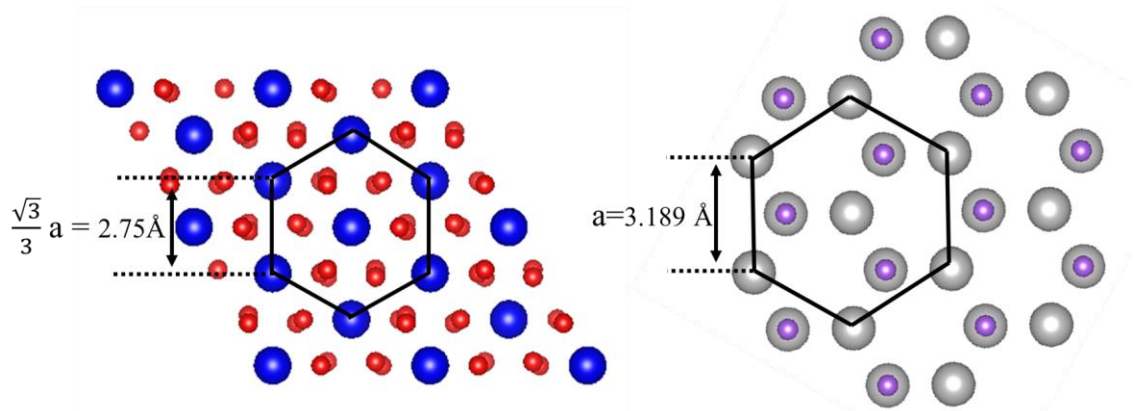


Figure 2.2. Atomic arrangements of the sapphire (0001) surface and the (0001) surface of GaN. Aluminum and oxygen atoms in sapphire are shown in blue and red, respectively while gallium and nitrogen atoms in GaN are shown in gray and purple, respectively.

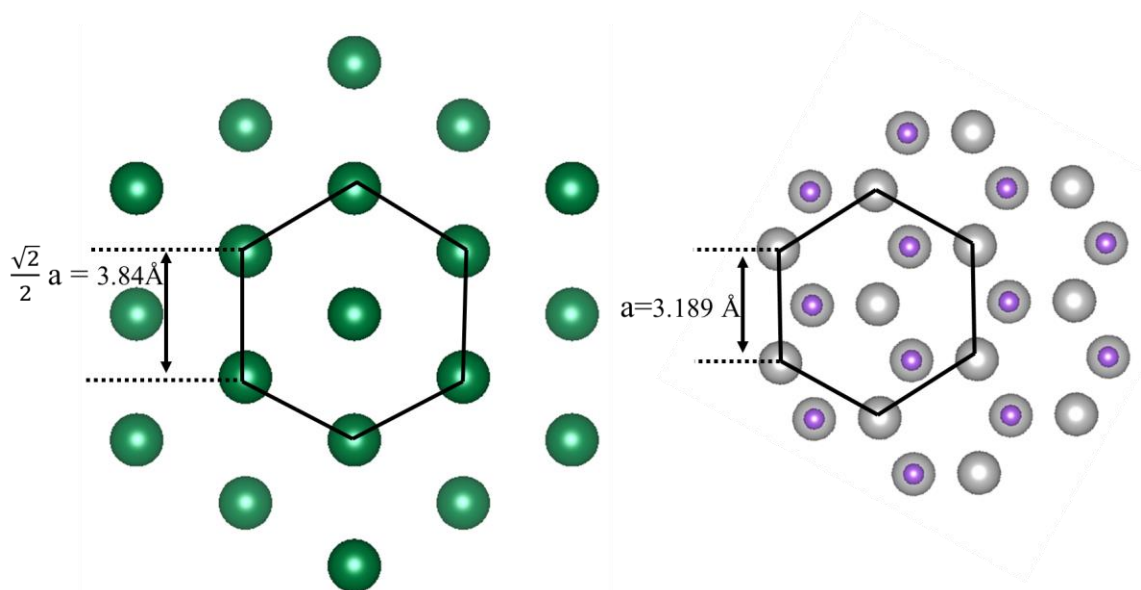
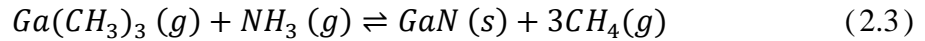


Figure 2.3. Atomic arrangements of the Si (111) surface and the (0001) surface of GaN. Silicon atoms are shown in green while gallium and nitrogen atoms in GaN are shown in gray and purple, respectively.

### 2.2.2. Metal organic chemical vapor deposition

Metal organic chemical vapor deposition (MOCVD), also known as metalorganic vapor phase epitaxy (MOVPE), is a gas phase technique used to deposit thin layers of single or polycrystalline materials. Gas phase precursors, of which at least one of them is a metal organic compound, are fed into a reaction chamber where a substrate is already placed. Inside the chamber, the precursors are subjected to a series of gas phase and surface reactions that lead to the nucleation of atoms of the material of interest on the surface of the substrate. Due to continuous nucleation of atoms and their ability to diffuse along the surface, atoms meet and coalesce to form a thin layer of the material of interest. The growth of GaN via MOCVD is typically performed using trimethylgallium (TMG) and ammonia (NH<sub>3</sub>). Although this process involves multiple steps it can be described by reaction 2.3. Typical growth rates of this process are between 1 and 3 μm/h.<sup>24</sup>



Alternatively, triethylgallium [(C<sub>2</sub>H<sub>5</sub>)Ga] and 1,3-[(dimethylamino)propyl]-1-gallacyclohexane can be used as a Ga source; whereas NF<sub>3</sub>, hydrazine (N<sub>2</sub>H<sub>4</sub>), 1,1-dimethylhydrazine [(CH<sub>3</sub>)<sub>2</sub>NNH<sub>2</sub>], hydrogen azide (HN<sub>3</sub>), tert-butylamine (tBuNH<sub>2</sub>), and isopropylamine (iPrNH<sub>2</sub>) can be used as a source of nitrogen.<sup>25</sup>

Different challenges have been addressed in the past to obtain high quality GaN. S. Nakamura identified that at high substrate temperature i.e. over 1000 °C, which is needed for the growth of high quality, single crystalline GaN films, thermal convection is induced. As a result a gas flow that is not favorable for uniform growth of GaN is created.<sup>19</sup>

Nakamura *et al.* proposed a system in which a second gas jet containing nitrogen and hydrogen is placed perpendicular to the surface. This new flow pushes the gases towards the surface of the substrate which leads to an improved crystal growth.<sup>26</sup> To improve the mixing of the precursors and still obtain excellent growth uniformity, Wang *et al.* proposed to add a third flow jet to the system.<sup>27</sup> Later, technologies that have been used in other systems like the planetary rotating discs and close-coupled showerhead (CCS) feeder were introduced into the growth of GaN films. The growth of GaN on non-native substrates causes poor GaN films and severe cracking. Akasaki *et al.* reported that the cracking of films could be suppressed by using an AlN buffer layer.<sup>28</sup> Later, S. Nakamura found that this effect could also be achieved by using a GaAlN or GaN buffer layer.<sup>29</sup>

Growth of conductive doped GaN films via MOCVD was instrumental in the development of the blue LED technology. N-type doping of GaN is easily achieved using silicon (Si) as the donor. Typically, a Si precursor is diluted in hydrogen and fed into the reactor where the precursor participates in the growth process. Common Si precursors in MOCVD processes are silane (SiH<sub>4</sub>) and disilane (Si<sub>2</sub>H<sub>6</sub>).<sup>30</sup> P-type doping of GaN is more complicated. Akasaki *et al.* discovered that to obtain conductive p-type doping in GaN, it was needed to initially obtain a Mg-doped GaN film and then activate the Mg acceptors by irradiation of low energy electrons (LEEBI). During growth, hydrogen passivates Mg acceptors by forming an Mg-H complex. The LEEBI process activates the Mg acceptors by removing the hydrogen. Later, Nakamura *et al.* reported that by annealing the Mg-doped GaN films in a nitrogen atmosphere it was possible to obtain highly conductive p-type GaN films without using the LEEMI process.<sup>31</sup>



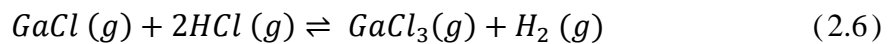
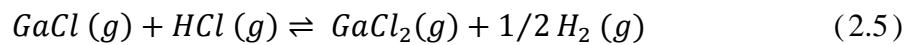
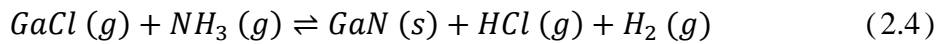
### 2.2.3. MBE

Molecular beam epitaxy (MBE) is a non-equilibrium technique used to grow epitaxially thin films of crystalline semiconductor materials. The process involves the reaction of one or more thermal molecular beams with a crystalline surface (substrate) under ultra-high vacuum conditions ( $10^{-8}$ - $10^{-12}$  torr).<sup>32</sup> The substrate is usually placed in a heated, rotatory substrate holder that allows to control the growth temperature and improve the growth homogeneity.<sup>33</sup> To obtain GaN epitaxial layers, a Ga vapor beam and an activated nitrogen beam are directed toward the heated substrate where deposition of Ga and N atomic planes takes place. The Ga beam is created using ultra-pure Ga and an effusion cell. The temperature of the cell plays an important role in the process as it allows to control the evaporation/sublimation rate which ultimately is reflected in the net Ga flux rate. To generate enough activated nitrogen atoms that react with the Ga source, a plasma source is utilized.<sup>19</sup> Typical growth rates of GaN using this technique are between 0.2 and 1.5  $\mu\text{m}/\text{h}$ .<sup>24</sup>

Growth of doped GaN films in MBE is performed by introducing molecular beams of the dopant materials. Similarly to the case of Ga, these beams are created using effusion cells containing the dopant source in its pure state. N-type and p-type doping are generally attained using Si and Mg, respectively. Because no hydrogen is used during the process, Mg does not passivate and therefore no annealing process is required.<sup>34-35</sup>

#### 2.2.4. HVPE

Hydride vapor phase epitaxy (HVPE) and halide vapor phase epitaxy are growth techniques that use gaseous chloride precursors to grow epitaxial layers of III-V semiconductors. These two techniques differ from each other by how the group V element is supplied. In halide phase epitaxy, both the anion and the cation are transported as chlorides whereas in the case of HVPE the group V element is supplied as a hydride.<sup>36</sup> HVPE is the only vapor phase epitaxy technique that operates close to equilibrium of deposit reactions. This condition allows HVPE processes to have high growth rates, and selective and anisotropic growth.<sup>36</sup> HVPE of GaN is carried out in a multi-temperature zone reactor using Ga, hydrogen chloride (HCl), and ammonia as precursors and H<sub>2</sub> as the carrier gas. HCl is fed into the source zone where reacts with Ga forming gallium chloride (GaCl). Then, GaCl and NH<sub>3</sub> are transported independently to the growth zone where the following chemical reactions occur simultaneously.<sup>37</sup>



As a result of the reaction between GaCl and NH<sub>3</sub>, reaction 2.4, GaN epitaxial layers are grown on the substrate. Growth of GaN via HVPE was reported for the first time by Maruska and Tietjen in 1969.<sup>38</sup> Since then, HVPE of GaN has been seen as a way to obtain freestanding GaN wafers.<sup>39</sup> GaN can be grown at growth rate as high as 1000

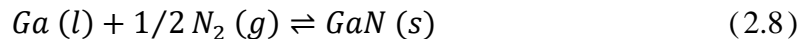
$\mu\text{m/h}$ .<sup>40</sup> Due to this high rate, HVPE is sometimes considered as a bulk GaN growth technique. The process to produce GaN wafers consists in growing a thick GaN layer on a foreign substrate, followed by substrate removal, crystal slicing, and wafer polishing.<sup>37</sup> Different techniques have been developed for substrate removal. Among them, the most widely used techniques are laser lift-off, self-separation, mechanical polishing, plasma etching, and chemical etching and spontaneous self-separation.<sup>37</sup> However, due to the use of non-native substrates, the HVPE-grown freestanding GaN wafers exhibit residual strain and extended defect concentration which makes them not suitable for demanding present and future devices.<sup>13</sup>

### 2.3. Growth of bulk GaN

As a consequence of the strong binding energy of the Ga-N bond, GaN melts at 2500 °C.<sup>41</sup> At that temperature, the nitrogen partial pressure in equilibrium with the solid GaN is over  $5 \times 10^4$  bar.<sup>42</sup> When the pressure of the system is lower than the equilibrium pressure, GaN does not melt but decomposes. Because of that, bulk GaN cannot be grown using standard melt-growth methods like Bridgman or Czochralski type of techniques. Different techniques have been proposed to produce bulk GaN. Among them, the high-pressure solution (HPS), the ammonothermal, and the Na flux techniques have been identified as the most promising. In this section a review of the experimental details as well as the advantages and challenges of these three techniques are presented. For a more extensive review in these techniques, the reader may refer to specific HPS,<sup>43-44</sup> ammonothermal,<sup>45-47</sup> and Na-flux review articles<sup>48</sup>.

### 2.3.1. High pressure solution

In the early 80s Bockowski *et al*, after studying the thermodynamics of the N<sub>2</sub>-Ga system, proved that the growth of GaN was possible from a Ga melt and molecular nitrogen at high temperature and pressure. They called this technique “high pressure solution”.<sup>42, 49</sup> The HPS method is based on the direct reaction between gallium and nitrogen (reaction 2.8) at high temperature (1400-2250°C) and high nitrogen pressure (0.75-2 GPa).<sup>50-51</sup> By combining high temperatures and pressures, the system is able to remain in equilibrium while the solubility of the nitrogen in the Ga is increased. This effect is illustrated in Figure 2.4. A rise in temperature increases the solubility of nitrogen in liquid Ga, Figure 2.4 (a), and decreases the Gibbs free energy of the reactants, Figure 2.4 (b). When the Gibbs free energy of the products is higher than that of the reactants, the reaction is no longer spontaneous. However, by increasing the pressure, the Gibbs free energy of the reactants shifts and the reaction can reach equilibrium again as seen in Figure 2.4 (b).<sup>42, 52-54</sup>



In a typical HPS process a crucible containing Ga is placed into a pressure chamber. The chamber is then pressurized with N<sub>2</sub> and heated up to the process pressure and temperature.<sup>55-56</sup> During the process, which lasts between 100 to 200 hours, N<sub>2</sub> dissociates into atomic nitrogen at the Ga surface and dissolves into the metal.<sup>57</sup> As a result, Ga supersaturates, leading to spontaneous nucleation of GaN crystals and their consequent enlargement into bigger crystals. To supersaturate the melt, two different approaches can be used. In the first one, a temperature gradient along the z-axis of the melt is used.<sup>58</sup> Usual values for the gradient are between 2 and 100 °C/cm.<sup>59-60</sup> In the second one, the N<sub>2</sub> pressure

is increased beyond the equilibrium condition and is maintain at that value during the crystal growth.<sup>56</sup>

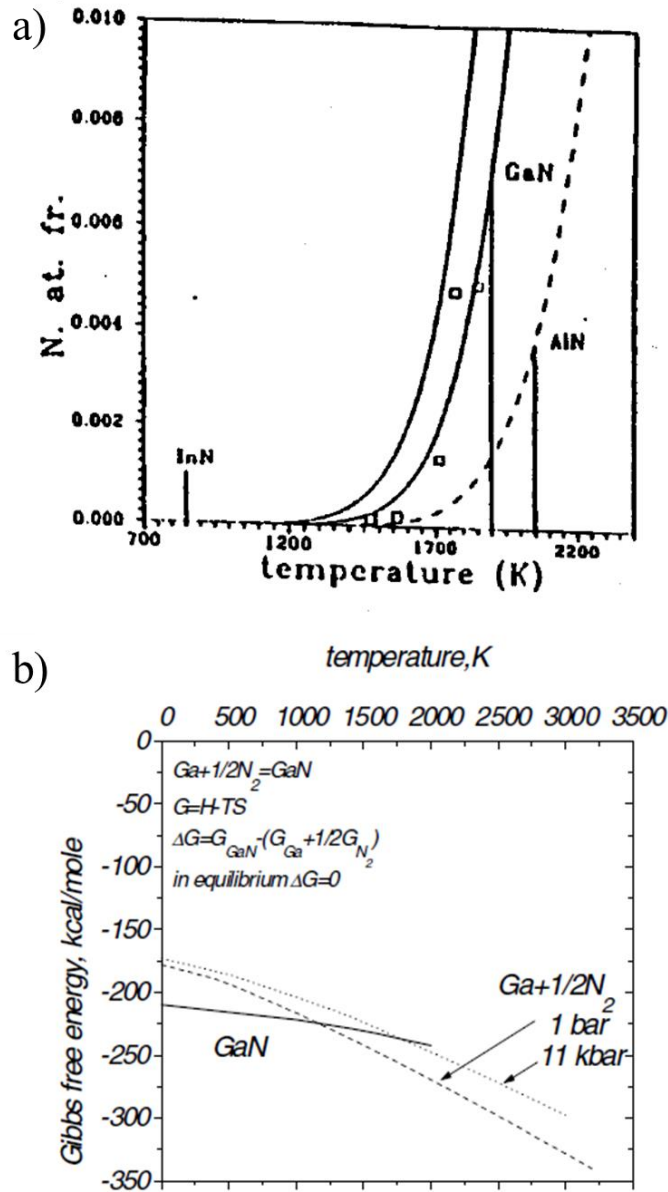


Figure 2.4 (a) Temperature dependence of the solubility of N in liquid Al, Ga, and In. Adapted from S. Porowski.<sup>52</sup> (b) Gibbs free energy of GaN and its constituents (reaction 2.8) in terms of pressure and temperature. Adapted from I. Grzegory.<sup>55</sup>

Unseeded growth of GaN via HPS was characterized by the growth of GaN thin hexagonal platelets. The platelets, which reached a lateral dimension of about 1 cm and a thickness of  $\sim 100 \mu\text{m}$ , exhibited, in the best of the cases, a dislocation density of  $10^1$ - $10^2 \text{ cm}^{-2}$ .<sup>55, 60</sup> The hexagonal surface of the platelets corresponded to the  $\{0001\}$  planes, whereas the side faces of the crystal were mainly the  $\{10\bar{1}1\}$  and  $\{10\bar{1}0\}$  planes. The strong anisotropy of the growth, i.e. 100 times faster in the directions perpendicular to the c-axis than the ones parallel to the c-axis, was explained by a slow nucleation rate on the  $\{0001\}$  surfaces.<sup>61</sup> The platelets obtained via the HPS method have been used as substrates for further growth of the GaN using HVPE, MBE, and MOCVD processes.<sup>54, 62</sup> GaN was grown along the c-direction of the platelets using HVPE at growth rates as high as  $50 \mu\text{m/h}$ . The dislocation density of the as-grown GaN layers was  $10^{-2} \text{ cm}^{-2}$ . The main drawback of the use of HVPE for further growth of GaN was the need to perform a surface preparation of the Ga-terminated face of the crystals. No growth on the N-polar surfaces was obtained.<sup>62</sup>

Seeded HPS growth of GaN has also been investigated. Initially, GaN platelets that were obtained through HPS were used as a substrate. The results showed that the use of a GaN seed promoted the growth along the c-axis.<sup>59</sup> The growth rate was reported to be 2-10  $\mu\text{m/h}$  depending on the temperature gradient. A small temperature gradient promoted slower growth rates, and larger temperature gradients promoted faster growth rates. Due to a radial temperature gradient, the growth rate at the center was different than at the edges of the seed, which resulted in the formation of macrosteps and step bunching.<sup>62</sup> Later, Bockowski *et al.* examined the use of SiC, sapphire, and GaN/sapphire as substrates for HPS growth of GaN. The growth of GaN on both SiC and sapphire was found to be

unsatisfactory. The HPS growth on SiC substrates was characterized by the formation of GaN hillocks that coalesce to each other, silicon nitride crystals, and free carbon bullets. These last two substrates were explained as a consequence of the decomposition of the SiC surface during the growth. When sapphire substrates were used, two different growth modes were observed. At the edges of the substrate the growth was reported as single crystalline, whereas close to the center the crystal growth was defined as polycrystalline. Lastly, the growth of GaN on GaN/substrates was promising. The growth mechanism, which was similar to the one observed when HPS GaN platelets were used as seeds, was described as propagation of macrosteps.<sup>63</sup> A following study showed that the dislocation density of GaN layers grown using the HPS technique was an order of magnitude lower than that of the GaN/sapphire substrates.<sup>18</sup> Proper growth was found to be dependent on the position of the seed inside the crucible. At the top, where the nitrogen concentration in the melt was higher, parasitic nucleation was observed. At the bottom, where the concentration of nitrogen is lower, the GaN seeds were dissolved. Stable homoepitaxial growth of GaN was observed only when the seed was placed at an intermediate place where the concentration of nitrogen inside the melt was optimal.<sup>51</sup> This zone is called the Ostwald-Miers region. For more discussion on the implications of the Ostwald-Miers region and spontaneous nucleation refer to sections 2.4.2 and 2.4.4.2.

More recently, Bockowski *et al.* proposed a novel concept in which free standing HVPE-grown GaN crystals are converted into HPS-grown GaN crystals.<sup>64</sup> (0001) oriented HVPE-grown GaN crystals were positioned one over the other with Ga in between them. Due to axial temperature gradient, the nitrogen side of the HVPE-grown GaN crystals dissolved, supplying atomic nitrogen to the melt. The nitrogen is then transported to the

adjacent HVPE-grown GaN seed where crystallization takes place on the crystal's Ga side. In this technique the HVPE seeds act as both feed and substrate. By converting the HVPE-grown crystals to HPS-grown crystals, it is possible to decrease the dislocation density and increase the free carrier concentration.<sup>65</sup>

### 2.3.2. Ammonothermal

Due to its more reactive nature, when compared to molecular nitrogen, ammonia has been used as nitrogen source in different chemical reactions. Above its critical values, i.e.  $T_C = 405.23$  K,  $P_C = 11.33$  MPa, and  $\rho_C = 0.225$  g cm<sup>-3</sup>, ammonia becomes a supercritical fluid allowing it to be used as a liquid solvent with gas-like properties, such as diffusivity, surface tension, and viscosity.<sup>66</sup> The synthesis of metal nitrides using supercritical ammonia was presented originally in 1984 by Jacobs *et al.*, but it was not until the mid-90s that it was applied to the synthesis of GaN.<sup>67-68</sup> The synthesis of GaN using supercritical ammonia is known as “ammonothermal” or “AMMONO” technique. Dwilinski *et al.* obtained micron-sized GaN crystals with good optical properties by exposing Ga to supercritical ammonia and alkali-metal amides (LiNH<sub>2</sub> or KNH<sub>2</sub>) i.e. mineralizers at 550°C and 0.5 GPa. The reaction between Ga and supercritical ammonia led to homogeneous crystallization of hexagonal GaN. The role of the mineralizers was found to be critical in the process. The authors pointed that the mineralizers facilitated the dissolution of undesired GaN and accelerated the chemical reaction.<sup>68-71</sup> Furthermore, the type of mineralizers influenced the structure of the GaN crystals. Purdy *et al.* reported that the use of acidic mineralizers (NH<sub>4</sub>X or LiX; X = Cl, Br, I), instead of the basic mineralizers used by Dwilinski *et al.*, promoted the crystallization of cubic-GaN.<sup>72-73</sup> Depending of the



type of mineralizers used during the process, the technique is identified as ammono-basic (basic ammonothermal) or ammono-acidic (acidic ammonothermal).

To obtain bulk GaN, Dwilinski *et al.*, in collaboration with Nichia Corporation, developed the ammonothermal bulk technique.<sup>45</sup> As a result of this collaboration, Ammono S.A. was created. The technique was described as a process in which GaN seeds are enlarged via epitaxial growth of GaN under ammonothermal conditions. To produce large crystals, a seed is enlarged and then used as a new seed in a new enlargement process. This sequence of processes is repeated until the desired size of the crystal is reached. In general, the process is carried out at 0.1-0.5 GPa and 400-750°C in an autoclave that is placed in a multiple-zone furnace, which enables a temperature gradient inside the chamber. In the warmer zone of the autoclave, a nutrient, such as metallic Ga or polycrystalline GaN, is dissolved in supercritical ammonia, and then transferred by convection to the crystallization zone (colder zone), where GaN is crystallized on the native seeds; this crystallization is due to the supersaturation of the solution.<sup>74-77</sup> When ammonothermal-grown crystals are used as a seed, the process is referred to as “true bulk ammonothermal”. Dwilinski *et al.* reported the growth of large GaN crystals with a low dislocation density of  $5 \times 10^{-2} \text{ cm}^{-2}$  using the true bulk ammono-basic method.<sup>78</sup> Crystals were sliced into polar (c-plane oriented), non-polar (m- and a-plane oriented) and semi-polar [(20-21)-plane oriented] GaN substrates. Up to 2-in. polar GaN wafers have been obtained.<sup>12</sup> These substrates exhibited a large lattice curvature ranging from  $10^2$  to  $10^3 \text{ m}$  and a small FWHM value of (0002) X-ray rocking curve of about 16 arcsec.<sup>79</sup> On the other hand, non-polar substrates and semi-polar substrates with sizes up to  $17 \times 8 \text{ mm}^2$  and  $9 \times 12 \text{ mm}^2$ , respectively, were initially obtained.<sup>80-81</sup> Continuous enlargement of those seeds allowed

the researchers to obtain 26 x 26 mm<sup>2</sup> m-plane substrates.<sup>82</sup> Although the final size of the crystals is limited only by the size of the autoclave, the slow growth rates of this process makes it difficult to obtain GaN crystals that fulfill the industry requirements.<sup>82</sup> Ammono's current growth rates for production of bulk GaN are 2 μm/day, 50 μm/day, and 80 μm/day in the m-, -c-, and a-direction, respectively.<sup>83</sup>

Epitaxial growth of GaN on HVPE-grown GaN substrates using the basic ammonothermal technique has also been reported.<sup>84-87</sup> GaN growth on flat c-oriented GaN substrates was characterized by a distinct growth on its two main surfaces. The Ga-polar surface exhibited the formation of pits, whereas the N-polar surface was featureless.<sup>84</sup> Furthermore, the dislocation density of the Ga surface, estimated by plain-view TEM observations, was less than  $1 \times 10^6 \text{ cm}^{-2}$ , which corresponds to an order of magnitude less than that of the N-surface. Finally, no dislocation generation was observed at the interface on the Ga face, while few dislocations were found at the interface on the N face.<sup>85</sup> The anisotropic nature of the growth rate resulted in the formation of crystals with a three-dimensional polyhedron shape.<sup>86</sup> The total growth rate in the c-direction was reported to be in the order of 50 μm/day.<sup>86-87</sup>

### 2.3.3. Na flux

In 1997, Yamane *et al.* introduced the concept of the sodium (Na) flux method.<sup>88</sup> In this technique, which works similarly to the HPS method, a Ga-Na flux is exposed to a nitrogen atmosphere at high pressure and temperature. The addition of Na into the Ga melt increases the solubility and reactivity of nitrogen in Ga.<sup>13</sup> This effect is reflected in the use of milder growing conditions compared to the other two techniques. In a typical Na flux growth, the pressure is <10 MPa and the temperature ranges from 700 to 900°C.<sup>48</sup> Initial

studies used  $\text{NaN}_3$  as the source of Na and reported the growth of GaN crystals with sizes of 1.0-2.0 mm and ~0.5 mm after 96 and 24 hours, respectively; these sizes differed depending on the process's conditions.<sup>88-89</sup> The morphology of the crystals varied between granules, platelets, and prisms and was determined by the Ga/Ga+Na ratio.<sup>90</sup> Further growth of the crystals was limited by the formation of a polycrystalline GaN layer on the surface of the flux.<sup>91</sup> Aoki *et al.* reported that by using a cone-shaped crucible they were able to control the formation of GaN crystals on the surface which enabled continuous crystal growth for over 360 hrs.<sup>92</sup> Furthermore, the researchers identified that by using high-purity (99.95%) Na also helped to reduce the formation of the GaN layer.<sup>93</sup> Finally, Kawamura *et al.* reported that by adding small amounts of carbon into the flux the formation of polycrystals was suppressed.<sup>94</sup>

Two different approaches have been attempted to obtain bulk GaN using the Na flux method. The first approach is to grow epitaxially a thick GaN layer on a MOCVD/HVPE/MBE-grown GaN substrate (layer). The second approach corresponds to the epitaxial enlargement of GaN crystals that were previously obtained via the Na flux method.<sup>95</sup> Independently of which approach is used, it is needed to guarantee that the epitaxial growth GaN is possible. Aoki *et al.* identified that depending on the process conditions, i.e. temperature and pressure, three different outcomes are possible: (1) decomposition of the GaN seed, (2) spontaneous nucleation of GaN crystals, and (3) epitaxial growth of GaN.<sup>96</sup> Therefore, the process conditions in the Na flux method are of utmost importance to obtain bulk GaN. The main advantage of the first approach is that large substrates are easily available. However, those substrates have a large dislocation density, which restrict the quality of the grown bulk GaN crystal. The first study in which

this approach was attempted, reported the growth of a 2 in crystal with a dislocation density of  $2.3 \times 10^5 \text{ cm}^{-3}$ , which is lower than that of the MOCVD-grown GaN substrate.<sup>97</sup> Kawamura *et al.* found that the dislocation density of the crystal reduced as the crystal gets thicker. The researchers explained this phenomenon as a two-step dislocation reduction process; they stated that the constant change in the propagation direction of the dislocations leads to the aggregation of dislocations and therefore the reduction of the dislocation density.<sup>98</sup> As a way to control the reduction of the dislocation density of the grown GaN crystals, different tactics have been reported. Imade *et al.* grew high quality GaN crystals using a GaN-on-sapphire wafer covered with a sapphire plate with a hole in the center as substrate. By limiting the initial growth of the bulk GaN to the volume of the hole (necking region), the dislocations, which are being originated from the substrate, cannot propagate further than the hole's sidewall. As a result, the GaN crystal that grows beyond the necking region is characterized for having a lower dislocation density.<sup>99</sup> Imashi *et al.* was able to grow GaN crystals with a dislocation density of  $\sim 10^3 \text{ cm}^{-3}$  by using the "point seed" tactic. In this tactic a GaN layer grown by MOCVD on a sapphire substrate is etched away leaving only a GaN point seed. Then, this point seed is used as a seed for epitaxial growth of GaN. In their study they used two different sizes of seeds i.e. 250 and 1000  $\mu\text{m}$ . When the smaller seed was used the dislocation density of the grown crystal was  $\sim 10^3 \text{ cm}^{-3}$ , whereas when the bigger seed was used it was  $\sim 10^3 \text{ cm}^{-3}$ . However, the mechanism in which the dislocation density decreases dramatically was not well understood by the researchers.<sup>100</sup>

The use of a GaN crystal as a seed allowed the researchers to obtain GaN hexagonal pillar crystals with a size of  $\sim 10 \text{ mm}$  in length and  $5 \text{ mm}$  in height. The corresponding growth rates of the process were  $30 \mu\text{m/h}$  in the c-direction and  $33 \mu\text{m/h}$  in the a-direction

(66  $\mu\text{m}/\text{h}$  in both directions).<sup>95, 101</sup> Further growth enabled crystals with over 20 mm in width and 15 mm in height to be obtained.<sup>102</sup> Imanishi *et al.* proved that when two GaN crystals coalesce along the a-direction no dislocations are formed.<sup>103</sup> This information was used by Mori *et al.* who proposed to obtain a larger crystal by the coalescence of GaN crystals from many isolated small seeds. The researchers, who were able to obtain a 2-in-diameter GaN crystal from multiple small seed crystals, believed that this technique could promote the fabrication of large-diameter, high quality GaN crystals.<sup>104</sup> Recently, Hayashi *et al.* came with a hybrid approach called the “multi point seed growth of GaN”. In this approach, multiple point seeds are created on a sapphire substrate. Then GaN crystals are grown from these seeds; as the crystals grow in the a-direction (growth rate of 80  $\mu\text{m}/\text{h}$ ) they coalesce. As a result, a large GaN crystal is created.<sup>105</sup>

Other alkali metals (lithium, potassium) and semi alkali metals (calcium) were successfully used in the growth of bulk GaN via the flux method.<sup>106-111</sup> Lithium (Li) and calcium (Ca) were used primarily as an additive to the Na flux technique. When used as an additive, both Li and Ca increased the solubility of GaN and nitrogen in the solution.<sup>106</sup> As a result, the process pressure can be reduced. Kawamura *et al.* reported that by adding 3 mol of Ca to a 138 Ga/Na mixture they were able to reduce the pressure from 20 to 10 atm and still obtain epitaxial growth of GaN.<sup>107</sup> They also reported that the yield of GaN grown in a Ca-Na flux drastically increased compared to that in the Na flux. However, an excessive amount of Ca in the flux reduces the yield and inhibits the growth of GaN at 700°C.<sup>108</sup> Additions of Li also improved the yield of the process. The crystals obtained using the Li-Na flux were larger crystals than that the ones obtained using the Ca-Na flux due to the low nucleation frequency. Furthermore, large addition of Li did not inhibit any

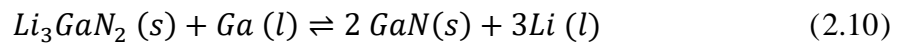
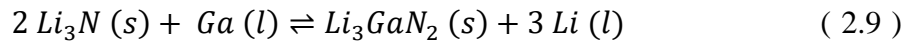
growth.<sup>109</sup> For more information involving the growth of GaN from a Li-based flux refer to section 2.4.1. Yamane *et al.* reported the growth of zincblende-type cubic GaN (c-GaN) using a potassium (K) flux. The researchers obtained a translucent single crystalline c-GaN crystal with a size of 40 x 30 x 30  $\mu\text{m}^3$  by exposing a K flux (Ga:K = 2:3 molar) to a nitrogen atmosphere at 70 bar and 750°C for 100 hours. The researchers, however, were not able to explain why cubic GaN was formed instead of hexagonal GaN.

#### 2.4. Low pressure liquid phase epitaxy of GaN

The reaction between Ga melt and nitrogen ( $\text{N}_2$ ), reaction 2.8, thermodynamically favors the GaN product only when the pressure of nitrogen in the system is higher than the equilibrium partial pressure of  $\text{N}_2$ . Unfortunately, the equilibrium partial pressure of  $\text{N}_2$  at the temperatures that bulk GaN is synthesized (1200-1750°C) are high (0.75-2 GPa), forcing the use of even higher pressures in the system. For more details in liquid phase epitaxy at high pressures refer to Section 2.3. However, it has been proven that the replacement of molecular nitrogen for alternative chemical species, which supply atomic nitrogen to the melt, allows GaN to grow at lower pressures. The growth of GaN from a melt at pressures of ~1 atm and below is labeled as low-pressure liquid phase epitaxy (LP-LPE) of GaN, or low-pressure solution growth (LPSG) of GaN. Those species can be grouped into three different groups: alkali and semi-alkali metal nitrides, ammonia, and nitrogen radicals. In this section, a review of these three groups is presented.

#### 2.4.1. Nitride flux

In the case of GaN growth, the term “nitride flux” refers to a liquid phase process in which a solution, made of an alkali or semi-alkali metal nitride and molten Ga, is used to dissolve nitrogen. The solution then transports the dissolved nitrogen to seed crystals where GaN crystallizes and grows.<sup>112</sup> X. L. Chen and collaborators were the first group to propose and use an alkali or semi-alkali metal nitride in conjunction to molten Ga to grow GaN.<sup>113-116</sup> Their process consisted of placing Li<sub>3</sub>N and Ga into a tungsten crucible and heating it to ~800°C in a growth furnace, which was pressurized up to 2 atm with N<sub>2</sub> gas at room temperature. The crucible was kept at those conditions for 120-180 h and then was cooled down at a rate of 2-3°C/d.<sup>113</sup> Initial results demonstrated the growth of hexagonal GaN platelet crystals with a size of 1-4 mm. The researchers believed that the process consisted of a two-step reaction, in which Li<sub>3</sub>N transforms to Li<sub>3</sub>GaN<sub>2</sub> and then to GaN. The process is described by reactions 2.9 and 2.10.<sup>113</sup>



Additional experimentation allowed them to construct a process map, which demonstrated that the type of growth depended on the experimental conditions. The process map is summarized in Table 2-6. It was found that crystalline GaN could only be synthesized when the moles of Ga exceeded the moles of Li<sub>3</sub>N. However, the yield of GaN was reported to increase by increasing the Ga content. The process temperature window was limited at the upper end by the reaction between Li<sub>3</sub>N and the W crucible and at the lower end by the thermodynamics of the process. The researchers hypothesized that at temperatures below 700°C the free energy of formation of Li<sub>3</sub>N is smaller than the free

energy of formation of GaN.<sup>113-114</sup> The process pressure was limited by the decomposition of Li<sub>3</sub>N. When the pressure was lowered to about 400 torr, Schönherr *et al.* reported the decomposition of Li<sub>3</sub>N into N<sub>2</sub> gas and liquid Li at 814°C.<sup>117</sup>

Table 2-6. Relationship between the experimental conditions and the type of outcome in a Li<sub>3</sub>N flux process for GaN growth. Adapted from Song *et al.*<sup>114</sup>

Variable	Value	Result
Li <sub>3</sub> N to Ga molar ratio	2:1	GaLi <sub>3</sub> N <sub>2</sub> granule
	1:1-20	Crystalline GaN
Reaction temperature (°C)	700	Li <sub>3</sub> N + Ga
	760	Poorly crystalline GaN
	800	Highly crystalline GaN
	850	WLi <sub>6</sub> N <sub>4</sub> granule
N <sub>2</sub> pressure (atm)	0.5	Li + Ga
	0.9	Crystalline GaN
	1.5-2.0	Crystalline GaN
Position of Li <sub>3</sub> N in crucible	Top	Poorly crystalline GaN
	Bottom	Highly crystalline GaN

New findings from Schönherr *et al.* allowed Chen *et al.* to reconceptualized the mechanism for the growth of GaN via the Li<sub>3</sub>N flux technique. They proposed in the first step that Li<sub>3</sub>N and Ga reacted to form Li<sub>3</sub>GaN<sub>2</sub> and liquid Li, reaction 2.9. Later, Li<sub>3</sub>N and Li<sub>3</sub>GaN<sub>2</sub> dissolved into the Li-Ga melt creating a Li-Ga-N melt. Finally, GaN crystallizes



from the Li-Ga-N melt.<sup>114</sup> This result implies that the growth of GaN does not occur by the direct reaction of  $\text{Li}_3\text{GaN}_2$  and Ga, as described in reaction 2.10. The dissolution of  $\text{Li}_3\text{N}$  in the Li-Ga melt is explained by the study performed by Yonco *et al.* who reported that  $\text{Li}_3\text{N}$  is highly soluble in Li.<sup>118</sup> Furthermore, Chen *et al.* constructed a Li-Ga-N phase diagram at 800°C and 1 bar using the calculation of phase diagrams (CALPHAD) methodology.<sup>115</sup> In the CALPHAD method, both the thermodynamic information of the compounds of interest and experimental data are used. The Li-Ga-N phase is presented in Figure 2.5. The diagram shows the presence a single-phase region composed of a Li-Ga-N melt (L), two two-phase regions composed of L and  $\text{Li}_3\text{GaN}_2$ , and L and GaN and a three-phase region comprised of L,  $\text{Li}_3\text{GaN}_2$  and GaN. In addition to the presence of pure Li, Ga and N at the corners, the diagram presents the presence of pure  $\text{Li}_3\text{N}$ ,  $\text{Li}_3\text{GaN}_2$  and GaN, denoted as dots in the diagram. According to the Li-Ga-N ternary phase diagram, GaN can only be obtained in the Ga-rich region. This result is consistent with the data presented in Table 2-6. Chen *et al.* was able to obtain  $\text{Li}_3\text{GaN}_2$  when the ratio of  $\text{Li}_3\text{N}$  to Ga was 2:1 (Li:Ga = 6:1). On the other hand, when the number of moles of Ga exceeded the number of moles of  $\text{Li}_3\text{N}$ , GaN was obtained. They believed that due to volatilization of  $\text{Li}_3\text{N}$  during the process, the Li to Ga molar ratio is actually lower than what it is expected from the composition of the precursor melt. Additionally, the researchers related the crystal size to the phase diagram. They found that, within the Ga-rich region, the higher the composition of N, the larger the size of the GaN crystals.<sup>114-115</sup> However, enlargement of the GaN crystals does not depend exclusively on the composition of the melt. X. L. Chen pointed that the main difficulty in enlarging the size of the GaN crystals is the homogeneous nucleation of GaN which is a competing process to crystal growth. The

author pointed that in order to obtain larger GaN crystals the parasitic growth of GaN must be prevented, and they acknowledged the need of further optimization of their process.<sup>116</sup>

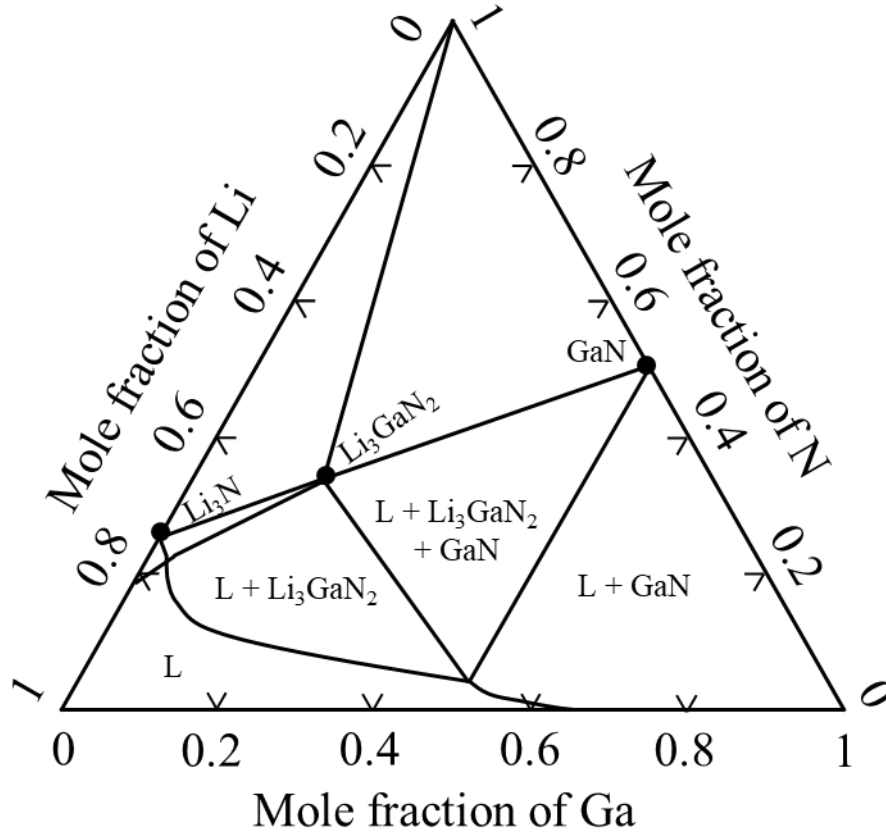


Figure 2.5 Li-Ga-N ternary phase diagram at 800°C and 1 bar. Data taken by Chen *et al.*<sup>115</sup>

In following studies, X.L. Chen *et al.* investigated the use of other alkali or semi-alkali metals in a nitride flux process. First, the authors added Ca metal to a Li<sub>3</sub>N flux and monitored the differences in the growth of GaN with respect of the pure Li<sub>3</sub>N flux. They found that additions of Ca improved the size distribution and changed the morphology of the grown GaN crystals. However, the use of excessive amounts of Ca prevented any type of growth.<sup>119</sup> Later the researchers proposed two new alkali or semi-alkali metal nitride fluxes for LPE of GaN. First, the researchers reported the use of a Ca<sub>3</sub>N<sub>2</sub>-based flux. Ca<sub>3</sub>N<sub>2</sub> and Ga were charged in a crucible and heat up at 900°C under a nitrogen pressure of about

2 atm. The results showed that GaN crystals, which were up to 1.5 mm in length and 100  $\mu\text{m}$  in width, were grown from a Ga-rich melt. The crystals that were characterized by its hexagonal prismatic morphology exhibited a preferential growth in the c-direction.<sup>120</sup> An additional advantage of a  $\text{Ca}_3\text{N}_2$  flux is that at 900°C, the vapor pressure of  $\text{Ca}_3\text{N}_2$  is less than  $1 \times 10^{-3}$  atm allowing to carry the process at lower pressures.<sup>121</sup> Secondly, Chen *et al.* investigated the outcomes of a  $\text{Ba}_3\text{N}_2$  flux in GaN growth. Their experimental set up was the same as they had done for their  $\text{Ca}_3\text{N}_2$  study. Similarly, to their previous  $\text{Ca}_3\text{N}_2$  study, they found that the type of flux used affected the morphology. The crystals obtained with the  $\text{Ba}_3\text{N}_2$  flux were described as pyramidal crystals with a flat top and hillock-like bottom. The researchers conjectured that this type of morphology was a result of an unbalance growth of the non-polar face.<sup>122</sup> The use of different nitride fluxes has been proven to be advantageous for different purposes. Nonetheless, their use at low pressures is limited by their decomposition temperature/pressure. For example,  $\text{Na}_3\text{N}$  decomposes at around 300°C when the pressure is lower than 100 atm which makes it not suitable for this type of process.<sup>92</sup>

Between 1997 and 2001 Ivantsov, Sukhoveev, Dmitriev, *et al.* reported the growth of GaN crystals from a Ga-based melt at a reduced temperature and pressure.<sup>123-126</sup> The growth of GaN was carried out by heating the flux up to  $\sim 1000^\circ\text{C}$  in a  $\text{N}_2$  atmosphere at a pressure not exceeding 2 atm for 30-120 minutes. The crystals, which grew spontaneously on the surface of the solution, were characterized by their regular hexagonal prism shape. The dimensions of individual single crystals reached up to  $2 \times 2 \times 0.1 \text{ mm}^3$ . XRD characterization indicated that the crystals were 2H-GaN and had a (0001) plane orientation.<sup>123-124</sup> Subsequent studies performed by these researchers focused on using this

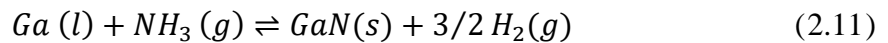
technique for seeded growth of GaN. A graphite rod, which was used as the growth seed, was inserted into a Ga-based melt at 850-1000°C in a N<sub>2</sub>-rich gas mixture at a total pressure of less than 2 atm. The rod was then lifted up slowly, allowing the growth of a GaN ingot. The linear velocity of the rod (~2µm/h) determined the process growth rate. GaN ingots of up to 21 mm in diameter and 15 mm in length were obtained via this approach. The ingots were sliced into 2 mm thick wafers for further characterization. XRD of the wafers revealed that the wafers had a polycrystalline structure with the [10-10] preferred orientation. Additionally, the wafers were used as substrates for homoepitaxial growth of GaN via HVPE. The results showed that the 3 µm thick HVPE-grown films were stress free and displayed an improvement in the structural and optical properties when compared with the substrate.<sup>125</sup> Further optimization of the process allowed them to obtain samples with up to 2.5 inches in diameter.<sup>126</sup>

Although it is not mentioned in the experiments by Ivantsov, Sukhoveev, Dmitriev, *et al*, the author of this dissertation believes that given the description and process conditions of the studies performed by these researchers., the melt could have contained alkali or semi alkali metal nitrides.

#### 2.4.2. Low pressure growth of GaN under ammonia atmosphere

The growth of GaN from molten Ga and ammonia at low pressures was reported for the first time in 1931 by Johnson *et al*. as an attempt to produce the only group III nitride, which had not been reported as being produced up to that date. The nitride, which was synthesized by exposing a boat containing Ga in a temperature-controlled system, appeared as a dark gray powder. The reaction was reported to proceed at temperatures as

low as 700°C. However, the process had to be carried out at 900-1000°C to obtain enough GaN for analysis due to the slow reaction rate at the lower temperature end. At temperatures higher than 1000°C, Ga was appreciably volatile, evaporating from the boat and condensing in the cooler regions of the reactor.<sup>127</sup> The volatility of Ga at high pressures brings additional problems to the LP-LPE of GaN. E. Ejder reported the growth of single crystalline whiskers of GaN from the vapor phase by the reaction of Ga and ammonia at 1000 and 1150°C.<sup>128</sup> Although the study of Johnson *et al.* provided some insights into the growth of GaN using Ga and ammonia, the mechanism in which GaN is formed was not discussed. It was not until 1972, after a series of studies from Logan and Thurmond, that the use of ammonia was seen as an alternative to N<sub>2</sub> for epitaxial growth of GaN from a Ga melt at significant lower pressure.<sup>129-130</sup> The equilibrium partial pressure of N<sub>2</sub> determines the minimum partial pressure of N<sub>2</sub> required to grow GaN from molten Ga and molecular nitrogen, reaction 2.8. In a similar way, the equilibrium partial pressure of ammonia determines the minimum partial pressure of ammonia required to grow GaN from molten Ga and ammonia, reaction 2.11.



The equilibrium partial pressure of N<sub>2</sub>,  $P_{N_2}^*$ , is related to the standard free energy of reaction 2.8,  $\Delta G_{2.8}^\circ$ , by the following expression.

$$1/2 RT \ln P_{N_2}^* = -\Delta G_{2.8}^\circ \quad (2.12)$$

The standard free energy of reaction 2.8 is, at the same time, related to the free energy of formation of GaN,  $\Delta G_{GaN}^f$ , and subsequently to the heat,  $\Delta H_{GaN}^f$ , and entropy,  $\Delta S_{GaN}^f$ , of formation of GaN. This relationship is expressed by equation 2.13.

$$-\Delta G_{2.8}^{\circ} = \Delta G_{GaN}^f = \Delta H_{GaN}^f - T\Delta S_{GaN}^f \quad (2.13)$$

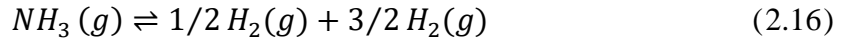
Similarly, the equilibrium partial pressure of ammonia,  $P_{NH_3}^*$ , can be expressed by:

$$\frac{P_{NH_3}^*}{P_{H_2}^{*3/2}} = K_{2.11} \quad (2.14)$$

Where  $P_{H_2}^*$  and  $K_{2.11}$  are the equilibrium partial pressure of  $H_2$  and the equilibrium constant for reaction 2.11, respectively. In addition, the pressure ratio  $P_{NH_3}^*/P_{H_2}^{*3/2}$  can be correlated to  $P_{N_2}^*$  using the following expression.

$$P_{N_2}^* = K_{2.16} \frac{P_{NH_3}^*}{P_{H_2}^{*3/2}} \quad (2.15)$$

Where  $K_{2.16}$  is the equilibrium constant for reaction 2.16.



Using the equations presented previously, available data in the literature, and some assumptions, Thurmond and Logan were able to calculate the equilibrium partial pressure of  $N_2$  and ammonia for reactions 2.8 and 2.11, respectively. The results, which are presented in Figure 2.6, showed that the growth of GaN using  $N_2$  requires significantly higher pressures than when ammonia is used as the nitrogen source. The calculated partial pressure of  $N_2$  in equilibrium is greater than 1 atm at 800°C. At 1200°C the pressure is  $\sim 1 \times 10^5$  atm and reaches  $\sim 1 \times 10^5$  atm at approximately 1700°C. In contrast, the calculated partial pressure of  $NH_3$  in equilibrium at 900 and 1200°C is  $\sim 1 \times 10^{-3}$  and  $\sim 3 \times 10^{-3}$  atm, respectively.<sup>129</sup>

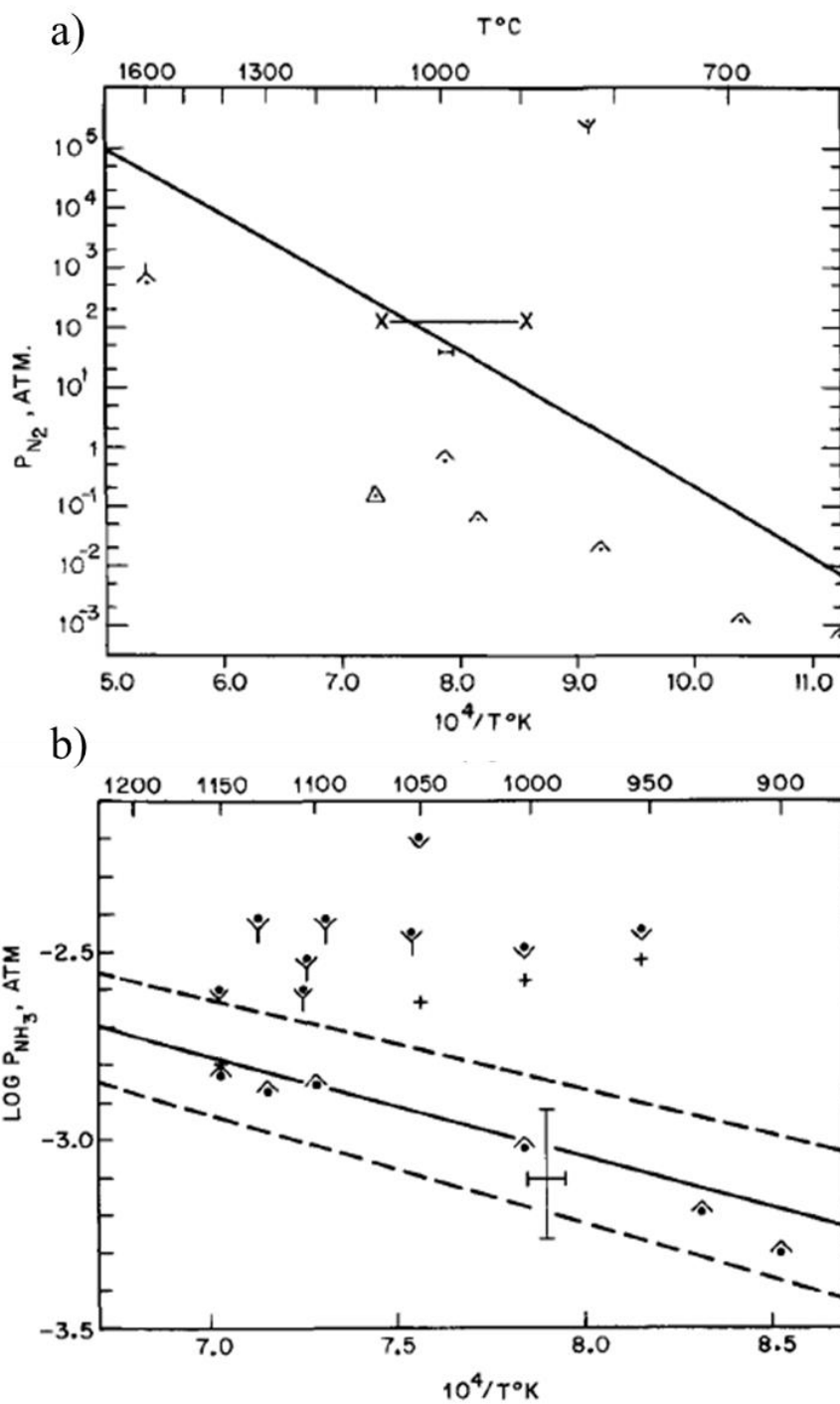


Figure 2.6. (a) Partial pressure of  $N_2$  in equilibrium with GaN when formed from Ga and  $N_2$ , ( $P_{N_2}$  vs.  $10^4/T$ ). (b) Partial pressure of  $NH_3$  in equilibrium with GaN when formed from Ga and  $NH_3$ , ( $\log P_{NH_3}$  vs.  $10^4/T$ ).  $P_{H_2}$  is 1 atm. Dashed lines represent a  $\pm 1$  kcal uncertainty in the free energy of formation of GaN. Adapted from Thurmond and Logan.<sup>129</sup>

Experimentally, Logan and Thurmond, grew epitaxial layers of GaN onto single crystal sapphire substrates by heating Ga under a partial pressure of ammonia in H<sub>2</sub>. Growths were carried out at a partial pressure of ammonia in the range of  $5 \times 10^{-4}$  -  $2 \times 10^{-2}$  atm and at temperatures in the range of 850-1050°C. The researchers found that the growth was only possible when the following three conditions were met: first, the partial pressure of ammonia is higher than the equilibrium partial pressure of ammonia at the temperature that the process is being carried out; second, there is a temperature gradient across the growth melt; and, third, the spontaneous homogeneous nucleation is controlled. The first condition was explained thermodynamically hereinbefore. The second condition states that by reducing the temperature of the end, where the growth takes place, the transport of dissolved nitrogen to the growing zone is improved. Finally, the third condition refers to the elimination of any GaN layer that was formed via homogeneous nucleation that limits the epitaxial growth of GaN. The researchers found that by adding Bi to the Ga melt, the homogeneous nucleation was decreased, allowing for the epitaxial growth of GaN. Nonetheless, the researchers claimed that the suppression of spontaneous nucleation of crystal growth by Bi addition was still not understood.<sup>130</sup>

Elwell *et al.*, who used a similar set of experiments as those utilized by Logan and Thurmond<sup>130</sup>, focused their attention on optimizing the conditions for the growth of GaN via LP-LPE and studied the influence of the addition of Bi or Sn to the Ga melt. In their experiments, a vitreous carbon crucible was charged with Ga, or Ga/Bi or Ga/Sn alloys and placed in a temperature gradient between 870 and 990°C and then exposed to ammonia and hydrogen. The partial pressure of ammonia was adjusted between  $3.4 \times 10^{-4}$  and  $2.3 \times 10^{-3}$  atm. They reported that the reaction between molten Ga and ammonia is primarily a



surface reaction. The initial stages of the growth took place either on the surface of the liquid, on the walls of the crucible, or onto the substrates that were introduced into the Ga. The full reaction of a Ga droplet would result in the formation of a hollow, dome-shaped GaN polycrystalline crust. It was believed that the GaN, formed on the surface of the Ga droplet in the initial stages, provided nucleation sites for further growth. The growth of GaN on the walls and substrates was determined by the wetting properties of the melt. The formation of a thin Ga film allowed for the relatively quick layer growth of GaN due to the large area of contact with the vapor phase. The addition of Bi and Sn was found to increase the nucleation of crystallites. Finally, the researchers found that the temperature gradient transport does not provide a significant effect in the growth of GaN from a Ga solution. They concluded that the growth occurs via a vapor-liquid-solid (VLS) mechanism with the Ga being supplied as a thin film by the outside flow of Ga.<sup>131</sup>

Following studies reported growth of GaN crystals and homoepitaxial growth of GaN via LP-LPE using ammonia as the nitrogen supplier specie.<sup>132-134</sup> Shibata *et al.* obtained large quantities of fine, good quality GaN crystals ( $1 \times 10 \mu\text{m}$ ) by injecting ammonia into molten gallium at  $900\text{-}980^\circ\text{C}$  under atmospheric pressure.<sup>132</sup> Alternatively, Meissner *et al.* reported the growth of millimeter sized GaN crystals using a MOCVD GaN layer as substrate.<sup>133</sup> The production of GaN crystals is of utmost importance as it allows the growth of bulk GaN via LPE. Klemenz *et al.* suggested that the LP-LPE of GaN is very sensitive to different substrate parameters. They found that among the different substrates that were used during experimentation, i.e. (0001) sapphire, (001)  $\text{LiGaO}_2$  (LGO), (001)  $\text{LiAlO}_2$  (LAO), and HVPE-grown GaN, the HVPE-grown GaN substrates provided the best results. The process in which homoepitaxial layers of GaN were grown was

characterized by an initial nucleation of GaN on existing defects of the seed followed by the growth of those nuclei and the formation of a continuous film.<sup>134</sup> The ammonia-based LP-LPE has shown to reduce the dislocation density remarkably during growth and can be easily scaled up. Up to three wafers have been produced in parallel without compromising the quality of the material.<sup>17</sup>

Sun *et al.* studied the formation reaction of GaN from Ga melts under ammonia atmosphere via a thermogravimetric technique. The authors described the process as a four-step process. The process is explained as follows: First,  $\text{NH}_3$  is decomposed and N is dissolved into the molten Ga; second, the nuclei are formed; third, nuclei grow to detectable size; and, finally, they grow into large GaN crystal through a crystal growth step. The first three steps are considered the induction period of the process. From these findings, they were able to introduce the concept of the Ostwald-Miers region for the growth of GaN via LP-LPE.<sup>135</sup> The Ostwald-Miers region is defined as the difference between the supersaturation and equilibrium concentrations. Therefore, the Ostwald-Miers region allows stable supersaturation without homogeneous parasitic nucleation of GaN. After a rigorous study, Hussy *et al.* constructed an GaN growth diagram in terms of the ammonia partial pressure and the experimental temperature, Figure 2.7. The diagram, which exhibits three different regions i.e. dissociation of GaN into Ga and  $\text{NH}_3$ , homogeneous nucleation and GaN growth (parasitic nucleation), and the Ostwald-Miers-Region, is used to predict the outcome of an ammonia-based LP-LPE process depending of the process conditions.<sup>136</sup>

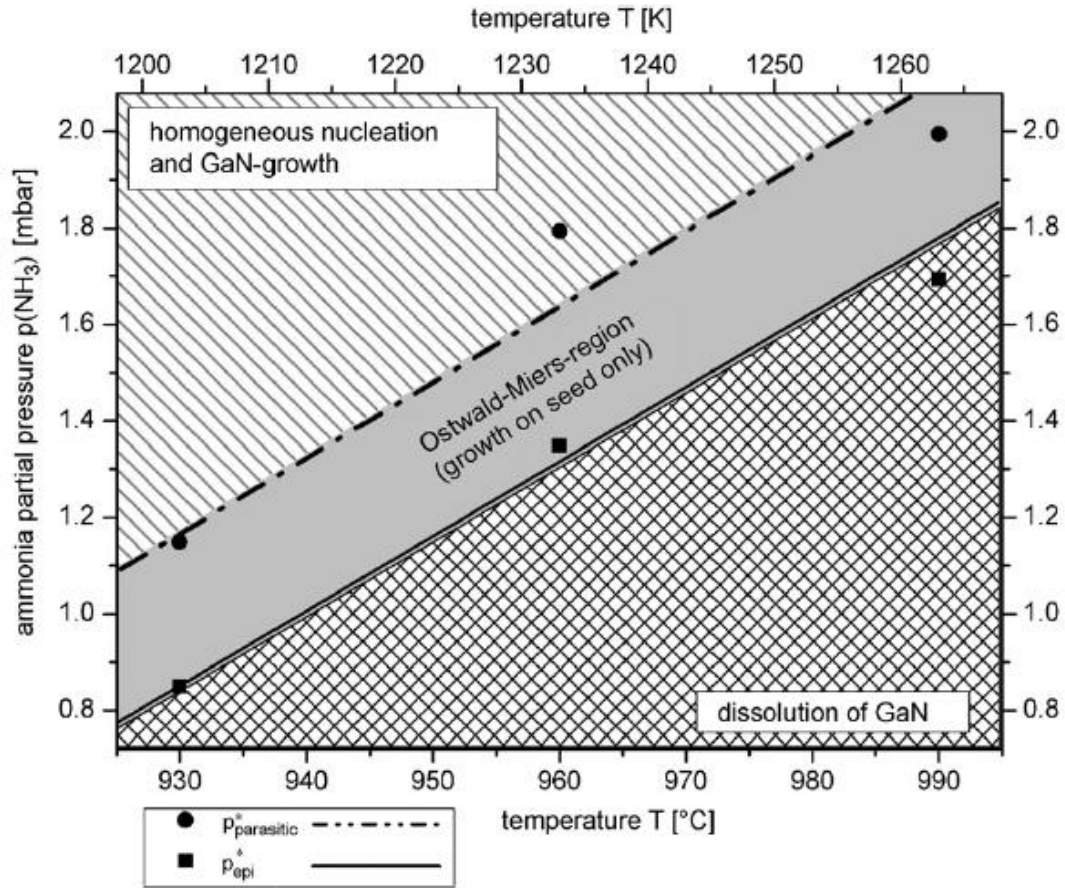


Figure 2.7. Diagram for the LP-LPE growth of GaN using ammonia. Ammonia partial pressure versus temperature with regions of dissociation of GaN (checkered), homogeneous nucleation and GaN growth (striped), and the Ostwald-Miers region (gray). Hydrogen and nitrogen were used as carrier gases and the total pressure was 1 atm. Adapted from Hussy *et al.*<sup>136</sup>

Proper epitaxial growth, however, does not depend exclusively on the partial pressure of ammonia and the process temperature. Hussy *et al.* reported that particles, which are generated by abrasion from sliding parts of the boat, or small crystals formed by homogeneous nucleation, can create macroscopic or secondary (misoriented areas, terraces or depressions) defects in the LPE layers. To limit the effect of the particles in the solution, the researchers proposed to increase the density of the melt to a value higher than that of

the particles. By doing that, the particles are not in contact with the substrate, which is placed at the bottom of the crucible. They also claimed that their methodology enables the process to be operated at supersaturation conditions as the particles, formed by homogeneous nucleation, float on top of the melt, allowing for higher growth rates.<sup>137</sup> Tanaka *et al.* argued that an adequate thickness of the melt is required to obtain the preferable nitrogen saturation that permits high-quality LPE. The authors used an inclined, rotatory substrate holder to create a Ga film with varying thickness on the substrate surface. Once the metal is exposed to ammonia, the concentration of nitrogen inside the melt depends on the ammonia partial pressure and the mass of the melt. Because the localized mass of Ga varies as the thickness of the film changes, the researchers were able to create a Ga film with a varying nitrogen concentration. The results showed that for the same process conditions i.e. overall pressure, carrier gas, and temperature, the nitrogen concentration inside the melt, and not the ammonia partial pressure, is what determines the process's growth region. The area in which the Ga film had the highest nitrogen concentration, which corresponds to the thinnest area of the film, depicted the presence of homogeneous nucleation. On the other hand, in the area where the concentration was the lowest and the film was the thickest, the process was characterized by growth of epitaxial layers of GaN.<sup>138</sup>

#### 2.4.3. Plasma-assisted growth of GaN

Angus *et al.* demonstrated that the growth of bulk GaN at under atmospheric pressures was possible when atomic nitrogen (N), derived from a microwave plasma source, is used as the nitrogen source. As explained by the researchers, the formation of

GaN using N, reaction 2.17, is favorable at N partial pressures ( $P_N$ ) which are easily reached in low pressure plasma environments.<sup>139</sup> The extreme difference in required pressures of  $N_2$  and N to achieve equilibrium, as seen in reactions 2.8 and 2.17, was calculated by J.S. Dyck.<sup>140</sup> The results are depicted in Table 2-7.



The N partial pressure,  $P_N$ , can be calculated in terms of  $P_{N_2}$  and thermodynamic data for the dissociation reaction of nitrogen (reaction 2.18).



The equilibrium constant for that reaction is,

$$K = \exp\left[-\frac{\Delta G^0}{RT}\right] \quad (2.19)$$

Where  $\Delta G^0$  is the standard Gibbs free energy of formation, R is the universal gas constant and T is the temperature in Kelvin. Alternatively, if ideal gases are assumed, K can be expressed in terms of the normalized partial pressures of the  $N_2$  and N.

$$K \approx \frac{P_N^2}{P_{N_2}} \quad (2.20)$$

Combining equations 2.19 and 2.20,  $P_N$  can be written as,

$$P_N \approx P_{N_2}^{1/2} \exp\left[-\frac{\Delta G^0}{2RT}\right] \quad (2.21)$$

In their study, Angus *et al.* exposed a liquid pool of Ga, held in a crucible, to a nitrogen plasma, which was generated by an electron cyclotron resonance (ECR) microwave (MW) source, at a pressure of 0.5 mTorr and a temperature of 1000°C. As a result, the researchers obtained a GaN deposit onto the molten gallium pool; the deposit

was characterized for its polycrystallinity and small domain size ( $<10\mu\text{m}$ ).<sup>139</sup> In a subsequent study they were able to obtain oriented GaN films on sapphire substrates via direct nitridation of a Ga film formed onto the substrates' surface. However, these films presented a high density of dislocations similar to those observed in vapor phase epitaxy techniques.<sup>141</sup>

Table 2-7. Equilibrium pressures of N<sub>2</sub> over GaN and the N equivalent. Adapted from J.S. Dyck.<sup>140</sup>

Temperature (°C)	N <sub>2</sub> pressure (bar)	N Pressure (bar)
1640	20000	$3.40 \times 10^{-08}$
1440	7000	$6.00 \times 10^{-10}$
1100	100	$1.5 \times 10^{-14}$

Later, Sunkara *et al.* demonstrated a self-oriented growth concept in which GaN platelet crystals nucleated and joined together (similar to the self-assembly phenomenon) when grown directly out of Ga films supported on amorphous substrates in the presence of N<sub>2</sub> plasma at sub-atmospheric pressures.<sup>14-16</sup> The proposed concept, Figure 2.8a, states that different platelets tend to move toward each other and form chemically bonded junctions at the edges where the growth is faster. The movement of the platelets, produced by the force of these bonds, causes the platelets to align themselves with respect to each other, which facilitates in their conjoining, see Figure 2.8b. Because the growth rate of the m-planes (10-10) is an order of magnitude faster than that of the c-plane (0001), the platelets bond at their m-planes which in turn causes their c-plane to be parallel to the substrate's

surface.<sup>14</sup> X-ray diffraction (XRD) spectrums showed that the primary reflections were from the (0002) and (0004) planes of wurtzite GaN, indicating a preferred c-plane orientation, which is in agreement with the self-assembly concept.<sup>14-15</sup> The researchers claimed that the physical movement of the platelets is only possible because of a thin film of molten Ga between the platelets and the substrate, which prevents the pinning of the platelets to the substrate by epitaxy. A cross-sectional scanning electron microscope (SEM) image of one of their typical as-deposited GaN films, Figure 2.8c, shows the presence of the Ga film in between the substrate and the GaN film.

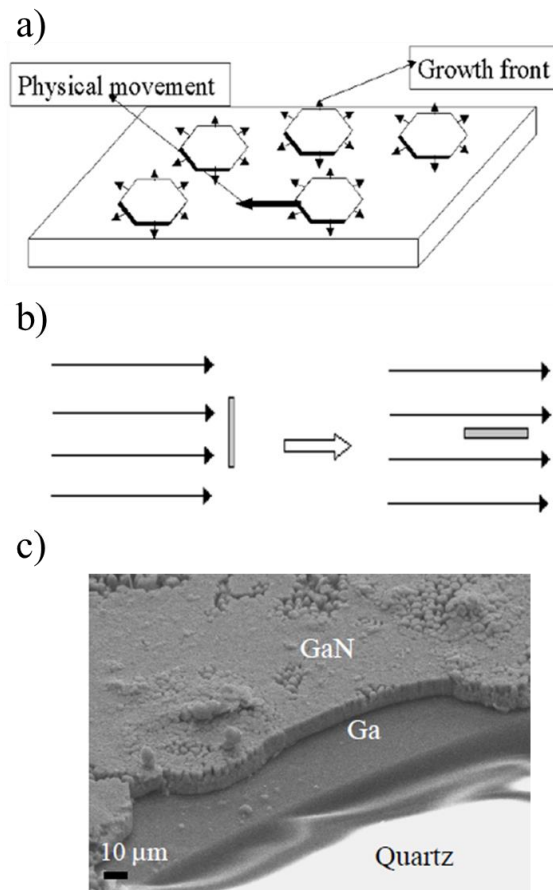


Figure 2.8. (a) Self-oriented growth of GaN. Adapted from Chandrasekaran et al<sup>14</sup>. (b) Self alignment of the platelets due to the movement. Adapted from Chandrasekaran et al<sup>14</sup>. (c) Cross-sectional SEM image of oriented GaN film. Adapted from Li et al.<sup>15</sup>

Novikov *et al.* identified that the plasma-assisted liquid phase epitaxy of GaN requires: (1) an efficient transport of N species from the surface of the Ga melt to the substrate, and (2) the prevention of the formation of polycrystalline GaN on the surface of Ga. The researchers proposed the use of a plasma-assisted electroepitaxy setup would fulfill these two conditions. By applying a DC current throughout the growth cell, the researchers were able to obtain the nitrogen concentration at the substrate-Ga interface required for GaN epitaxy. The researchers reported that the nucleation of GaN islands on sapphire (0001) and GaN-on-sapphire substrates at  $\sim 650$  °C and  $\sim 3 \times 10^{-5}$  torr. By increasing the growth time, those islands coalesced into a continuous layer.<sup>142-143</sup> It was found that the nucleation density of GaN on GaN-on-sapphire was higher than that of sapphire. The researchers hypothesized that this was a consequence of an improved wetting behavior of Ga on GaN compare to sapphire.<sup>143</sup> However, the results showed that the growth rate was very low and the uniformity was poor. After 60 hours of growth, it was possible to observe pin holes as big as  $10 \mu\text{m}$ .<sup>144</sup>

#### 2.4.4. Challenges

According to the information presented hereinbefore, two main challenges have been identified for the LP-LPE growth of GaN: (1) control of the wetting properties of the Ga melt and (2) prevention of the parasitic nucleation. In this section both challenges are discussed.

##### 2.4.4.1. Wetting properties

The formation of a film has been reported during the growth of GaN at low pressure via the ammonia and nitrogen plasma techniques. This phenomenon has caught the



attention of several scholars. Tanaka *et al.*, who grew epitaxial layers using ammonia as precursor, suggested that an adequate thickness of the film is required to obtain a nitrogen concentration in the melt that leads to epitaxial growth of GaN. If the film is too thin, the melt saturates, and parasitic nucleation occurs. Contrary, if the film is too thick the nitrogen concentration in the melt is not enough to grow GaN.<sup>138</sup> Similarly, Chandrasekaran *et al.* pointed the importance of having a Ga film on top of the substrate in order to obtain highly oriented GaN films via the plasma-assisted technique.<sup>14</sup> The formation of the film and its thickness depend on the wetting properties of Ga in its liquid state.

The wettability of a liquid resting on a solid and surrounded by a gas or vapor is determined by the interaction of the phases at the different interfaces i.e. solid-liquid (SL), liquid-gas (LG) and solid-gas (SG). These interactions create a surface energy,  $\gamma$ , characteristic of each interface. The total energy of the liquid-solid-gas system at equilibrium is minimized by moving the triple line, which is where the three interfaces meet, see Figure 2.9. A balance of forces at this line results in the Young's equation (equation 2.22).

$$\cos \theta = \frac{\gamma_{SG} - \gamma_{LS}}{\gamma_{LG}} \quad (2.22)$$

The contact angle,  $\theta$ , is used to determine the degree in which a liquid wets a solid surface. When the liquid molecules are strongly attracted to the solid molecules, the liquid spreads out completely and forms a thin liquid film. In this case, the contact angle corresponds to  $0^\circ$ . Conversely, when the liquid does not wet, the solid surface and a liquid sphere are formed, and the contact angle is  $180^\circ$ .

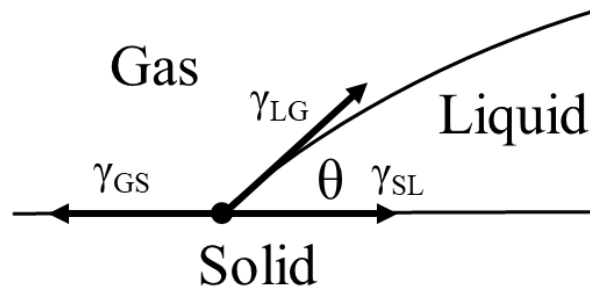


Figure 2.9. Interaction between liquid, solid, and gas in a liquid-solid-gas system.

In accordance to equation 2.22, the wettability of Ga depends on the interaction between Ga, the substrate, and the atmosphere used during experimentation. Furthermore, preliminary results indicate that the process temperature also affects how much Ga wets a certain substrate.<sup>14, 16</sup> Although different authors have reported the ability of Ga to wet different substrates, the reason why this happens is still unclear. Logan *et al.* described how, during their GaN growths via liquid phase epitaxy (LPE), Ga flows up the inside walls of the boat when it was exposed to a  $H_2/NH_3$  atmosphere at temperatures above  $850^\circ C$ . As an explanation for this phenomenon, the authors proposed that Ga spreads over an adjacent GaN film which is formed by Ga when Ga evaporated and reacted with  $NH_3$ .<sup>130</sup> If true, this would indicate that interfacial energy between Ga and GaN,  $\gamma_{Ga/GaN}$ , is very small.<sup>145</sup> T. J. Peshek, who also grew GaN by exposing Ga to  $NH_3$ , observed a similar phenomenon but held an alternative explanation. The author attributed the spreading phenomena to a decrease in the surface tension due to nitrogen saturation of the metal.<sup>146</sup> Ga has been also reported to wet different substrates when exposed to plasma. J. S. Dyck reported how molten Ga, which was saturated by nitrogen due to its exposure to nitrogen plasma, wet the walls of a boron nitride crucible at temperatures above  $900^\circ C$ .<sup>140</sup> H. Li studied the wetting properties of Ga on a quartz substrate. The results showed that Ga only

spread onto the surface of substrate when it was exposed to nitrogen plasma at high temperatures. The author suggested that the incorporation of nitrogen into the Ga melt induced the spreading behavior of the metal onto the quartz substrate.<sup>147</sup> In a similar manner, additions of other metals like, bismuth (Bi), tin (Sn), and indium (In) to Ga have been shown to reduce the surface tension of the alloy compared to that of pure Ga.<sup>148</sup> Moreover, Kleinbaum *et al.*, who obtained GaN films via plasma-assisted LPE, stated that the ability of Ga to wet a surface is increased by adding hydrogen to the nitrogen plasma. As explained by the authors, the use of hydrogen plasma in the process promotes the spreading of Ga by removing a native oxide layer that holds the liquid together.<sup>149</sup> This effect is well seen in Dickey's work where he used this native oxide "skin" for a variety of applications, which include: self-healing circuits, shape-reconfigurable conductors, stretchable antennas, wires, and interconnects and 3D printing.<sup>150</sup>

#### 2.4.4.2. Homogeneous nucleation

"Nucleation" refers to the initial step in the formation of a crystal from a solution, a liquid or a vapor. The process is described as the arrangement of a small number of ions, atoms, or molecules into a pattern characteristic of a crystalline solid, which creates a site upon which additional particles are deposited as the crystal grows.<sup>151</sup> There are two types of nucleation: heterogeneous and homogeneous. In heterogeneous nucleation, a surface of a different substance acts as the center upon which the first atoms, ions, or molecules of the crystal become properly oriented.<sup>151</sup> On the other hand, homogeneous nucleation refers to a process in which nuclei are randomly and spontaneously formed without the need of any nucleation site.<sup>152</sup> Homogeneous nucleation has been found to be harmful to LP-LPE of

GaN in three different ways. First, crystals that have been grown through homogeneous nucleation compete with the substrate (seed) used in this process as centers for epitaxial growth.<sup>116, 135-136</sup> Second, crystals can precipitate and deposit onto the substrate surface inducing defects in the LPE grown layers.<sup>137</sup> Lastly, homogeneous nucleation near the surface of the melt promotes the formation of a polycrystalline crust on top of the molten metal. This film acts as a diffusion barrier that prevents the incorporation of any gaseous species into the melt limiting further growth.<sup>14, 130</sup> Logan and Thurmond reported the formation of a polycrystalline GaN crust when a Ga melt was exposed to ammonia at temperatures below 950°C. They found that if the melt was agitated by mechanical vibration or placed on a temperature gradient the formation of the crust could be suppressed. In a similar way, the researchers pointed that carrying the experiment at higher temperatures also inhibited the formation of the crust. Furthermore, they reported that by adding Bi to the melt, the homogeneous nucleation was considerably reduced.<sup>130</sup> However, an explanation of this phenomenon was not provided.

Sun *et al.* and Hussy *et al.* determined the existence of an Ostwald-Miers region in relation to the partial pressure of ammonia and the process temperature for LP-LPE of GaN.<sup>135-136</sup> This region determines the conditions in which the growth of GaN occurs only on the seed (heterogeneous nucleation). When the partial pressure of ammonia in the system was higher than the ammonia partial pressure at the upper limit of the Ostwald-Miers region for a given process temperature, homogeneous nucleation was observed.<sup>135-</sup>  
<sup>136</sup>This behavior is similar to the one reported by Chandrasekaran *et al.* in regard to the synthesis of nanowires using low-melting point metals. The researchers found that the

growth of Ge nanowires from a Ga melt was only possible between the liquidus and the spinodal lines.<sup>153</sup> This behavior is depicted in Figure 2.10.

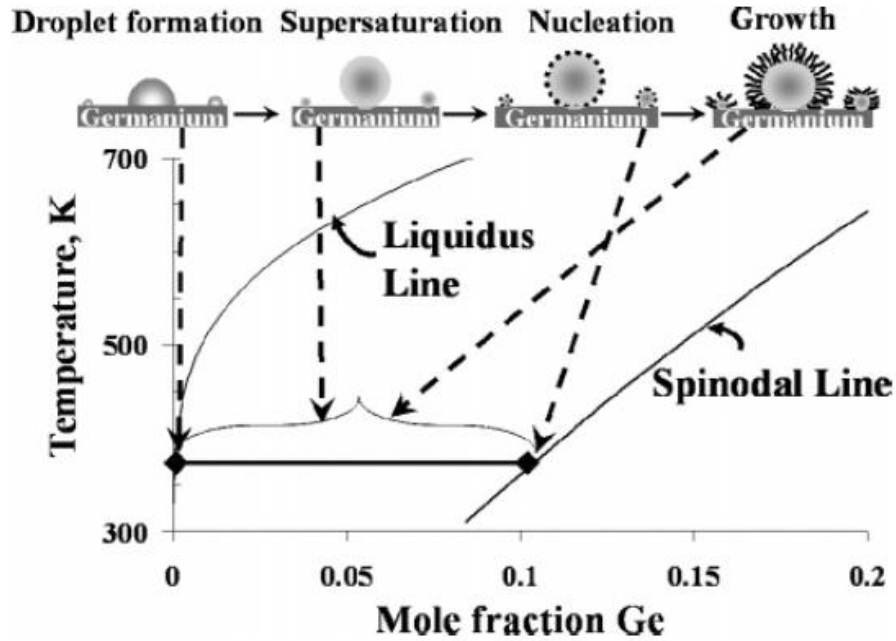


Figure 2.10 Synthesis of Ge nanowires from a Ga melt. The region between the liquidus and the spinodal line depicts the condition in which the growth of nanowires is promoted.

The liquidus line is defined as the locus of temperatures above which only the liquid phase is stable. Mathematically, the liquidus line can be obtained by solving equation 2.23.<sup>153</sup>

$$\left(\frac{\partial G_l}{\partial X_S}\right)_{T,P} = 0 \quad (2.23)$$

Where  $G_l$  is the Gibbs free energy of the liquid (mix) and  $X_S$  is the concentration of the solute in the mix. For a given temperature, the concentration that satisfies equation 2.23 corresponds to the equilibrium solubility of the solute.<sup>153</sup> Conversely, the spinodal line determines the conditions at which the solute nucleates. When a system crosses this line, the phases separate spontaneously without the need of any nucleation step. This process is

known as spinodal decomposition and in the case of a binary mixture can be described by the Cahn-Hilliard equation (equation 2.24 ).<sup>154-155</sup>

$$\frac{\partial C_B}{\partial t} = D\nabla^2 C_B - 2M\kappa\nabla^4 C_B = 0 \quad (2.24)$$

Where  $C_B$  is the composition of the of homogeneous material,  $D$  is the diffusion coefficient, and  $M$  and  $\kappa$  are a positive constant and a positive parameter, respectively. Due to the positive value of  $M$ , the sign of the diffusion coefficient (defined by equation 2.25) is determined by the sign of  $\partial^2 f / \partial C_B^2$ .<sup>154</sup>

$$D = M \left( \frac{\partial^2 f}{\partial C_B^2} \right) \quad (2.25)$$

Where  $f$  is the free energy of homogeneous material with composition  $C_B$ . When  $\partial^2 f / \partial C_B^2 > 0$  the solution is stable and the diffusion, if any, occurs from higher to lower concentration. Conversely, when  $\partial^2 f / \partial C_B^2 < 0$  the solution has crossed the spinodal line and is unstable. In this case, diffusion takes place from lower to higher concentration. However, the second term on the right-hand side of equation 2.24 is responsible for stabilizing the system against short distance scale fluctuations when  $D < 0$ . The latter means that spinodal decomposition only occurs when mass is moved over long distances i.e. large distance fluctuations.<sup>154</sup>

The region between the liquidus line and the spinodal line in the Ge-Ga system, depicted in Figure 2.10, is analogous to the Ostwald-Miers region in the ammonia-based LP-LPE growth of GaN via, Figure 2.7. In both cases, homogeneous nucleation can be prevented by operating far from the supersaturation limit of the system. The ability to suppress parasitic nucleation by modifying the experimental conditions represents an

advantage for any LP-LPE technique. However, in order to effectively control the parasitic nucleation, a proper understanding of the system is needed.

## CHAPTER 3

### EXPERIMENTAL METHODS

The experimental methods and characterization techniques employed for the completion of this work are presented in this chapter.

#### 3.1. Nitridation experiments

In this work, nitridation experiments refer to the process in which a material reacted with nitrogen radicals to form a nitride. Experiments were performed using two distinct systems. For purposes of this document the systems are referred as RF-plasma reactor and ECR plasma reactor. In this section an overview of the systems used during experimentation and a description of the procedure of a generic nitridation experiment is presented. Specific experiments are described as experimental details in Chapter 4, Chapter 5, and Chapter 6.

##### 3.1.1. RF-plasma reactor

The RF-plasma reactor is described as a custom-built, capacitively-coupled, radio-frequency (RF) plasma reactor. The piping and instrumentation diagram (P&ID) of the system is presented in Figure 3.1. The reaction chamber is a 30-mm-diameter quartz tube (90 cm in length) that is placed inside a tube furnace with temperature control. The maximum temperature of the furnace is 1100 °C. The system has 4 different gas connections with their respective mass flow controllers which allows to obtain different



gas mixtures. However, in most of the cases, during the nitridation experiments only  $N_2$  and  $H_2$  were used. The gases are fed at the front end of the tube and two-concave stainless-steel parallel plate plasma electrodes are positioned outside the tube between the gases' inlet and the tube furnace, immediately adjacent to the furnace. The working electrode is connected to a 600 W, 13.6 MHz, RF power generator (Seren R601) through an automatic matching network controller (Seren MC2). This configuration allows the control of the forward power and the reduction of the reflected power to zero during operation. The counter electrode is connected to a common ground. During operation, the glow discharge region of the plasma extends to approximate 45 cm into the tube furnace. Vacuum is achieved using a roughing pump (Edwards 18) with a maximum pumping speed of 12.1 cfm. The pressure inside the reaction chamber is measured downstream the tube using an absolute capacitance manometer with an accuracy of  $\pm 0.50\%$  at the pressures observed during this study. The base pressure of this system is in the order of  $10^{-3}$  torr.

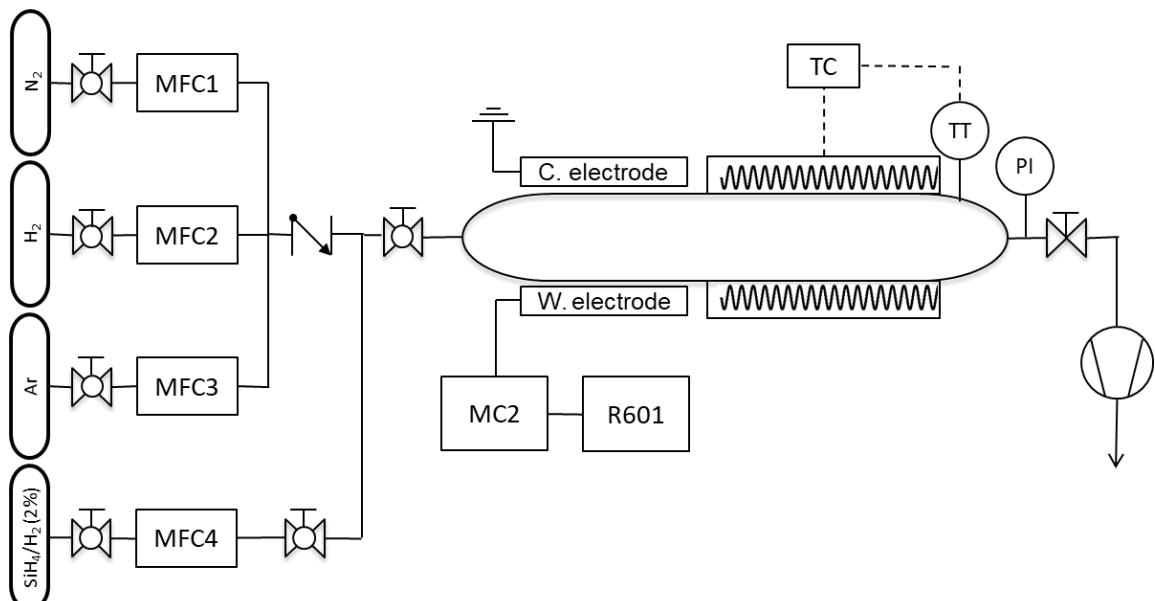


Figure 3.1 RF-plasma reactor P&ID.

### 3.1.2. ECR-plasma reactor

The ECR plasma reactor is a system that consists of a 15 in. long, 8 in. diameter, water-cooled, stainless-steel vacuum chamber equipped with an ASTeX AX4500 electron cyclotron resonance (ECR) plasma source. The chamber, which is aligned vertically, has six different flanges: two 8-in. conflat flanges (CF), one at each end of the cylinder, and four lateral 2.75-in. CF. The lateral flanges are located at the same height and are distributed evenly around the chamber. The plasma source, which has a standard NW160 flange, is connected to the top of the vacuum chamber using a NW/CF adapter. An 8-in to 2.75-in. water cooled CF reducer equipped with electrical feedthroughs is used to make the gas exhaust connections and to set up a rotatory, substrate heater. The substrate heater, which consists of a tungsten strip and a substrate susceptor, is positioned in such way that the substrate susceptor is aligned with the lateral flanges. Two viewports were installed in two of the lateral flanges. One of the viewports is used for monitoring the process while the other one is used exclusively to measure the substrate susceptor temperature. The temperature is measured using an infrared temperature sensor (Mikron M770/780). The temperature is controlled using an Omega PLATINUM Series PID controller that is connected to the temperature sensor and that sets the power that is sent through the tungsten strip. The system has 3 different gas connections with their respective mass flow controllers which allows to obtain different gas mixtures. The gases are fed at the top of the chamber through the gas inlet included in the ASTeX AX4500. Vacuum inside the chamber is achieved using a rotatory vane (Alcatel 2063) pump and a turbomolecular pump (Edwards 18) connected in series. The pumping speed of the rotatory vane and turbomolecular pumps

are 45 cfm and 40-50 l s<sup>-1</sup>, respectively. The pressure inside the chamber is measured with two different MKS Baratron capacitance manometers that are connected to the remaining two lateral flanges. One of the sensors is used to measure pressures in the 1-1000 torr range while the other one is used in the 1 x 10<sup>-3</sup>-1 torr range. Additionally, an ion gauge (SRS GW-100F) is connected downstream the chamber to measure the base pressure of the system. This gauge is not used during experimentation. The base pressure of the system is in the order of 10<sup>-6</sup> torr. The P&ID of the ECR plasma reactor is presented in Figure 3.2

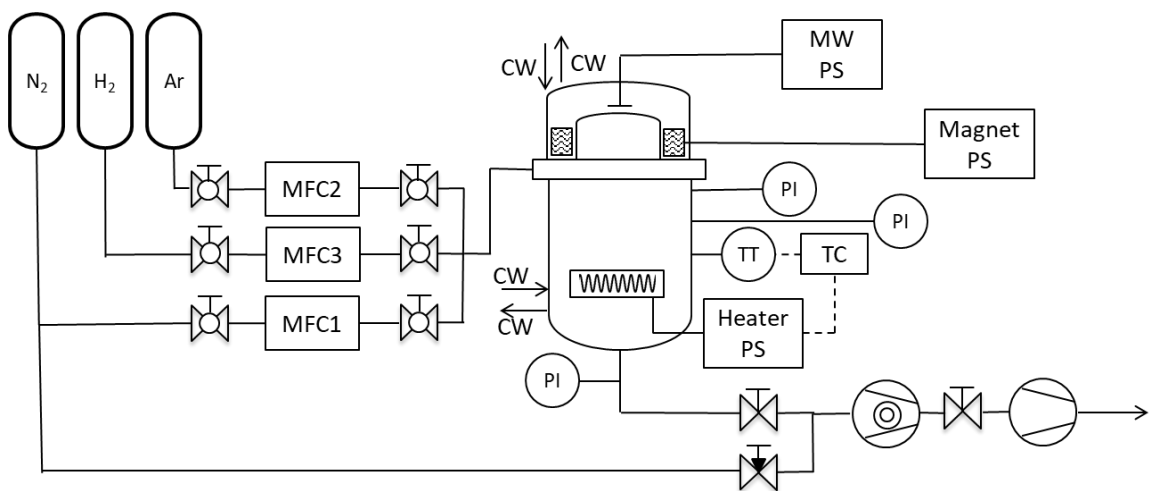


Figure 3.2 ECR-plasma reactor P&ID.

The ASTeX AX4500 ECR plasma source system is a high density, low pressure, low temperature plasma source used for a variety of plasma applications. The system consists of a water-cooled plasma source, a microwave power generator, a coaxial slug tuner, a coaxial cable, and a magnet power supply.<sup>156</sup> The configuration of the system is shown in Fig. 4.2.

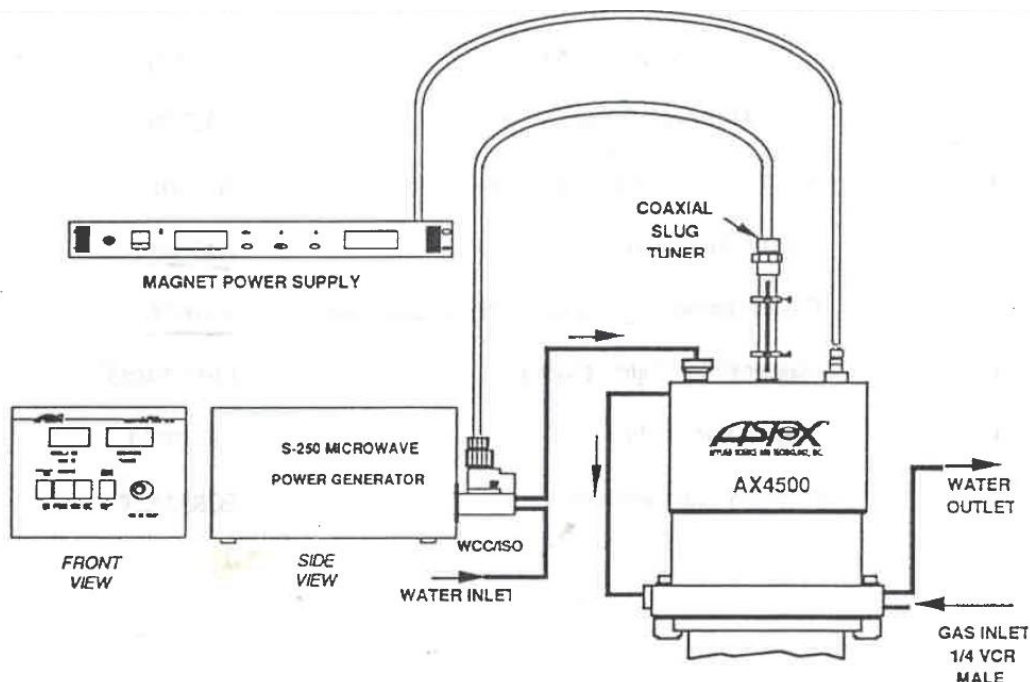


Figure 3.3 ASTeX AX4500 source configuration. Adapted from the operation manual of the ASTeX AX4500 ECR Plasma Source.<sup>156</sup>

### 3.1.3. Typical nitridation experiment

The experiment is started by cleaning the substrates that are going to be used in the experiment. The cleaning procedure consists of three steps. The substrates are sonicated first in acetone for 20-30 minutes and then in DI water for 5-10 minutes, and finally blown dried using dry air. Once the substrates are cleaned, Ga (99.99 % purity) is placed on top of the substrate either as a droplet or as a film. The substrates are then placed inside the chamber and the chamber is pumped down until it reaches the base pressure of the system. Subsequently, at least three purging cycles are performed. In a purging cycle, a valve downstream the reaction chamber is closed, and nitrogen gas is fed into the reactor causing the pressure inside the chamber to rise. Once the pressure has increased by at least two orders of magnitude, the valve is slowly opened, and the flow of nitrogen is stopped. When

the pressure in the system has reached its base pressure, the next purging cycle is initiated. After completion of the purging cycles, the temperature of the substrate holder is raised to 500-600 °C without flowing any gases. At that temperature the samples are exposed to hydrogen or hydrogen plasma for 5-10 minutes to reduce any gallium oxide layer that is present on the surface of the molten Ga. After the reduction period, the flow of hydrogen is stopped, and the temperature is raised to the desired experimental temperature. The samples are then exposed to nitrogen plasma. In the case of the RF plasma reactor the forward power used during experimentation is 100 W with a nitrogen flow of 100 sccm. On the other hand, in the ECR plasma reactor the microwave power is 260 W and the nitrogen flow is 3-20 sccm. Due to the lack of a pressure controller in both systems, the pressure inside the chamber is determined by the total gas flow. The pressure in a nitridation experiment ranges between 0.5 and 0.75 torr in the RF plasma reactor and between 5 and 30 mtorr in the ECR plasma reactor. After the desired plasma exposure time has been met the plasma is shut off and the cooling process is started.

### 3.2. Contact angle experiments

A contact angle experiment consists of six steps. First, a droplet of Ga or Ga alloy is placed onto a substrate. Second, the surface oxide layer on the Ga/Ga alloy is removed by using a solution of hydrochloric acid (HCl). Third, the substrate is placed on one of the contact angle experiment setups. Fourth, the experimental temperature is set. Fifth, a picture of the Ga/Ga alloy droplet is taken. Lastly, the image is analyzed using an image processing software and the contact angle value is obtained.

Two different setups were used. The first one, which is performed under ambient conditions, consists of a perfectly flat aluminum plate that is placed on a hot plate and a digital camera. The camera is placed next to the plate in such way that the lens of the camera is at the same height of the plate and perpendicular to the plate. The samples are placed on the plate and the temperature of the plate is raised to the experimental temperature. Temperature was measured using thermocouple type K. Due to the rapid formation of an oxide layer at high temperatures, the experiments performed using this setup did not exceed 300 °C. The second setup, which is performed under vacuum, consists of the ECR plasma reactor and a digital camera. The camera is positioned in front of one of the view ports in such way that it was aligned with the substrate susceptor. The samples are placed onto the substrate susceptor and the chamber is evacuated. Once the base pressure of the reactor has been reached, the temperature of the substrate susceptor is increased to the experimental temperature. The temperature sensor equipped in the ECR plasma reactor does not record temperatures below 500 °C thus this setup was used for experiments in which the experimental temperature exceeded 500 °C.

### 3.3. Characterization techniques

This section describes the characterization techniques utilized in this work.

#### 3.3.1. X-ray diffraction

X-ray diffraction (XRD) is a rapid, analytical, non-destructive technique that is used to study the structure, composition, and physical properties of crystalline materials. This technique is based on the scattering of X-ray photons by regularly spaced atoms in a crystalline material. A material is exposed to a monochromatic beam of X-rays and the

scattered X-rays are recorded using an X-ray detector. When constructive interference of the scattered monochromatic X-rays occurred, the detector records a peak in the intensity. Because constructive interference only occurs when the Bragg's law, equation 3.1, is satisfied, the lattice spacing of the material can be determined.<sup>157</sup>

$$n \lambda = 2 d \sin \theta \quad ( 3.1 )$$

Where  $n$  is an integer called the order of reflection,  $\lambda$  is the wavelength of the X-rays,  $d$  is the interplanar spacing, and  $\theta$  is the angle between the incident beam and the crystal plane. To identify the composition of a material, a diffraction pattern is recorded as a function of  $\theta$  and compared with standard line patterns available for various compounds in the Powder Diffraction File (PDF) database.<sup>157</sup>

In this study XRD was used to determine the chemical composition of the intermediate and final products in the nitridation experiments. This information was used to understand the different mechanisms of our proposed concepts. Additionally, this technique was used to obtain the crystalline quality and orientation of the films. All samples were characterized using a Bruker Discovery D8 XRD system equipped with Cu  $K\alpha$  radiation. Generally, the scans were performed between 10 and 90° utilizing a scan speed of 0.2-1 seconds per step with angle steps of 0.01°.

### 3.3.2. Scanning electron microscopy

The interaction between a high-energy electron beam and the atoms of a material leads to the generation of a variety of signals, i.e. Auger electrons, secondary electrons, backscatter electrons, X-rays, visible light, diffracted beam, transmitted beam, and inelastically scattered electrons, that can be used for characterization of a given material.

Scanning electron microscopy (SEM) is a type of electron microscopy that is used primarily to obtain topological images of surfaces in the millimeter and nanometer-scale. Imaging is accomplished by scanning a finely focused beam of electrons over an area of interest while a desired signal is collected. Among the different signals, secondary electrons and backscatter electrons are used for this purpose. Secondary electrons, which are low energy electrons, are usually limited to the beam impact area. As a result, the resolution of the images that are obtained using secondary electrons are in the order of the electron beam size. Backscatter electrons, which electrons that have been scattered out of the sample, provide a lower resolution than that of secondary electrons but allow to discriminate areas of a sample that is composed of different materials. The number of backscatter electrons increases with the atomic number of the material that is interacting with the electron beam, thus different materials generate different backscatter electron intensity. Energy dispersive spectroscopy (EDS) is used in conjunction with SEM to obtain the elemental composition of a sample. The X-rays that are emitted by the electron beam-sample interaction are characteristic of each electron transition of each element which allows to perform elemental mapping of the sample.<sup>158</sup>

In this work, surface morphology, layer thickness, uniformity, and qualitative chemical composition were routinely controlled using SEM. Two different system were used in this work: a FEI Nova NanoSEM 600 in secondary electron mode and a TESCAN VEGA3 also in secondary mode. The TESCAN VEGA3 is equipped with an EDS detector thus all EDS imaging and analysis was performed using the TESCAN VEGA3.



## CHAPTER 4

### FUNDAMENTAL PROPERTIES OF GA IN THE PRESENCE OF PLASMA<sup>1</sup>

#### 4.1. Introduction

As mentioned in section 2.4.4, proper wettability of the substrate by molten Ga and the prevention of homogeneous nucleation of GaN have both been identified as the main challenges for LP-LPE of GaN. Poor wetting is reflected in low substrate coverage and non-uniform nucleation of GaN on the surface of the substrate. On the other hand, spontaneous nucleation of GaN leads to the formation of crystals that compete with the substrate as centers for epitaxial growth, as well as creates defects in the LPE grown layers and promotes the formation of a GaN crust that prevents further incorporation of gaseous species into the melt. Homogeneous nucleation occurs due to a localized high concentration of nitrogen in the melt. Because of this, the prevention of spontaneous nucleation of GaN can only be achieved by controlling the concentration of nitrogen in the melt. Nitrogen concentration in the melt is determined primarily by the dissolution of nitrogen radicals into the metal. However, other processes also participate in what has been identified as a synergistic interaction between molten Ga and plasmas. Thus, in order to control the

---

<sup>1</sup> The texts in Section 4.3 were reproduced with the permission of AIP Publishing (Appendix I). Original article was published as “M.L Carreon<sup>§</sup>, D.F Jaramillo-Cabanzo<sup>§</sup>, I. Chaudhuri, M. Menon, and M. K. Sunkara (2018), Synergistic interactions of H<sub>2</sub> and N<sub>2</sub> with molten gallium in the presence of plasma, *Journal of Vacuum Science & Technology A* 36, 021303 (2018), <https://doi.org/10.1116/1.5004540> (<sup>§</sup>*Authors contributed equally to this work*)”.

concentration of nitrogen in the metal, the interaction between nitrogen plasma and molten Ga needs to be studied.

The synergistic effect of molten Ga in the presence of plasmas can be utilized in a variety of applications, other than the growth of GaN. For example, Si nanowires (NWs) have been grown in a tip-led fashion by dissolving Si radicals into molten Ga. For this type of process a non-wetting characteristic of Ga is needed; the process needs multiple nanometer-sized Ga droplets that can be used as individual seeds instead of a continuous film.

In this chapter a set of fundamental studies regarding the wetting properties of Ga and the interaction between nitrogen plasma and molten Ga is presented. These studies aim for: (1) understanding the influence of different variables on the wetting properties of Ga; and (2) gaining insights into the interaction between nitrogen plasma and molten Ga and how this interaction is related to the nitrogen concentration in the melt. The interaction between molten Ga and hydrogen plasma is also discussed herein. Additionally, an example in which Ga is used as catalyst to grow Si NWs on Cu foils is presented.

#### 4.2. Wetting properties

A set of contact angle experiments were performed to identify the influence of different variables in the wetting properties of Ga. Specifically, the influence of the surface that is in contact with the metal, the temperature, and additions of other elements were evaluated. The effect of the surface was assessed by using quartz and GaN-on-sapphire substrates. In the case of the temperature, this variable was evaluated by carrying the experiments at four different temperatures. The following temperatures were used during experimentation: 50, 250, 650, and 950 °C. Finally, the effect of additions of other metals

to the melt was assessed by alloying Ga with three different metals i.e., In, Sn, and Bi. As a result, four different materials were tested: pure Ga and three different alloys i.e.,  $\text{Ga}_{0.95}\text{In}_{0.05}$ ,  $\text{Ga}_{0.95}\text{Sn}_{0.05}$ , and  $\text{Ga}_{0.95}\text{Bi}_{0.05}$ . The experimental procedure of the contact angle experiments is explained in section 3.2. The results of the contact angle experiments are summarized in Table 4-1 and Table 4-2. The experiments performed in the ambient setup are presented in Table 4-1, while the ones that were performed in the vacuum setup are presented in Table 4-2. No data was collected for  $\text{Ga}_{0.95}\text{Bi}_{0.05}$  at 50 °C because at that temperature the alloy was a solid.<sup>159</sup>

Although, in most cases, the contact angle was lower when GaN was used as a substrate. There is no experimental evidence that supports that Ga and/or Ga alloys wet easier on GaN surfaces than on quartz surfaces. Furthermore, the contact angle values presented in Table 4-1 and Table 4-2 indicate bad wettability of Ga and Ga alloys. Except for three of the experiments, the contact angles were larger than 90°. These observations disagree with the hypothesis presented by Logan *et al.* in which they explain the spreading behavior of Ga by a small interfacial energy between Ga and GaN.<sup>130</sup> On the other hand, the temperature and the addition of other elements to the melt were found to have an effect in the wetting properties of the molten metal. In the case of temperature, it was found that as the temperature increased, the contact angle was reduced. Similar behavior was found when Ga was alloyed with other elements. The  $\text{Ga}_{0.95}\text{In}_{0.05}$  and  $\text{Ga}_{0.95}\text{Bi}_{0.05}$  alloys depicted lower contact angles than that of Ga and  $\text{Ga}_{0.95}\text{Sn}_{0.05}$  at the same experimental conditions. There was no significant difference between Ga and  $\text{Ga}_{0.95}\text{Sn}_{0.05}$  in terms of the resulting contact angle. These results can be explained by a change in the surface tension of the alloy. As the surface tension of the alloy decreases, the contact angle of the droplet also

decreases.<sup>160</sup> To support this hypothesis the surface tension of the different melts were calculated at the temperatures that the experiments were performed.

Table 4-1. Contact angle experiments results. Ambient setup.

Temperature	Melt	Substrate	Angle	
50	Ga	Quartz	120.3	
		GaN	120	
	Ga <sub>0.95</sub> In <sub>0.05</sub>	Quartz	117.5	
		GaN	115.3	
	Ga <sub>0.95</sub> Sn <sub>0.05</sub>	Quartz	122.2	
		GaN	123.7	
	Ga <sub>0.95</sub> Bi <sub>0.05</sub>	Quartz	-	
		GaN	-	
	300	Ga	Quartz	118
			GaN	110.7
Ga <sub>0.95</sub> In <sub>0.05</sub>		Quartz	110.7	
		GaN	104.6	
Ga <sub>0.95</sub> Sn <sub>0.05</sub>		Quartz	118.8	
		GaN	108.3	
Ga <sub>0.95</sub> Bi <sub>0.05</sub>		Quartz	87.6	
		GaN	55.2	

Table 4-2. Contact angle experiments results. Vacuum setup.

Temperature	Material	Substrate	Angle	
650	Ga	Quartz	117.1	
		GaN	122.5	
	Ga <sub>0.95</sub> In <sub>0.05</sub>	Quartz	109.7	
		GaN	108	
	Ga <sub>0.95</sub> Sn <sub>0.05</sub>	Quartz	115.9	
		GaN	116.7	
	Ga <sub>0.95</sub> Bi <sub>0.05</sub>	Quartz	110.4	
		GaN	93.1	
	950	Ga	Quartz	115.2
			GaN	121.7
		Ga <sub>0.95</sub> In <sub>0.05</sub>	Quartz	106.4
			GaN	104.5
Ga <sub>0.95</sub> Sn <sub>0.05</sub>		Quartz	104.1	
		GaN	110.4	
Ga <sub>0.95</sub> Bi <sub>0.05</sub>		Quartz	112.8	
		GaN	88.4	

Dogan *et al.* calculated the surface tension of the Ga-In and Ga-Sn alloys at different temperatures as a function of the In and Sn concentrations, respectively.<sup>148</sup> Assuming that the surface tension changes linearly with temperature, it was possible to create a relationship between the surface tension and the temperature at a given concentration. Similarly, Aqra *et al.* calculated the surface tension of different Ga-Bi alloys as a function of temperature.<sup>161</sup> Although the study did not report the surface tension of  $\text{Ga}_{0.95}\text{Bi}_{0.05}$ , this one was estimated by utilizing data that was provided in the study and some assumptions. Specifically, the surface density of  $\text{Ga}_{0.95}\text{Bi}_{0.05}$  was estimated by averaging the surface tensions of  $\text{Ga}_{0.96}\text{Bi}_{0.04}$  and  $\text{Ga}_{0.94}\text{Bi}_{0.06}$ . The surface tension of the different melts is presented in Table 4-3. As seen in this table, the surface tension in all melts decreases as the temperature increases which explains why the contact angle tended to get smaller as the temperature was increased. When other elements were added to Ga, it was found that Bi is the element that reduces the surface energy the most, which is in good agreement with the contact angle experiments. At the temperatures that the experiments were performed  $\text{Ga}_{0.95}\text{Sn}_{0.05}$  exhibits a lower surface tension than that of  $\text{Ga}_{0.95}\text{In}_{0.05}$ . This result is contradictory with the results obtained from the contact angle experiments in which at the same conditions  $\text{Ga}_{0.95}\text{In}_{0.05}$  exhibited a lower contact angle than  $\text{Ga}_{0.95}\text{Sn}_{0.05}$ . However, it was found that in the calculations presented by Dogan *et al.*<sup>148</sup> the surface tension of pure Ga (i.e., when the concentration of In or Sn is equal to zero) varied depending of the system. The surface tension of Ga in the Ga/In system was higher than the surface tension calculated in the Ga/Sn system. These values are also included in Table 4-3. A comparison between the surface tension of Ga and the surface tension of its alloy for each system shows that the absolute change in surface tension is higher when In is incorporated. This means

that under the same conditions it is expected that  $\text{Ga}_{0.95}\text{In}_{0.05}$  has lower surface tension than  $\text{Ga}_{0.95}\text{Sn}_{0.05}$ . Therefore, a smaller contact angle in the Ga-In alloy, in comparison to the Ga-In alloy, is expected. This behavior is in good agreement with the results presented in Table 4-1 and Table 4-2. In the same way the small difference between the contact angles that were obtained with pure Ga and  $\text{Ga}_{0.95}\text{Sn}_{0.05}$  can be explained by the small change in surface tension after Sn is added to the melt.

Table 4-3. Estimated surface tension of different Ga alloys at the temperatures that the contact angle experiments were performed.

Temperature (°C)	Surface tension (mN/m)				
	Ga/In		Ga/Sn		Ga/Bi
	Ga	$\text{Ga}_{0.95}\text{In}_{0.05}$	Ga	$\text{Ga}_{0.95}\text{Sn}_{0.05}$	$\text{Ga}_{0.95}\text{Bi}_{0.05}$
50	690.98	679.91	676.33	670.46	603.02
300	683.23	672.11	668.86	663.09	545.02
650	672.38	661.19	658.39	652.76	463.82
950	663.08	651.83	649.42	643.91	394.22

The influence of nitrogen and hydrogen plasmas in the wettability of Ga was also investigated. Due to constraints in the experimental setup it was not possible to perform a systematic study as done previously for the other variables. In the presence of hydrogen plasma, Ga agglomerates as a droplet and is maintained in this shape independently of the exposure time. The process in which Ga is exposed to hydrogen plasma is presented in Figure 4.1. A solid Ga film [Figure 4.1(a)] was heated to 350 °C which caused the

formation of a liquid Ga film [Figure 4.1(b)]. Liquid Ga maintained its shape as a film due to a native oxide layer that prevents the movement of the liquid.<sup>150</sup> Once the film is exposed to hydrogen plasma the  $\text{Ga}_2\text{O}_3$  layer started reduce causing the film to agglomerate [Figure 4.1 (c)]. After approximately 20 minutes of plasma exposure, the oxide layer is completely removed, and the film has been shaped into a big droplet [Figure 4.1 (d)]. Continuous exposure of up to 45 more minutes to hydrogen plasma did not modify the shape of the droplet.

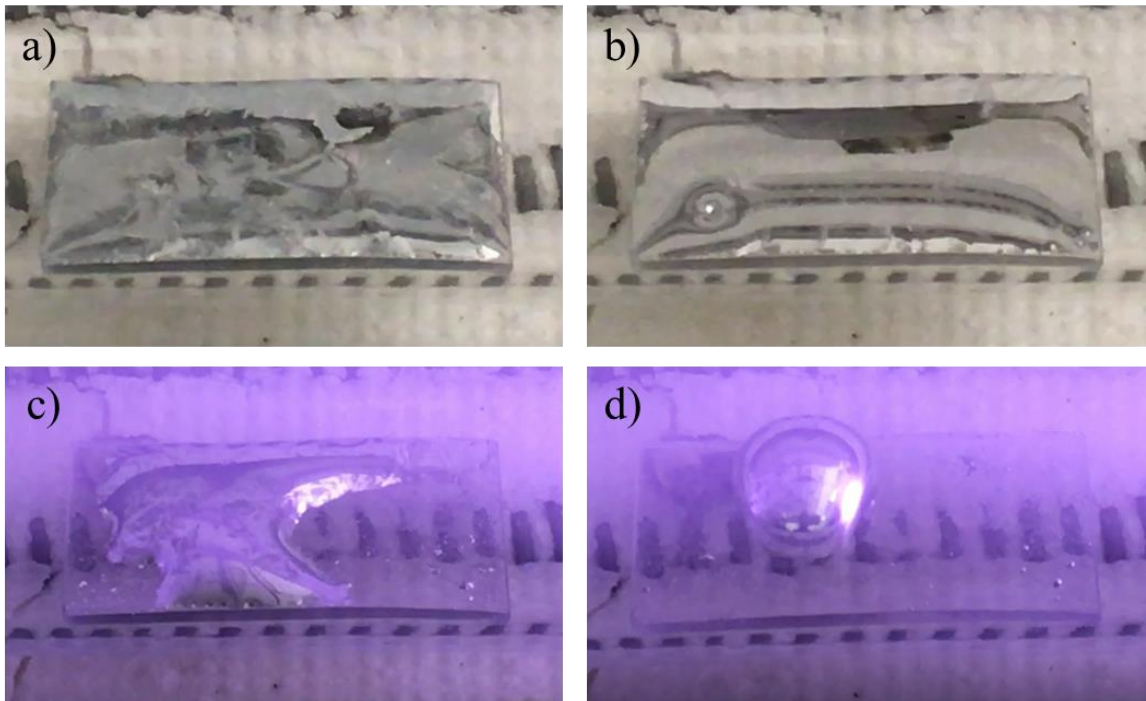


Figure 4.1 Process that explains the wetting behavior of Ga under hydrogen plasma. (a) A solid Ga film is transformed into a (b) liquid Ga film by increasing the temperature of the system. Hydrogen plasma exposure removes the oxide layer of the melt, which causes (c) agglomeration of the film. Finally, after the oxide layer has been completely removed a (d) Ga droplet is formed.



The effect of nitrogen plasma in the wetting properties of Ga was evaluated by exposing the Ga to nitrogen plasma at different temperatures. Before the nitrogen plasma exposure, the Ga<sub>2</sub>O<sub>3</sub> layer was removed either ex-situ utilizing HCl or in-situ by exposing the samples to hydrogen or hydrogen plasma. At low temperatures the metal agglomerated into a big droplet similarly to the hydrogen plasma case. However, when Ga was exposed to nitrogen plasma at high temperature i.e. over 800 °C, the behavior was found to be different. In this case, Ga agglomerated into a droplet initially and then as the droplet was exposed to nitrogen plasma, it started to spread. Continuous exposure to nitrogen plasma resulted in the formation of GaN on the surface of the droplet, which prevented the droplet from spreading any further. The spreading effect was not seen in any of the other contact angle experiments which suggests that the dissolution of nitrogen radicals into Ga is the most effective way to increase the wettability of Ga. This conclusion is in good agreement with previous studies.<sup>140, 146-147</sup> An example of a Ga droplet exposed to nitrogen is presented in Figure 4.2 (a). Proper wetting of Ga is the result of increasing Ga's wettability without promoting the formation of a GaN crust. The dissolution of nitrogen radicals into the melt increases the wettability of Ga but also the local nitrogen concentration. When the concentration of nitrogen in the melt is too high, spontaneous nucleation of GaN is promoted. However, as it is discussed in Chapter 5, it was found that by maintaining the concentration of nitrogen inside the melt below the spinodal concentration it was possible to wet different surfaces. A Ga droplet contained in a reservoir made of GaN-on-sapphire [Figure 4.2 (b)] was used in a pulse experiment, which is also explained in Chapter 5, as a way to control the concentration of nitrogen inside the melt. After the experiment was performed it was found that the metal wetted the walls of the reservoir even though these

were aligned vertically. Additionally, it was observed that Ga spread freely on GaN and sapphire surfaces. Details of the Ga/reservoir arrangement after the pulse experiment are shown in Figure 4.2 (c).

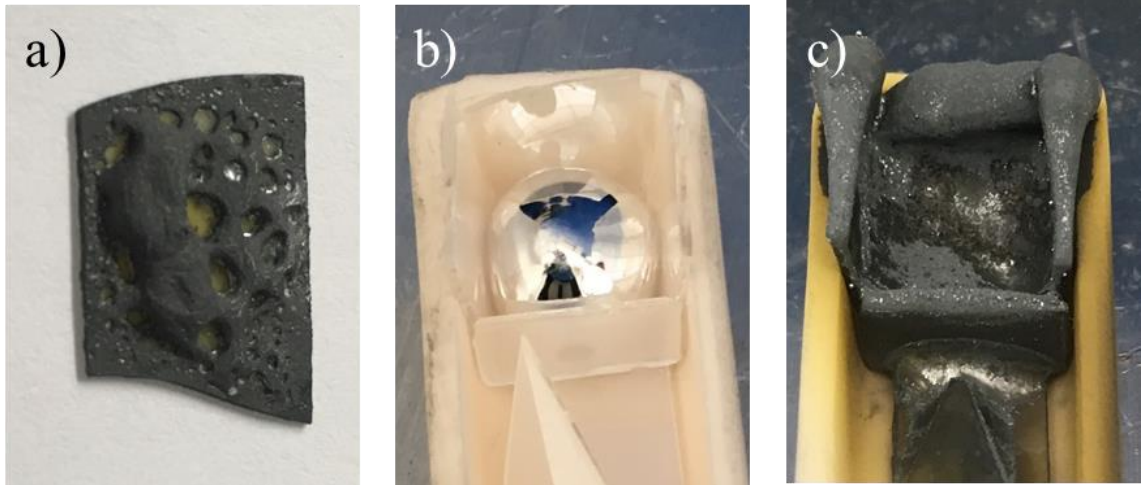


Figure 4.2 Ga film after being exposed to nitrogen plasma at 800 °C. (b) Ga droplet contained in a reservoir made of GaN-on-sapphire. (c) Same Ga/reservoir arrangement after pulse experiment.

#### 4.3. Interaction radicals into molten Ga

In order to control the concentration of nitrogen in Ga, it is necessary to understand first how nitrogen plasma and Ga interact. M. Carreon presented through absorption/desorption experiments that both nitrogen and hydrogen radicals produced from plasma dissolve into Ga. Additionally, the researcher calculated the number of moles absorbed of each type of radicals at different conditions. Results showed that (1) absorption of hydrogen and nitrogen radicals reduces with temperature, and (2) the absorption of species is higher at low power plasmas.<sup>162</sup> However no mechanism or explanation of how these plasmas and Ga interact was provided. Additionally, due to the nature of the reactor

that was used by the researcher during experimentation, i.e. the plasma discharge did not extend throughout the whole length of the reactor it is believed that their setup acted as a dynamic system where a constant recombination and generation of radicals take place. If the rate of diffusion of molecules is faster than the recombination of the radicals outside the plasma zone, one could expect a gradual increment in pressure, which could alter the absorption/desorption experiments results.

To understand the relationship between the concentration of nitrogen inside the metal, which is directly related to the moles that are absorbed, and the interaction between molten Ga and plasmas, a new set of adsorption/desorption experiments, in which Ga was exposed intermittently to nitrogen and hydrogen plasmas, was performed.<sup>163</sup> By limiting the exposure to plasma, it was possible to identify different processes that are happening and decrease the diffusion issues that arise from the experimental setup. The experiments were carried out in the RF-plasma reactor operated in a batch mode, Figure 4.3. Details of the RF-plasma reactor are provided in section 3.1.1. Ga-coated and uncoated capillaries were exposed intermittently, 10 minutes at the time, to nitrogen and hydrogen plasmas, Figure 4.4 and Figure 4.5, respectively. Similar results were obtained for both nitrogen and hydrogen. By limiting the plasma exposure to 10 minutes it was possible to identify the different phenomena that are taking place in the process. During the first 10 minutes of plasma exposure the uncoated and coated capillaries behaved differently but in good agreement with the results previously presented in M. Carreon's work.<sup>162</sup> The increment in pressure observed when the uncoated capillaries were exposed to plasma follows the same behavior as the first regime explained hereinbefore, suggesting that, by reducing the plasma exposure time, the diffusion effects are limited. The opposite behavior was observed when

coated capillaries were used, i.e., a rapid decrease in pressure followed by stabilization followed by an exponential decay in pressure. In the case of nitrogen, a slight increase before the exponential decay was perceived. Once the plasma was shut off the pressure decreased for both cases. Nonetheless, when gallium was used, the decrement rate was slower. In the case of hydrogen after approximately 5 minutes of shutting the plasma off, the pressure started to increase. The difference between both cases indicate that while the decrease in pressure of the system without gallium is a response exclusively of the almost instantaneous recombination of radicals, the system with gallium-coated capillaries present two different coexisting phenomena. The recombination of radicals due to the lack of plasma excitation and the desorption of species from the molten metal is suspected to be responsible for the overall number of species in that system. The samples were exposed to plasma for 10 minutes one more time. The results show a similar response in pressure in the gallium free configuration compared to the response obtained during the first plasma exposure, whereas the pressure in the other system decreases initially and then increases. The shape of the curve once the pressure increases is similar to the curve obtained in the system without gallium, suggesting that the metal got saturated, reducing considerably the amount of species that are being dissolved and acting like a non-catalytic material. Finally, the pressure after shutting the plasma off was monitored for an extra 10 minutes. The curves obtained in this period are in accordance with the ones obtained the first time the plasma was turned off.

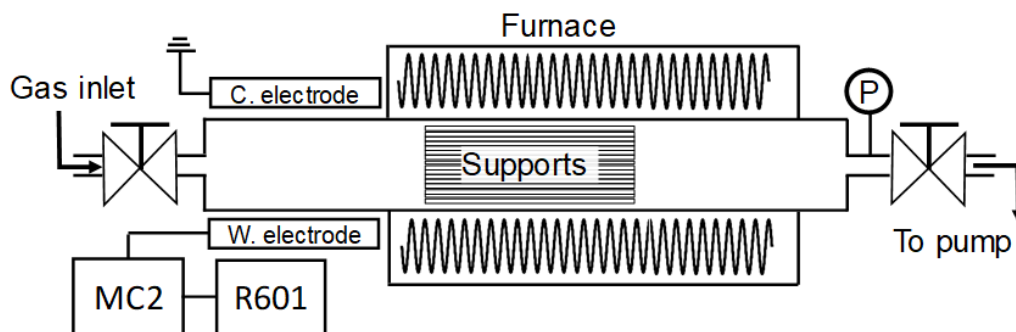


Figure 4.3 Schematic of the system used for the absorption/desorption experiments.

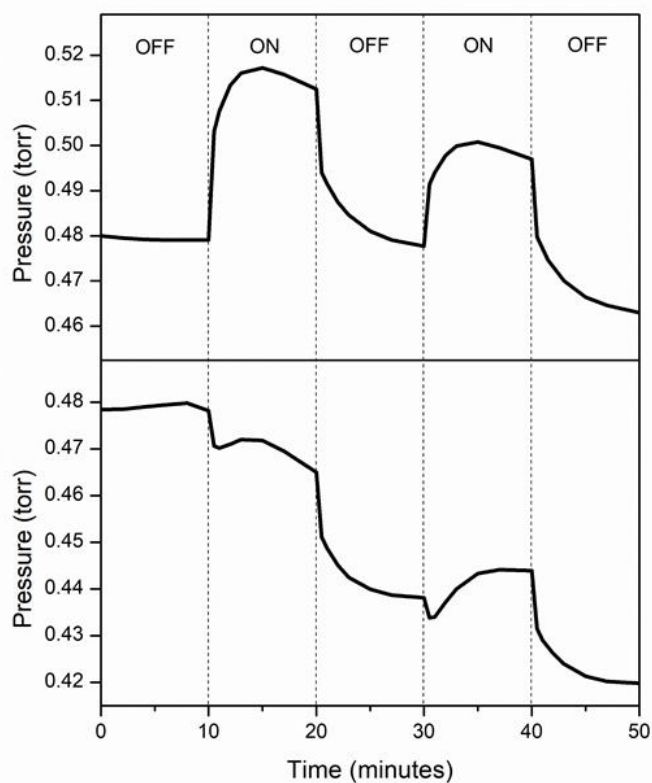


Figure 4.4. On/off experiments. Change in pressure when uncoated (top) and Ga-coated (bottom) supports are exposed intermittently to nitrogen plasma. Experiments were performed at 400 °C and a power of 100 W.

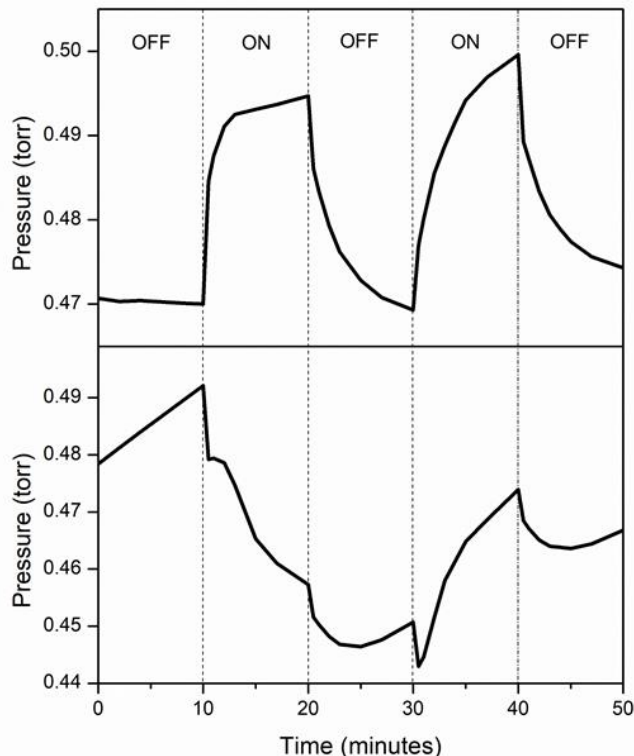


Figure 4.5. On/off experiments. Change in pressure when uncoated (top) and Ga-coated (bottom) supports are exposed intermittently to hydrogen plasma. Experiments were performed at 400 °C and a power of 100 W.

The overall interaction of molecular nitrogen with molten Ga is proposed to be as follows: (1) creation of atomic nitrogen species; (2) surface adsorption of nitrogen on molten gallium, i.e., formation of Ga-N species; (3) diffusion of N or Ga-N into the bulk; (4) recombination inside the gallium bulk; (5) surface recombination between atomic nitrogen in the gas phase and adsorbed species on the surface; and (6) desorption of molecular nitrogen. A graphical representation of the mechanism is presented in Figure 4.6. Nitrogen was chosen as an illustrative example; it is believed that the mechanism for the interaction of molecular hydrogen with molten gallium is the same.

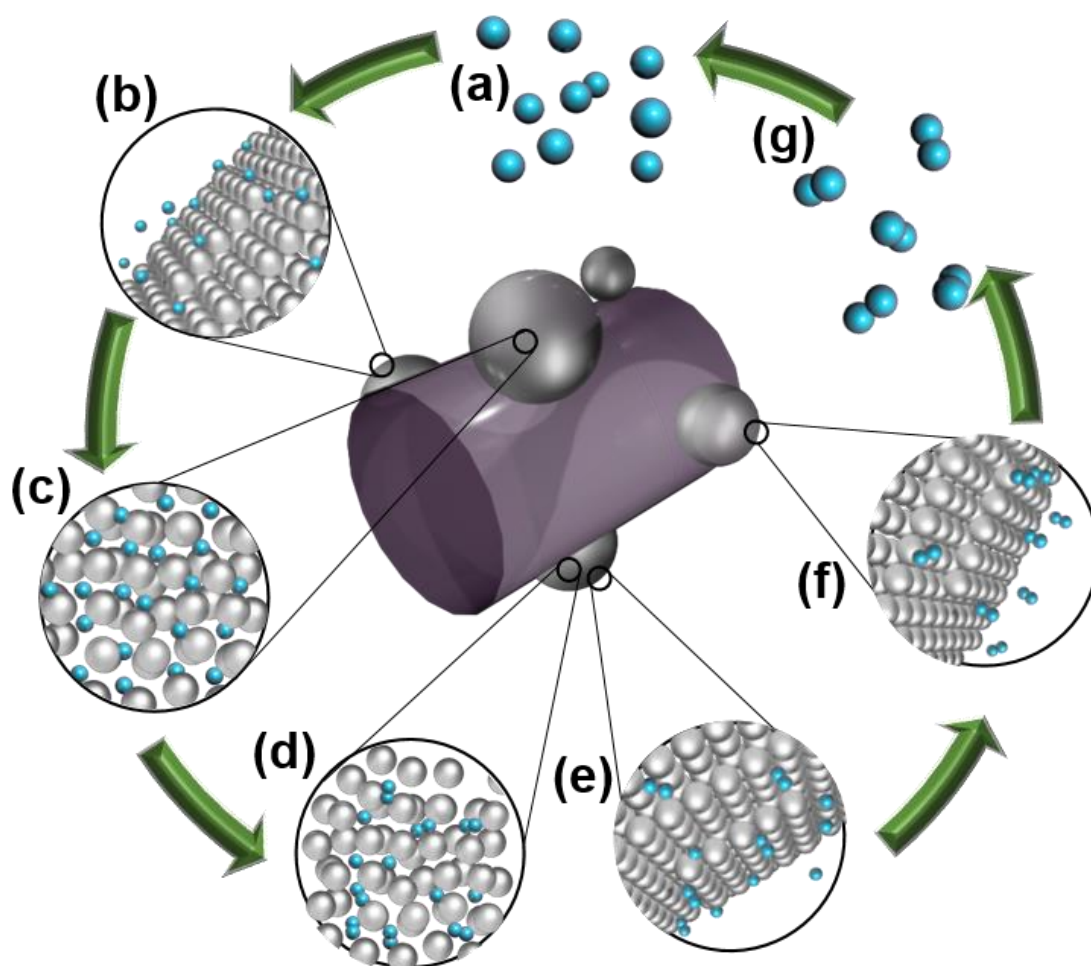


Figure 4.6. Proposed mechanism: (a) creation of atomic species, (b) surface adsorption, (c) diffusion into the bulk, (d) recombination inside the bulk, (e) surface recombination, (f) desorption of molecular species, and (g) molecular species in the gas phase.

Besides the diffusion and the desorption steps, all the steps can be represented by a chemical reaction. The enthalpy of reaction ( $\Delta H_{\text{rxn}}$ ) of a particular reaction can be estimated by subtracting the total energy of the bonds formed from the sum of the broken bonds' energy, Equation 4.1. This approximation becomes useful for determining the thermal behavior of a reaction; for example, when the bonds that are being broken are stronger than the ones that are being formed ( $\Delta H_{\text{rxn}} > 0$ ), the reaction will be endothermic. This expression

does not provide exact values for  $\Delta H_{rxn}$  because it uses average bond energies. The bond enthalpy of a chemical bond depends upon the molecular environment in which the bond exists. Therefore, the bond energy values reported in the literature are averaged. Table 4-4 presents the different reactions that take place in the gallium-nitrogen and gallium-hydrogen plasma systems with their respective  $\Delta H_{rxn}$ . In the case of hydrogen, it is important to notice that while the surface adsorption and the surface recombination processes are exothermic, the gas dissociation and the bulk recombination are endothermic. It is believed that the energy in the gas dissociation step is supplied principally by the RF generator, whereas the energy in the bulk recombination step is provided by the temperature of the system. Accordingly, while bulk recombination rates should increase with increasing temperatures, the production of radicals should remain unaffected, independent of temperatures, thus leading to a decrease in the quantity of moles absorbed. Even though the bulk recombination of nitrogen atoms is exothermic, this energy is smaller in magnitude than both the surface adsorption and the surface recombination, which explains why the bulk recombination is favored over the other reactions at higher temperatures. This statement is in good agreement with the experimental data presented by M. Carreon<sup>162</sup> i.e., the higher the temperature, the lower the number of molecules absorbed.

$$\Delta H_{rxn} \approx \sum (\text{broken bond energy}) - \sum (\text{formed bond energy}) \quad (4.1)$$



Table 4-4. Chemical reactions and their enthalpy of formation for the Ga - N<sub>2</sub> and Ga - H<sub>2</sub> plasma systems.

	Nitrogen		Hydrogen	
	Reaction	$\Delta H_{rxn}$ (kJ/mol)	Reaction	$\Delta H_{rxn}$ (kJ/mol)
Gas dissociation	$N_2 \rightarrow N + N$ ( 4.2 )	945 (Ref. <sup>164</sup> )	$H_2 \rightarrow H + H$ ( 4.3 )	436 (Ref. <sup>164</sup> )
Surface adsorption	$Ga + N \rightarrow Ga-N$ ( 4.4 )	-218 (Ref. <sup>165</sup> )	$Ga + H \rightarrow Ga-H$ ( 4.5 )	-262 (Ref. <sup>166</sup> )
Surface recombination	$Ga-N + N \rightarrow Ga + N_2$ ( 4.6 )	-727 <sup>a)</sup>	$Ga-H + H \rightarrow Ga + H_2$ ( 4.7 )	-174 <sup>a)</sup>
Bulk recombination	$Ga-N + Ga-N \rightarrow 2Ga + N_2$ ( 4.8 )	-509 <sup>a)</sup>	$Ga-H + Ga-H \rightarrow 2Ga + H_2$ ( 4.9 )	88 <sup>a)</sup>

<sup>a)</sup>Enthalpies calculated using Equation 4.1 and reported bonds energies (Equations. 4.2-4.5).

Nitrogen and hydrogen atoms recombine differently on dissimilar surfaces. Rahman and Linnett studied the recombination of nitrogen on pyrex and different metals. In the case of Pyrex surfaces, they found that the recombination of nitrogen is first order at pressures  $\sim 0.1$  Torr; a second order process is noticeable at higher pressures (i.e. 0.9 Torr). Because of this observation, the authors proposed that both Hinshelwood and Rideal mechanisms occur on a varying sticking coefficient surface. In their study, the recombination coefficient,  $\gamma$ , which is defined as the fraction of atoms striking the surface which recombine, was reported in the order of  $10^{-6}$ .<sup>167</sup> In another study, Rahman and Linnett presented  $\gamma_N$  for different metals:  $2 \times 10^{-3}$ ,  $6.7 \times 10^{-5}$ , and  $6.8 \times 10^{-2}$  for Fe, Ni, and Cu, respectively.<sup>168</sup> Argoitia *et al.* exposed molten gallium to nitrogen plasma at low pressure. They found that the surface recombination is slow enough that nitrogen atoms diffuse into the bulk and form GaN crystals.<sup>139</sup>

In the case of hydrogen radical recombination on surfaces, Wood and Wise reported that the formation of a hydrogen molecule from two hydrogen atoms on Pyrex glass and fused quartz surfaces occurs through two varying mechanisms: Rideal (R) and Hinshelwood (Hi) with two binding states: strongly bound (a) and weakly bound (b). They concluded that the overall recombination of hydrogen is composed of four different regimes: Rideal-strongly bound (R-a), Rideal-weakly bound (R-b), Hinshelwood-strongly bound (Hi-a), and Hinshelwood-weakly bound (Hi-b). Depending on the temperature, one of these terms becomes dominant. Specifically, Hi-a, Hi-a, Hi-b and R-b are the predominant regimes for temperatures  $>500$ , 500-120, 120-50 and  $<50$  K, respectively. Additionally, Wood and Wise reported a recombination coefficient in the order of  $10^{-3}$ , as well as recombination rates of  $\sim 10^{17}$  and  $\sim 10^{15}$  atoms/cm<sup>2</sup>s at 500 and 77 K, respectively.<sup>169</sup>

The recombination of hydrogen onto diamond has also been reported. Gat and Angus found that for this system,  $1 > \gamma > 0.23$  with a recombination rate of  $\sim 10^{19}$  atoms/cm<sup>2</sup>s. The authors suggested that due to this high recombination rate and the exothermic behavior of the reaction, much of the energy that reaches the surface during diamond deposition is transported by atomic hydrogen.<sup>170</sup> In the case of metals, recombination of hydrogen atoms is strongly dependent on the metal surface where atoms recombine. Melin and Madix reported the hydrogen recombination coefficient on Ag (0.05), Au (0.03), Co (0.13), Cu (0.09), Fe (0.1), Ni (0.1), Pt (0.06), and W (0.08).<sup>171</sup>

#### 4.4. Growth of Si NWs on Cu foils

To increase the capacity of carbon-based anodes in lithium ion batteries, other group IV elements have been investigated to replace carbon as the anode material. Among these, silicon has gained significant attention from scientists from all over the world mainly due to its high specific capacity. At room temperature each Si atom can alloy with up to 3.75 Li atoms which is reflected in a theoretical specific capacity of 3579 mAh/g. Unfortunately, this materials presents a substantial volumetric change during cycling of up to 310%.<sup>172</sup> This causes, in most cases, the pulverization of the material and the subsequent fade in the battery's overall capacity. To overcome this issue, researchers have decided to use nanostructured materials that can buffer the change in volume. Thin films,<sup>173</sup> nano-sized porous materials,<sup>174</sup> nanoparticles,<sup>175-177</sup> nanowires<sup>178-179</sup> and nanotubes<sup>180</sup> have been tested, showing a significant improvement when compared to bulk material. Out of these morphologies 1D nanostructures have shown to be advantageous over the other type of morphologies due to their facile strain relaxation, enhancement in the power rate, efficient

1-D electron transport, and when grown directly onto the substrate, a good contact with the current collector. Nevertheless, the volumetric expansion is not the only problem that these two materials must address in order to break into the market.

The use of 1D Si anodes in commercial applications is promising but the reduction of the dead weight needs to be resolved for this technology to succeed. Freestanding 1D materials are generally mixed with conductive carbon and some binder into a slurry and coated onto a thin copper film. The overall specific capacity of the anode is determined by the contributions of all the materials that comprise anode. Equation 4.10 is used to estimate the overall specific capacity of the anode in terms of the specific capacity ( $C_i$ ) and mass ( $W_i$ ) of all materials that conform the anode. As seen in Equation 4.10, the overall specific capacity of the anode is calculated by adding the specific capacities of all materials used in the anode. Thus, by adding materials with a lower specific capacity like carbon and/or inactive materials, like a binder or the metal current collector, to the freestanding 1D Si material, the overall specific capacity of the anode is reduced. In the case of arrays, no carbon black or binder is needed. Nevertheless, 1D Si arrays have been mostly grown on thick stainless-steel substrates, which substantially increases the weight of the anode when compared to the thin copper films used in commercial Li-ion batteries. Some studies have shown 1D Si arrays on other substrates like Ti<sup>181</sup>, Si<sup>182</sup> and Cu.<sup>183-184</sup> In both cases where copper was used as the substrate, the 1D Si structures were made with the same top down approach. Bundle type nanorods were prepared by etching a previously deposited Si film (~2 $\mu$ m) using the metal-assisted chemical etching technique (MACET).<sup>78,184</sup> The problem with this approach is that in order to prevent the oxidation of the Cu foil by the etching solution and the consequent detachment of the Si array from the substrate, a thin Si film is

used at the interface between the substrate and the array.<sup>183</sup> The underlayer film can cause loss of capacity due to delamination of the array during cycling.<sup>185</sup> In fact, the Si nanorods on Cu foil exhibit a poor reversible capacity retention of 46.0% after 100 cycles.<sup>184</sup> No bottom up method has been reported for growth of Si NWs or Si NTs on copper foils. Memarzadeh et al. pointed that the growth of Si NWs on Cu foil is not possible due to the high reactivity of Au, which is the most widely used catalyst for the growth of Si NWs, with Cu and the high reactivity of the SiH<sub>4</sub> with Cu to form copper silicides.<sup>186</sup> Utilizing other catalysts has seen as way to overcome these issues. For example, Ga has been proposed as a catalyst to grow Si NWs. Carreon *et al.* grew Si NWs on Si, quartz and stainless-steel (SS) substrates at temperatures as low as 200°C by utilizing Ga in the presence of a SiH<sub>4</sub>/H<sub>2</sub> (2%) plasma.<sup>162, 187</sup> The potential for using silicon nanowires as a replacement of carbon as anode material in Li-ion batteries is indeed promising, but more efforts are needed to overcome current challenges and limitations. Specifically, it is important to develop a new method for the large-scale growth of highly packed SiNWs on thin Cu substrates.

$$\text{overall specific capacity} = \frac{\text{total capacity}}{\text{total weight}} = \frac{\sum C_i W_i}{\sum W_i} \quad (4.10)$$

In this work, we present our more recent results regarding the production of Si NWs on Cu foils. Si NWs were grown in the RF plasma reactor using SiH<sub>4</sub>/H<sub>2</sub> mixture plasma. Cu foil (0.025 mm thick) was cut into circles with a diameter of 15.5 mm which could be

use directly in CR2032 coin-type cells. A solution of Ga<sub>2</sub>O<sub>3</sub> particles (<10 μm) was drop-casted on the Cu substrates. The substrates were introduced to the reactor and then exposed to hydrogen plasma for 30-60 min at 350-400 °C. This step is performed to obtain individual, uniformly distributed Ga droplets on the surface of the Cu substrate that can act as catalyst for the growth of Si NWs. It is important to mention that due to the wetting characteristics of Ga in the presence of H<sub>2</sub> plasma, the Ga droplets maintained their shape throughout the length of the process. Once the reduction step had concluded, the temperature of the reactor was changed to the growth temperature (i.e. 400 °C) and then the substrates were exposed to SiH<sub>4</sub>/H<sub>2</sub> mixture plasma for 60-180 min. Initial results showed that no wires were grown, instead a copper silicide layer was formed. To prevent the formation of the silicide layer, a diffusion layer was used. This approach was already reported by Memarzadeh *et al.* who minimized the formation of a silicide on their SS substrates by coating them with a TiN layer.<sup>186</sup> Different materials were utilized as diffusion blocking layer. Specifically, amorphous carbon, copper oxide, titania (TiO<sub>2</sub>) and alumina (Al<sub>2</sub>O<sub>3</sub>) were tested as diffusion blocking layers. Results showed that after the exposure to SiH<sub>4</sub>/H<sub>2</sub> plasma, the carbon and copper oxide-coated substrates exhibited the formation of a metal silicide all over the surface. In the case of the TiO<sub>2</sub>-coated (20 nm) substrates it was found that the surface was covered by patches of Si NWs and metal silicide. Finally, densely packed Si NWs (d~100 nm) were grown uniformly all over the surface of the alumina-coated (20 nm) substrates, Figure 4.7.

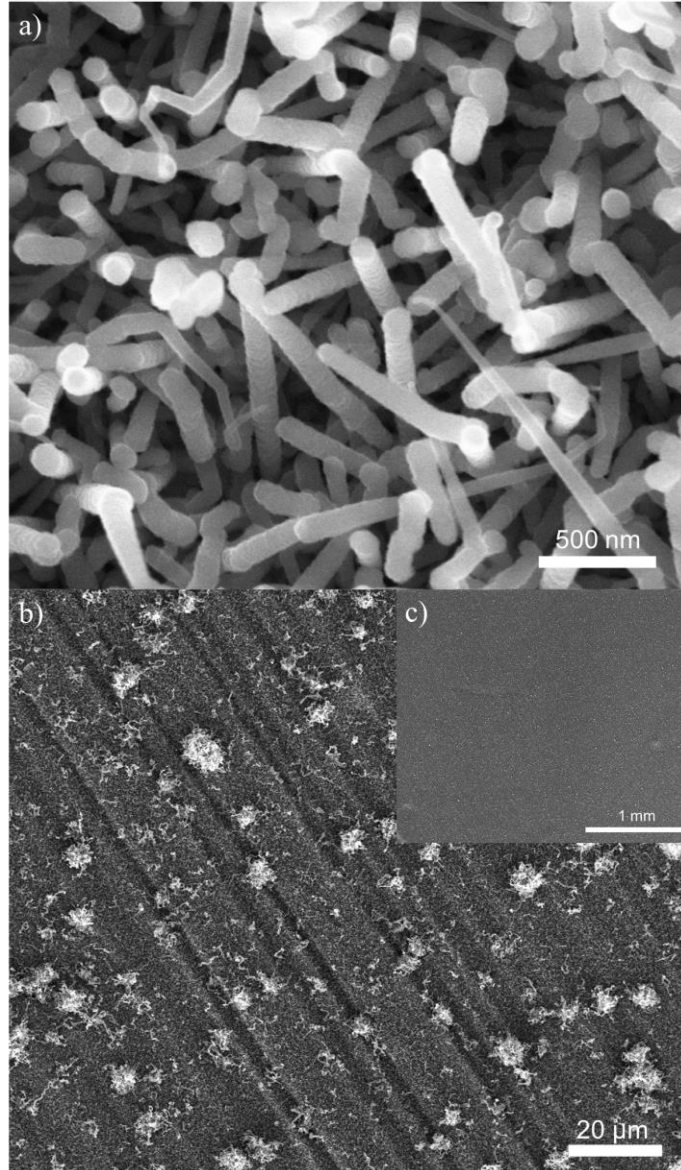


Figure 4.7 Growth of Si NWs on  $\text{Al}_2\text{O}_3$ -coated Cu substrates. Densely packed (a) Si NWs ( $d \sim 100$  nm) were grown (b) uniformly all over the surface of the alumina-coated substrates. (c) Formation of silicides was not observed.

The difference in the results obtained from the different coating materials is explained by the way these materials interact with hydrogen.  $\text{Sp}^2$ -bonded carbon is easily etched away when is exposed to hydrogen plasma.<sup>188</sup> Thus it is expected that during the

process that the carbon layer is removed allowing the reaction between Cu and Si to occur. Similarly, hydrogen plasma can reduce metal oxides into metals which can limit the efficiency of the film as a diffusion blocking layer. The degree in which a metal oxide is reduced depends on its stability; the more stable the metal oxide is the harder it is to be reduced. The Ellingham diagram is a plot used to determine the ease of reduction of different metal oxides. From the Ellingham diagram reported by S.M Howard<sup>189</sup> it was found that the reduction of copper oxide is significantly easier than that of TiO<sub>2</sub> or Al<sub>2</sub>O<sub>3</sub>. Furthermore, Al<sub>2</sub>O<sub>3</sub> is a more stable oxide compared to TiO<sub>2</sub> and copper oxide. Among the different oxides utilized as diffusion blocking layers, Al<sub>2</sub>O<sub>3</sub> is the most difficult to reduce. Additional experiments using Al-coated Cu substrates were performed. The results showed the formation of a continuous silicide layer on the surface of the substrate which indicates that Al does not perform adequately as a diffusion blocking layer. This result suggests that when Al<sub>2</sub>O<sub>3</sub> was used as diffusion blocking layer it was not completely reduced to Al. To test the hypothesis that the oxide blocking layers are reduced to metals during the process, a new set of experiments, in which the thickness of the Al<sub>2</sub>O<sub>3</sub> coating was varied, was performed. Specifically, Si NWs were attempted to grow on Cu substrates coated with a 5, 10, 15, 20, and 30 nm-thick Al<sub>2</sub>O<sub>3</sub> layer. Results showed that the outcome depended on the thickness of the diffusion blocking layer. The substrates with 5 and 10 nm-thick Al<sub>2</sub>O<sub>3</sub> layers only exhibited a copper silicide layer on their surface. When the thickness of the layer was 15 nm both Si NWs and metal silicide were found on the surface of the substrate. Finally, when the thickness of the Al<sub>2</sub>O<sub>3</sub> layer was 20 nm or larger, only densely packed Si NWs were found. The results suggest that during the process, at least 15 nm of the Al<sub>2</sub>O<sub>3</sub>



layer are reduced into Al. By having a layer thicker than that value is possible to guarantee that a  $\text{Al}_2\text{O}_3$  layer is still left to prevent the reaction between Cu and Si.

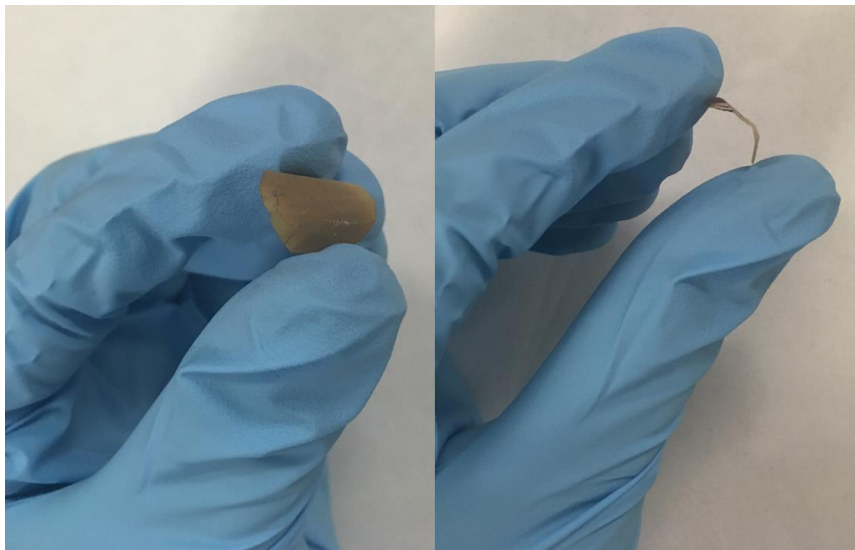


Figure 4.8 Flexible anode for Li-ion batteries. Anode is composed Si NWs arrays grown on  $\text{Al}_2\text{O}_3$ -coated Cu.

The Si NWs arrays on  $\text{Al}_2\text{O}_3$ -coated Cu, which exhibited flexibility as seen in Figure 4.8, were tested as anode material for Li-ion batteries. Charge/discharge measurements were performed using CR2032 coin-type cells assembled in a dry argon-filled glove box. The test cell consisted of the Si NWs arrays on  $\text{Al}_2\text{O}_3$ -coated Cu as the working anode electrode and lithium metal as the counter electrode. The measurements were performed at a current density of  $100 \text{ mA g}^{-1}$  in the potential range between 0.05 and 2.20 V. The results are shown in Figure 4.9 Charge/discharge cycle performance of Si NWs arrays grown on  $\text{Al}_2\text{O}_3$ -coated Cu as anode material in Li-ion batteries.. The anode exhibited a high initial reversible specific capacity of  $3083 \text{ mAhg}^{-1}$ . This value is over eight times higher than the theoretical specific capacity of carbon. The specific reversible

capacity of the anode after 13 cycles was  $2988 \text{ mAhg}^{-1}$  which is reflected in a capacity retention of 96.9 %. The high capacity retention can be a consequence of the small number of cycles that the anode was tested. Assuming that the capacity loss per cycle ( $7.30 \text{ mAhg}^{-1}$ ) is constant, the capacity of the anode after 100 cycles would be  $2345 \text{ mAhg}^{-1}$ , which is still very competitive compared to current technologies. On the other hand, it was found that the Coulombic efficiency was constant at  $\sim 74\%$ . In 1D Si-based anodes, the anodes are expected to have low efficiency in the first cycle due to irreversible secondary reactions like the SEI formation. Additionally, it is also expected that, once these reactions have taken place, the Coulombic efficiency increases to over 95%. The fact that the Coulombic efficiency of the tested anode did not improve within 13 cycles indicates the presence of secondary reactions. However, due to the low capacity loss per cycle it is believed that these reactions do not involve the Si NWs, as it could be continuous SEI formation due to SEI cracking or delamination. Although the low Coulombic efficiency is not well understood, and further studies are needed to understand this behavior properly, the results presented in this work are a immense step towards obtaining Si NWs arrays on thin Cu foils in a large-scale.

The eutectic temperature between Au and Si occurs at  $363 \text{ }^\circ\text{C}$  which limits the use of gold as catalyst for growth of Si NWs at lower temperatures. Conversely, Si NWs can be obtained at temperatures below the Si-Au eutectic temperature when Ga is used as catalyst. A set of experiments in which Si NWs were grown on Si substrates at  $200\text{-}350 \text{ }^\circ\text{C}$  were performed. The results showed that at  $200$  and  $250 \text{ }^\circ\text{C}$  the reduction of gallium oxide particles did not occur, thus in those cases, the reduction step was performed at  $400 \text{ }^\circ\text{C}$ . When the process was performed at  $200 \text{ }^\circ\text{C}$ , Si NWs were only observed coming out of big

(larger than 500 nm) Ga particles. A similar behavior was observed when the process was performed at 250 °C. At 300 °C, two different regimes were identified. At the center of the substrate, the growth of NWs was observed only around big Ga particles. On the other hand, at the edges of the substrate the growth was dense and uniform. Finally, when the process temperature was 350 °C the resultant growth of Si NWs was identified as uniform and dense. This type of growth is very similar to the one previously obtained at 400 °C. Results are shown in Figure 4.10 Growth of Si NWs on Si substrates at (a) 200, (b) 250, (c) 300, and (d) 350 °C. Figure 5.14.

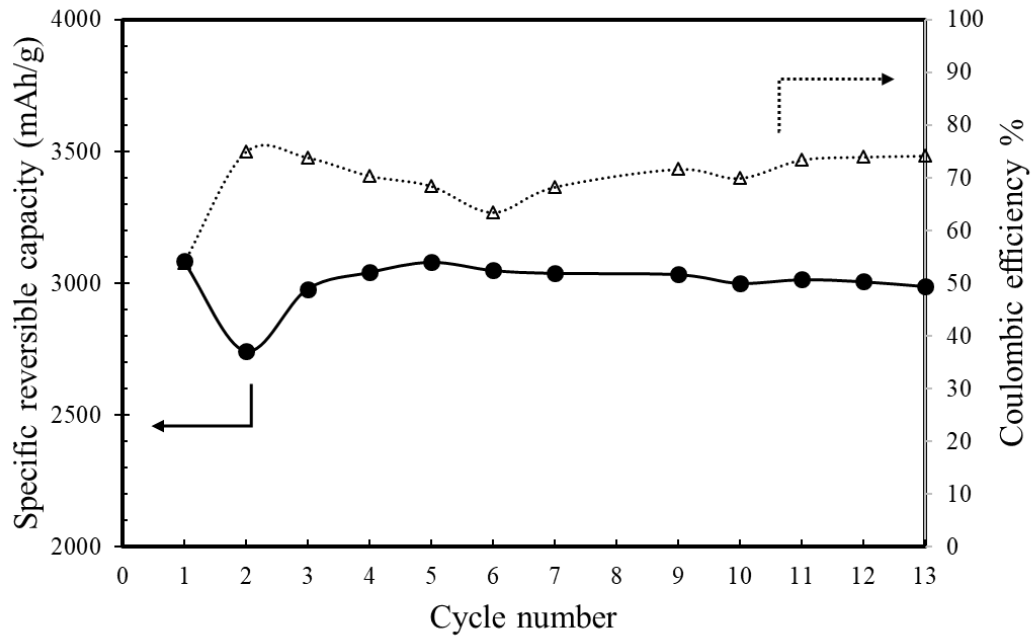


Figure 4.9 Charge/discharge cycle performance of Si NWs arrays grown on Al<sub>2</sub>O<sub>3</sub>-coated Cu as anode material in Li-ion batteries.

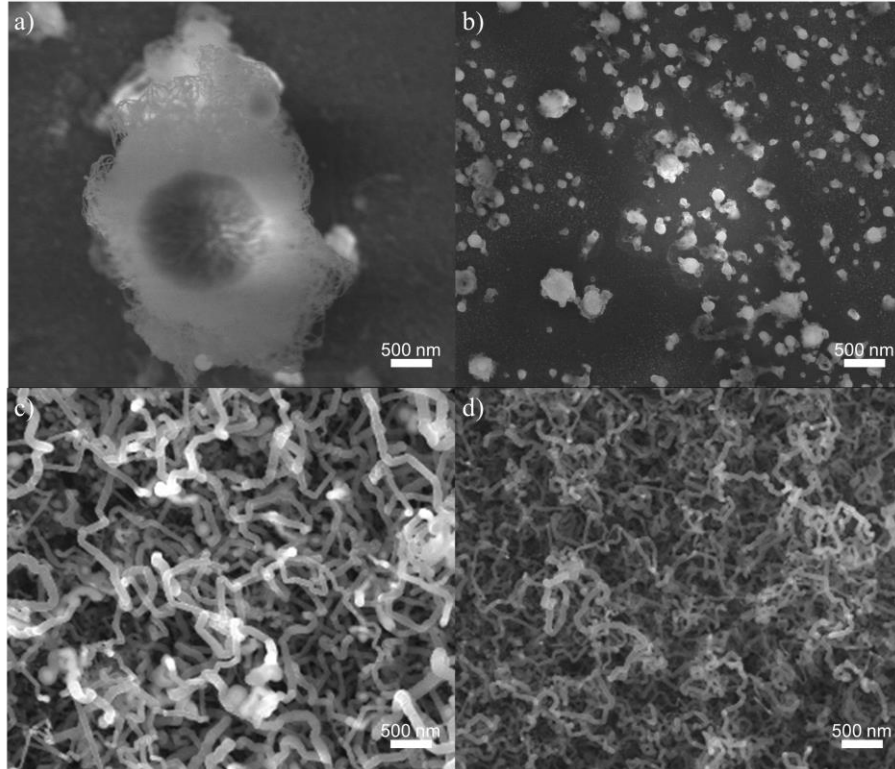


Figure 4.10 Growth of Si NWs on Si substrates at (a) 200, (b) 250, (c) 300, and (d) 350 °C.

Finally, the use of ultrananocrystalline diamond (UNCD) was explored as an alternative to the  $\text{Al}_2\text{O}_3$  coating. UNCD has several advantages over  $\text{Al}_2\text{O}_3$ . First, UNCD is more conductive than  $\text{Al}_2\text{O}_3$ . Second, the UNCD coating process is easier to scale up than the ALD process in  $\text{Al}_2\text{O}_3$  coating. Finally, UNCD consists mostly of  $\text{sp}^3$ -bonded carbon which makes it more resistant to etching than graphite when exposed to hydrogen plasma. Previously, we showed that UNCD does not etch under high-power hydrogen microwave plasma.<sup>188</sup> UNCD-coated Si was used as substrate for the growth of Si NWs. The results of the growth, which was performed at 350 °C, are shown in Figure 4.11. As seen from the figure the growth of Si NWs was successful. Si NWs were grown uniformly all over the surface of the substrate without etching the UNCD coating. These results suggest that UNCD or diamond-like carbon coatings can be used as diffusion blocking layers for growing Si NWs on Cu foils.

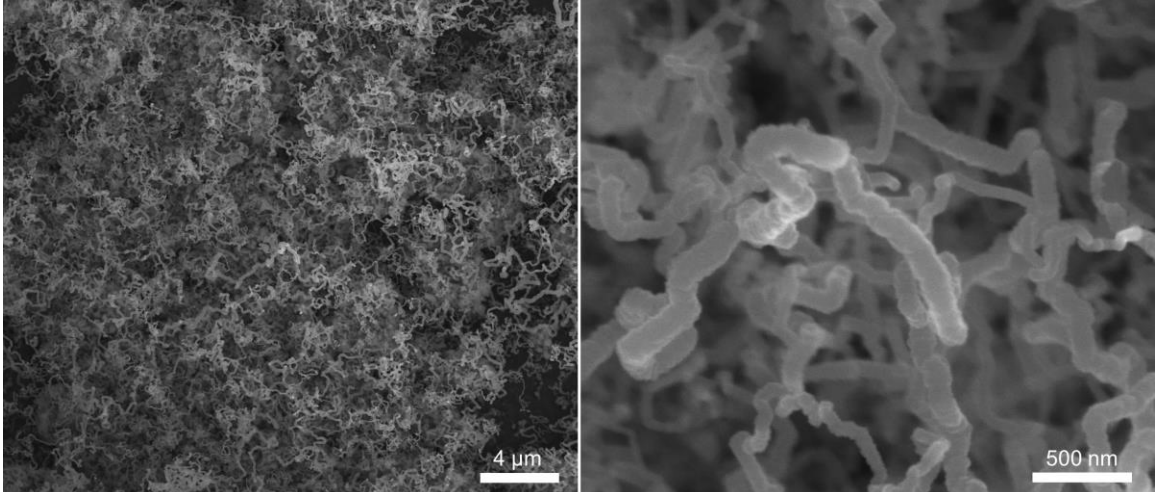


Figure 4.11 Growth of Si NWs on UNCD-coated Si substrates. The temperature of the growth was 350 °C.

#### 4.5. Summary

In this chapter a set of fundamental studies were presented in order to understand the influence of different variables on the wetting properties of Ga and gain insight into the interaction between nitrogen plasma and molten Ga. The results obtained from contact angle experiments suggested that both an increment in temperature and the addition of other elements can improve the wettability of Ga by reducing the surface tension of the molten metal. However, these variables were not as effective as the dissolution of nitrogen radicals into the melt. Nitrogenated-Ga melts were found to spread freely on different substrates. Absorption/desorption experiments indicated a rapid adsorption/dissolution of the gas into the molten metal when gallium was exposed to plasma. The overall interaction between Ga and plasmas is composed of five processes: (1) surface adsorption, (2) diffusion into the bulk, (3) recombination inside the bulk, (4) surface recombination, and (5) desorption of species from the bulk. The concentration of radicals inside the metal is determined by the rate in which each process is completed. Finally, the growth of Si NWs on Cu foils was presented to elucidate the potential of the synergism between molten Ga

and plasma in other applications different than the growth of GaN. Si NWs were tested as anode in Li-ion batteries showing a promising result. The anode exhibited a high reversible specific capacity in the first cycle of  $3083 \text{ mAhg}^{-1}$  with a capacity retention of 96.9 % after 13 cycles.

## CHAPTER 5

### PLASMA-ASSISTED LIQUID PHASE EPITAXY OF GAN

#### 5.1. Introduction

As stated in Chapter one, there is a need to develop a cost-effective technique for the production of bulk GaN. Two different approaches, which are based on the synergistic interaction between molten Ga and nitrogen plasma, have been proposed for this task. The first approach is a film-based method, in which a GaN film, grown through exposure of metallic Ga to plasma-activated nitrogen atoms, is grown into a millimeter-thick crystal via HVPE. Plasma nitridation of Ga can be performed using foreign or MOCVD/HVPE-grown GaN substrates. When foreign substrates are used, the resulting GaN film acts either as a buffer layer or as a substrate for the second step depending if the film adheres to the substrate or if it is a free-standing film, respectively. Previous reports suggest that when quartz is used as a substrate highly oriented GaN flakes are obtained.<sup>14</sup> On the other hand, when the process is performed on a native substrate, the homoepitaxial growth of GaN can be used to reduce the dislocation density of the original substrate, which promotes the growth of higher quality GaN in the second step.<sup>17-18</sup> The second approach is a crystal-based method in which single-crystalline GaN seed crystals, grown by exposing a Ga-based flux to nitrogen plasma, are enlarged into bulk GaN crystals via plasma-assisted liquid-phase epitaxy. Because the success of these two approaches is determined primarily by the

step in which the epitaxial growth of GaN takes place, this work focuses on providing a reliable plasma-assisted liquid phase epitaxy process. Among the existing challenges in liquid-phase epitaxy of GaN, homogeneous nucleation of GaN has been identified as the most critical. Spontaneous nucleation of GaN is a consequence of a supersaturation of nitrogen in the melt. Different researchers have identified the existence of an Ostwald-Miers region in their high and low-pressure LPE processes.<sup>51, 135-136</sup> This region determines the conditions in which the nitrogen concentration in the melt promotes the growth of GaN only on the seed. Outside this region neither growth nor spontaneous nucleation occurs. To find an equivalent region in the plasma-assisted LPE process presented in this work, the concentration of nitrogen needs to be control by one of the process variables.

In this chapter, pulsed-plasma-assisted liquid phase epitaxy is introduced as a process to grow homoepitaxial GaN layers which simultaneously reduces the homogeneous nucleation of GaN. A parametric analysis of this technique is also presented to provide a relationship between the concentration of nitrogen inside the melt and the process variables. The analysis also indicates the advantages of performing pulse over non-pulse plasma-assisted liquid phase epitaxy of GaN. The growth of highly oriented GaN films is also presented in this chapter. Finally, this chapter presents the growth of single-crystalline GaN crystal seeds.

## 5.2. Highly oriented GaN films

Based on the self-oriented growth concept reported by Sunkara *et al.*<sup>14-16</sup>, GaN films up to 1 cm<sup>2</sup> were grown on quartz substrates. In a typical growth experiment, Ga-coated substrates were placed inside the ECR-plasma reactor. Once the chamber was



purged, the substrates were exposed to nitrogen plasma and the heater was turned on. As the temperature was ramped up, the Ga film agglomerated into droplets with a considerable size distribution. These gallium droplets started to spread about 10 minutes after exposure to the atomic nitrogen at  $\sim 950^{\circ}\text{C}$ . Gradually, the nitrogenated gallium melt covered the substrate, and a thin, gray colored solid film is formed on top of the gallium layer. The spreading of the gallium melt during the growth phase was found to be critical in growing smooth textured films. XRD characterization showed that flat GaN films only presented reflections of the (0002) and (0004) planes of the hexagonal GaN, whereas the non-flattened GaN films showed the presence of all the characteristic planes of the wurtzite GaN. Differences between flat and non-flatten GaN films are shown in Figure 5.1. Thus, in order for GaN films to be produced effectively for a large-scale industrial need, this process necessitates flat and uniform Ga film, which can ultimately be nitridated into large-area highly oriented GaN films. In this work, two adjustments were necessary for obtaining flat, uniform films. The first adjustment was to utilize Ga as a film instead of a drip. When the Ga film is heated up, the film is transformed into several small Ga droplets that later spread and form a film. Conversely, when the drip is heated up it forms one big droplet that does not spread uniformly due to the formation of a GaN crust. The second adjustment was to expose the sample to nitrogen plasma at a mid-temperature, i.e.  $\sim 650\text{-}750^{\circ}\text{C}$ , for 15-45 minutes before raising the temperature to the process temperature. By performing the second adjustment, the concentration of nitrogen inside the melt was increased without having GaN nucleation. As mentioned in section 4.2, the incorporation of nitrogen into Ga improves the wettability of Ga by reducing its surface tension.

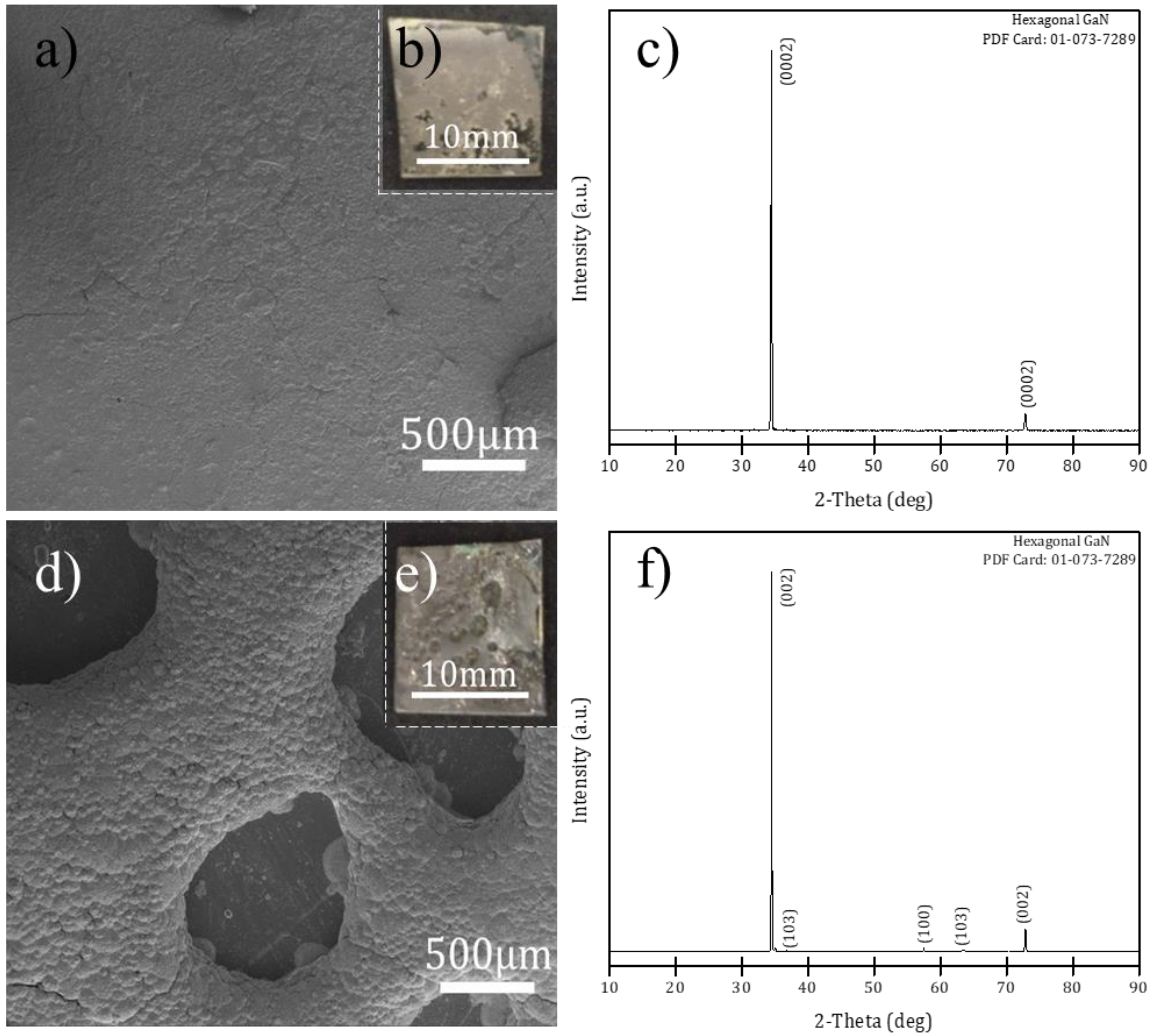


Figure 5.1. (a) Top morphology of flat GaN film, with the top right corner (b) showing the film as deposited. (c) X-ray spectra for the flat film. (d) Top morphology of non-flatten GaN film with the top right corner (e) showing the film as deposited. (f) X-ray spectra for the non-flatten film.

### 5.3. GaN seeds for growth of GaN

The use of both alkali or semi alkali metals and nitrogen plasma to grow bulk GaN, for the best of our knowledge, has not been reported. As a proof of concept, a series of experiments, where a mixture of Ga and LiCl is exposed to nitrogen plasma, were performed. The experiments were carried out in a custom-built, capacitively-coupled, RF

plasma reactor. The mixture, which had a molar ratio of 1:4 (Ga:LiCl) was spread onto a quartz substrate and placed inside the chamber. After a couple of purging cycles, the temperature was raised to 800°C and a nitrogen/hydrogen plasma was ignited. Hydrogen was added to reduce any oxide that might be in the system and to prevent any oxidation of Ga during the experiment. Hydrogen represented 10% of the total flow. After two hours, the plasma was shut down and the samples were cooled at a rate of ~10°C/min.

The post-processed samples, which were identified as yellow/gray powders, were characterized by SEM and XRD. Morphological analysis of the powders showed the presence of two different growth patterns. The first one, Figure 5.2 (a)-(b), corresponds to hexagonal platelets that stack on each other, forming a particle. The second one, which is described as hexagonal pillars, was found to be either on the surface of micron-size agglomerates, Figure 5.2 (c)-(d), or as crystals with hexagonal or cubic shapes, Figure 5.2 (e)-(f). The size of these pillars was found to be ~10 µm in length and ~2 µm in width. Moreover, XRD studies suggested that the powders are composed primarily of hexagonal GaN. In addition to all characteristic planes of the wurtzite GaN, the XRD spectrum, Figure 5.3, shows the presence of cubic GaN, Li<sub>3</sub>N and hydrated LiGaO<sub>2</sub>. It was not possible to identify the existence or absence of metallic Ga in the sample because its peaks slightly overlap with the ones of GaN. The other precursor, LiCl, was not found in the sample.

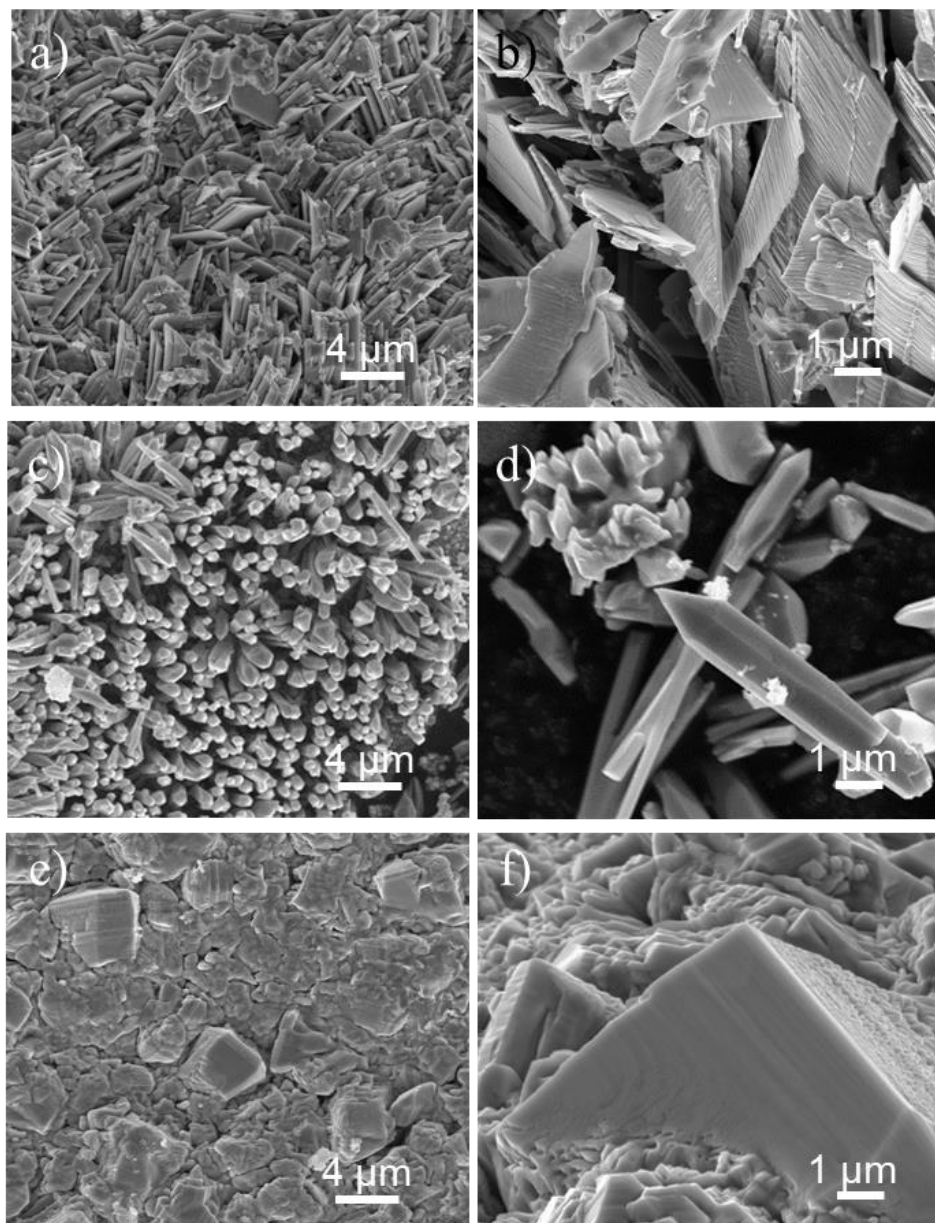


Figure 5.2. Morphological analysis of the samples synthesized by exposing a Ga-LiCl melt to  $N_2$  plasma. (a) Particle formed out of platelets. (b) Close-up of the platelets. (c) Agglomerates with pillars on their surface. (d) Close up of one of the pillar structures. (e) Agglomerates of hexagonal and cubic crystals. (f) Close up of a cubic crystal.

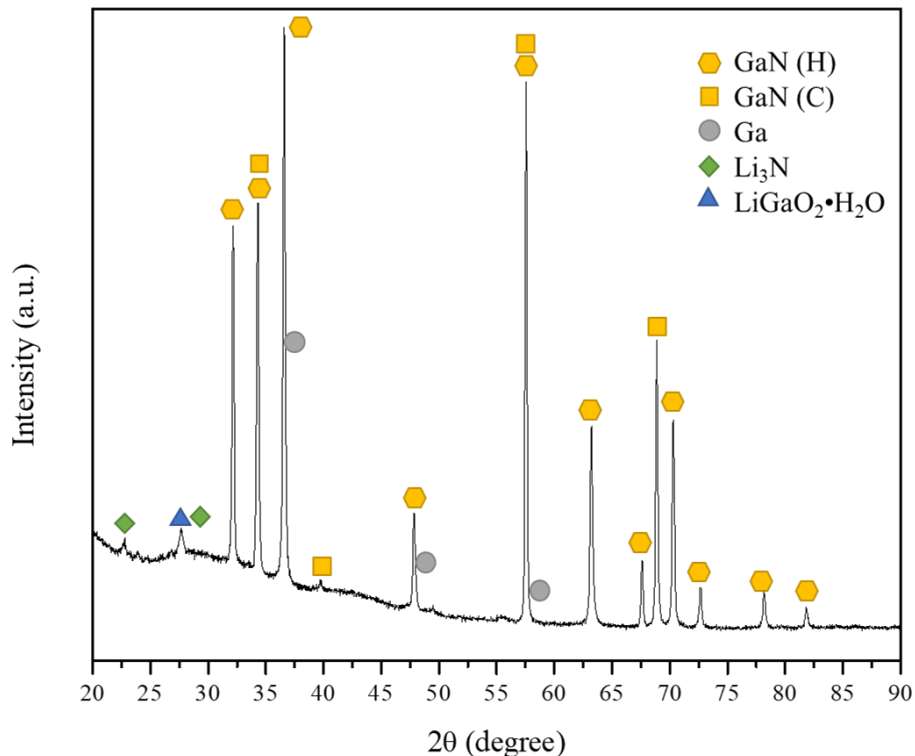


Figure 5.3. XRD spectrum of powders synthesized by exposing a Ga-LiCl melt to  $N_2$  plasma.

The presence of  $Li_3N$  indicates that there was a reaction between Li and N radicals and suggests that  $Li_3N$  is an intermediate product in the process of producing GaN. This statement is backed by Song *et al.* who proposed that the first step in the growth of GaN via a Li flux is the reaction between  $Li_3N$  and Ga to form  $Li_3GaN_2$  and liquid Li, Reaction 2.9. Later,  $Li_3N$  and  $Li_3GaN_2$  dissolved into a Li-Ga melt creating a Li-Ga-N melt from which GaN crystallizes.<sup>114</sup> Although no chlorine compounds were found, the results suggest that LiCl might have participated in the process. It is believed that LiCl promoted the crystallization of cubic GaN. The XRD spectrum, Figure 5.3, shows the presence of cubic GaN in the sample. Purdy *et al.* reported that the use of acidic mineralizers like LiCl promoted the crystallization of cubic-GaN in ammonothermal processes.<sup>72-73</sup> The presence of  $LiGaO_2$  is attributed to  $Ga_2O_3$ , which was already present in the sample and was not

reduced by the hydrogen plasma. Nonetheless, the possibility of a leak in the system that allows oxygen to enter the chamber was not discarded. It is believed that the big agglomerates were indeed LiCl particles, which were coated with gallium; the gallium reacted very quickly with N creating a GaN layer that prevented the particle from melting completely. The powders were washed in acidic solutions and water to remove any metal or salt that might still be present. No significant changes were found after these washes, suggesting that these particles are GaN coated. It is believed that the process takes place at the surface of the LiCl, which explains why the growth of platelets and pillars was observed primarily on the surface these particles. It is believed that if the area of contact between Ga and Li is enlarged and the formation of a GaN film at the interface between these two elements can be suppressed, the size of the crystals can be improved significantly.

#### 5.3.1. Regrowth of GaN seeds

Regrowth experiments of these seeds were attempted by taking the powders obtained in Section 5.3 and immersing them into a drip of Ga that was previously placed onto a substrate. Then Ga and seeds were exposed to nitrogen plasma following the same process as the pulsed plasma-assisted LPE explained in Section 5.4. Due to the good wettability of nitrogenated Ga, the Ga droplet that contained the crystals spread onto the substrate. This created a film in which the powders appeared at the surface. As a result, the powders were mixed with the eventually formed GaN crust. The resultant crust was milled and examined using SEM. Due to similar morphology between the platelets and the crust it was not possible to identify which crystals were a part of the powders that were immersed into the Ga and which crystals were obtained because of spontaneous nucleation. No crystals with pillar morphology were observed. However, larger amorphous particles were

found. The presence of these types of particles suggests that the agglomerates contained in the powders were covered by a layer of GaN. Similarly, when the GaN powders were incorporated into a Ga-LiCl mixture and exposed to nitrogen plasma it was not possible to differentiate between old and new GaN crystals. It is believed that in order to obtain proper regrowth of the seeds, only single crystals, like the one presented in Figure 5.2 (d), should be used. In the Recommendations chapter, a variation of the process in which these crystals are formed is presented in an attempt to reduce the formation of agglomerates and promote the formation of crystals with pillar morphology.

#### 5.4. Plasma-assisted liquid phase epitaxy of GaN

Liquid phase epitaxy growth of GaN was performed in RF plasma reactor using N<sub>2</sub> and Ga precursors following the experimental procedure explained in section 3.1.3. GaN crystals ~1mm<sup>2</sup>, purchased from Ammono, were used as substrates by immersing them into the molten Ga. The furnace temperature was held at 800-900°C. Initially, it was found that a GaN crust was being formed on top of the Ga. This phenomenon is seen in Figure 5.4. As seen in Figure 4.4, the dissolution of N into Ga is significantly faster than the recombination of radicals. This phenomenon can cause a rapid saturation of the melt and the consequent precipitation of GaN via the spinodal decomposition mechanism. This mechanism is explained in detail in Section 2.4.4.2. To promote the growth while decreasing the spontaneous nucleation, a pulse experiment, in which the sample is exposed intermittently to nitrogen plasma, was performed. The dissolution of radicals takes place only when the plasma is on. Conversely, the recombination of radicals can occur when the plasma is on or off. Thus, pulse experiments are intended to promote the recombination over the dissolution of radicals as an attempt to reduce the concentration of nitrogen inside

the melt. The pulse was described as five minutes of plasma exposure, followed by five minutes without plasma and so on until the end of the experiment. A cross sectional view of the substrate used in this experiment, Figure 5.5, depicts the growth of GaN on top of the GaN substrate. Evidence of growth on top of the substrate suggests that the reduction of radicals dissolved in the melt helped the reduction of spontaneous nucleation. Although the results obtained in this experiment were promising, it was needed to gain a better understanding on how the degree of saturation of the Ga melt affects the nucleation and the homoepitaxial growth of GaN.

Utilizing substrates with small surface areas was found to be difficult. Due to the good wettability of nitrogenated Ga, the Ga that was placed on top of the substrates spread freely, displacing the crystals and leaving just a thin layer of Ga on top of the substrate. If the Ga film is too thin, it is difficult to identify whether or not the growth of GaN is occurring via liquid phase epitaxy or through the vapor-liquid-solid (VLS) mechanism. To prevent the displacement of the substrates and the formation of a thin layer all over the surface of the substrate, the small GaN crystals were replaced by large surface area MOCVD grown (0001) GaN-on-sapphire substrates, which are not easy to displace by the movement of Ga.



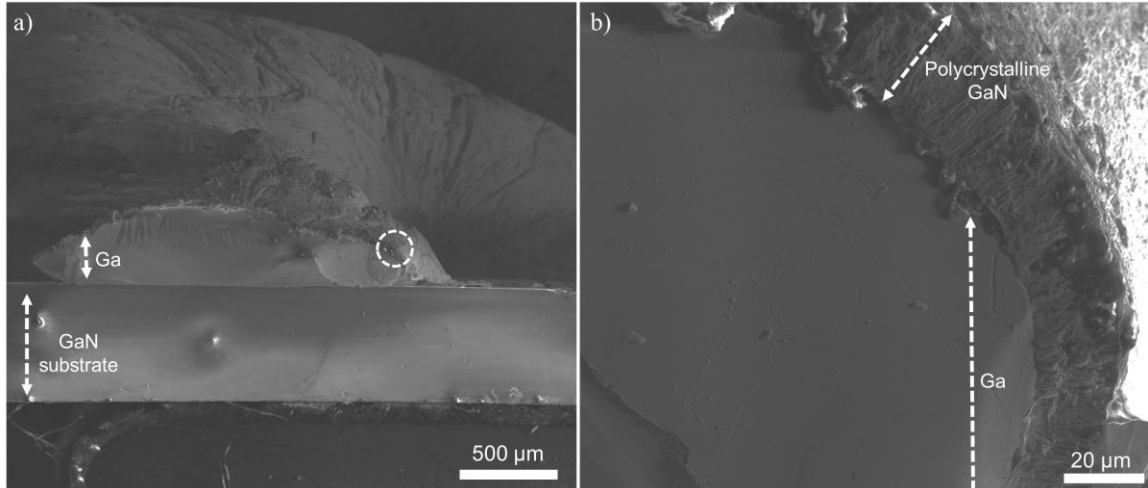


Figure 5.4 (a) Formation of a GaN crust on top of Ga after continuous exposure to nitrogen plasma. Dashed circle indicates (b) the interface between Ga and the GaN crust.

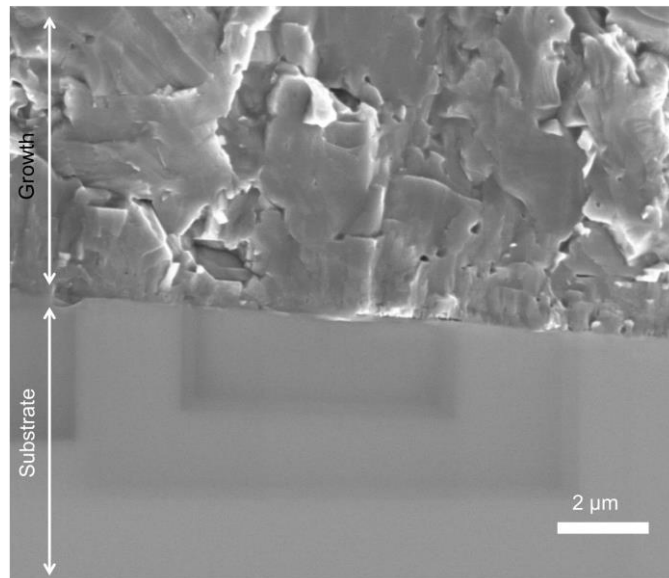


Figure 5.5. Growth of GaN via pulsed plasma-assisted liquid phase epitaxy was performed at 900 °C utilizing a five-minutes on, five-minutes off pulse.

To confirm that GaN was obtained via liquid phase epitaxy and not through the VLS mechanism, a new pulse experiment using a GaN-on-sapphire substrate was performed. The experiment was shorter than previous experiments in an attempt to guarantee that not all Ga was consumed. A cross-sectional view of the substrate after the

experiment is presented in Figure 5.6. It was found that the on top of the grown GaN layer there was a Ga film. Thus, the growth of GaN took place underneath the Ga which indicates that the growth of GaN was indeed obtained via liquid phase epitaxy and not through the VLS mechanism.

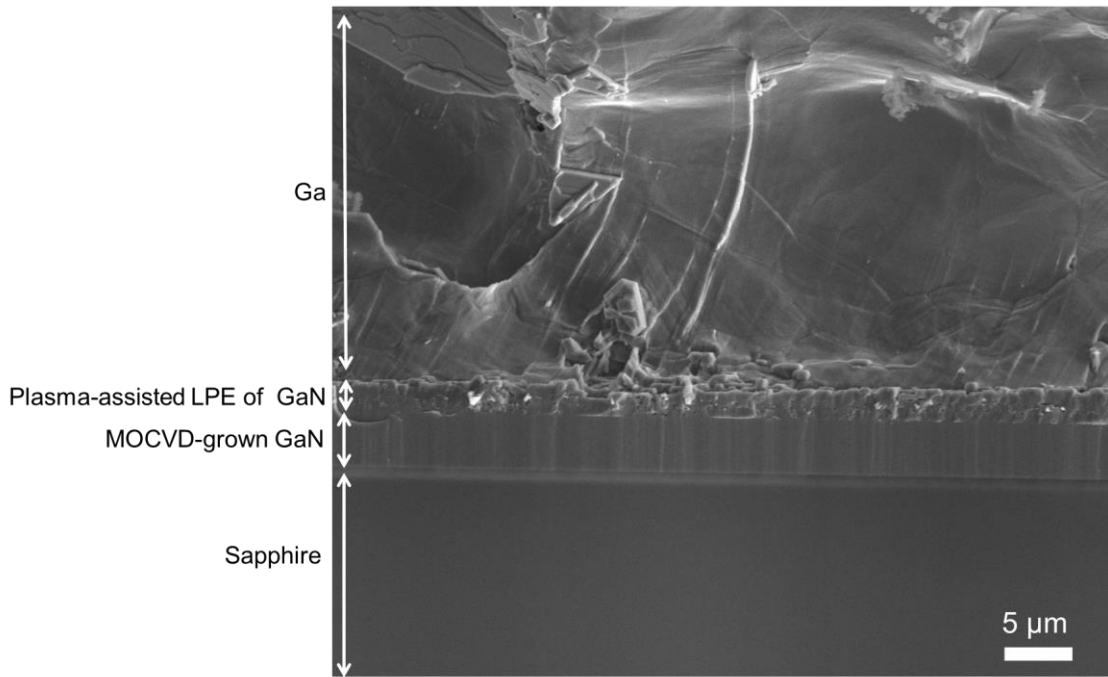


Figure 5.6 Pulse experiment performed for a short period of time.

In the pulse experiments Ga was placed on top of the GaN-on-sapphire substrate as a drip. During the process, Ga agglomerates into a big droplet and then as the concentration of nitrogen inside the melt is increased it begins to spread. As a consequence of this phenomenon a Ga film with varying thickness was formed on top of the surface of the substrate. A graphical description of this phenomenon is presented in Figure 5.7.



Figure 5.7 Ga film formation during LPE experiments. A Ga film with varying thickness is formed on top of the substrate due to the incorporation of nitrogen into the melt.

The type of GaN growth was found to be dependent of the thickness of the Ga film. Close to the edge where the thickness was the thinnest, a highly polycrystalline GaN film was obtained, Figure 5.8 (a). In a mid-point, between the edge and the center of the Ga film, a GaN film sample was obtained. The film, Figure 5.8 (b), indicates that the film was formed by GaN columns that merged together. It is believed that the film was obtained due to a faster growth rate in the c-direction of GaN crystals, which were grown epitaxially in the beginning of the process. In between of some of the columnar structures, the presence of voids was observed, suggesting a low the quality of the film. Finally, towards the center of the film, where the film was thickest, nucleation of individual GaN crystals was observed. A cross-sectional view of one of the crystals shows good growth quality as the interface between the substrate and the crystals is almost unnoticeable, Figure 5.8 (d). The crystals were described as hexagonal pyramids with a flat top, which is characteristic of crystals that are oriented in the c-direction. The size of the crystals varied between 1 and 5  $\mu\text{m}$  in length and between 0.1 and 1  $\mu\text{m}$  in height, Figure 5.8 (e). The crystals were analyzed using transmission electron microscopy (TEM). The results, Figure 5.9, indicated that the crystals were grown epitaxially. High-resolution TEM images of the interface show that the atomic arrangement of the GaN substrate is maintained in the GaN crystal. Additionally, no differences were found between the electron diffraction patterns of the substrate and the crystal, Figure 5.9 (e)-(f). The ring pattern in the electron diffraction pattern of the GaN crystal corresponds to amorphous platinum that was deposited on top of the GaN crystal to make the TEM lamella. Imanishi *et al.* proved that when two GaN crystals coalesce along the a-direction no dislocations are formed.<sup>103</sup> Thus, the enlargement of c-oriented crystals induces the coalescence of crystals along the a-direction, which, at

the end, results in the formation of a single crystalline film. The nucleation density of crystals obtained in this area however is low, which means that crystals need to grow significantly in the a-direction to coalesce with their neighbors. In order to obtain homoepitaxial GaN films, the process needs to be adjusted to promote the nucleation of crystals and their growth in the a-direction.

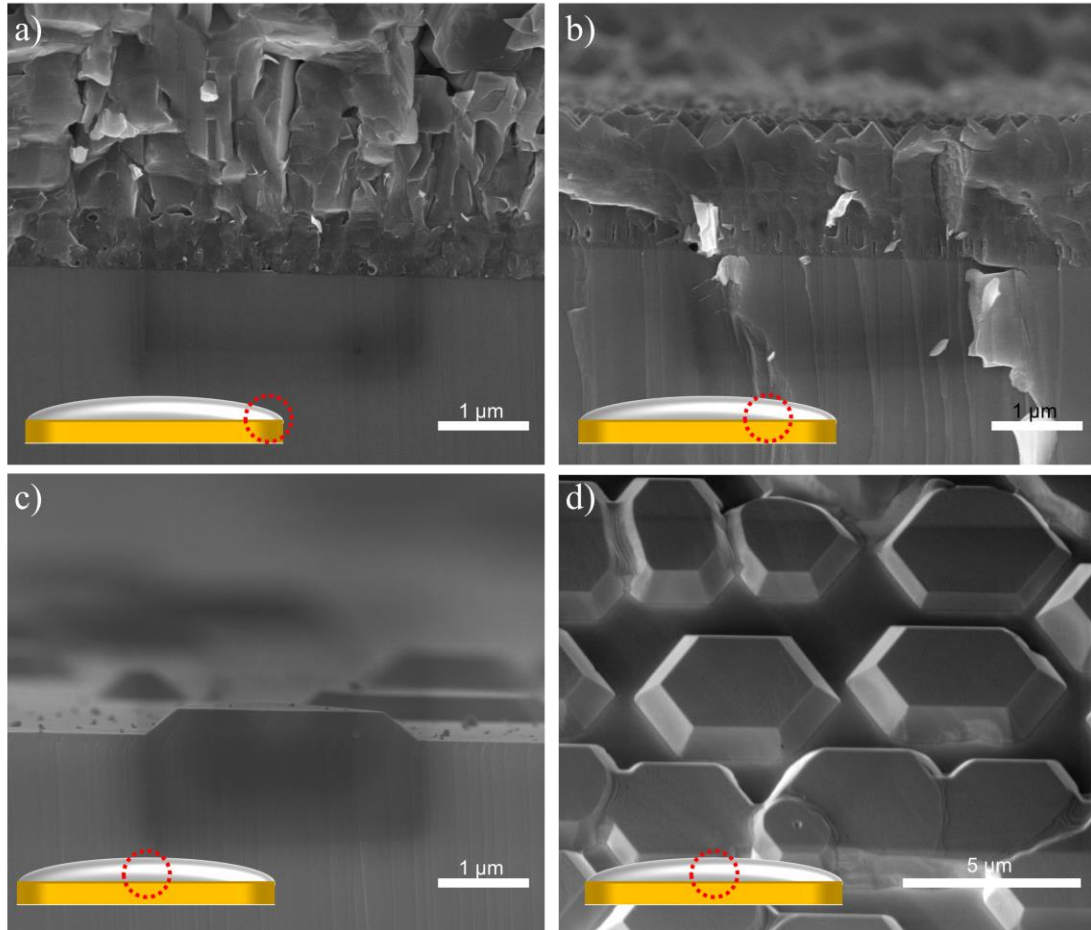


Figure 5.8 Growth of GaN via pulsed plasma-assisted LPE utilizing a Ga film with varying thickness. (a) Polycrystalline GaN was obtained in the thinnest area of the film. (b) Epitaxial growth of GaN was obtained in a mid-point between the edge and the center of the film. (d)-(e) GaN crystals were obtained in the thickest area of the film.

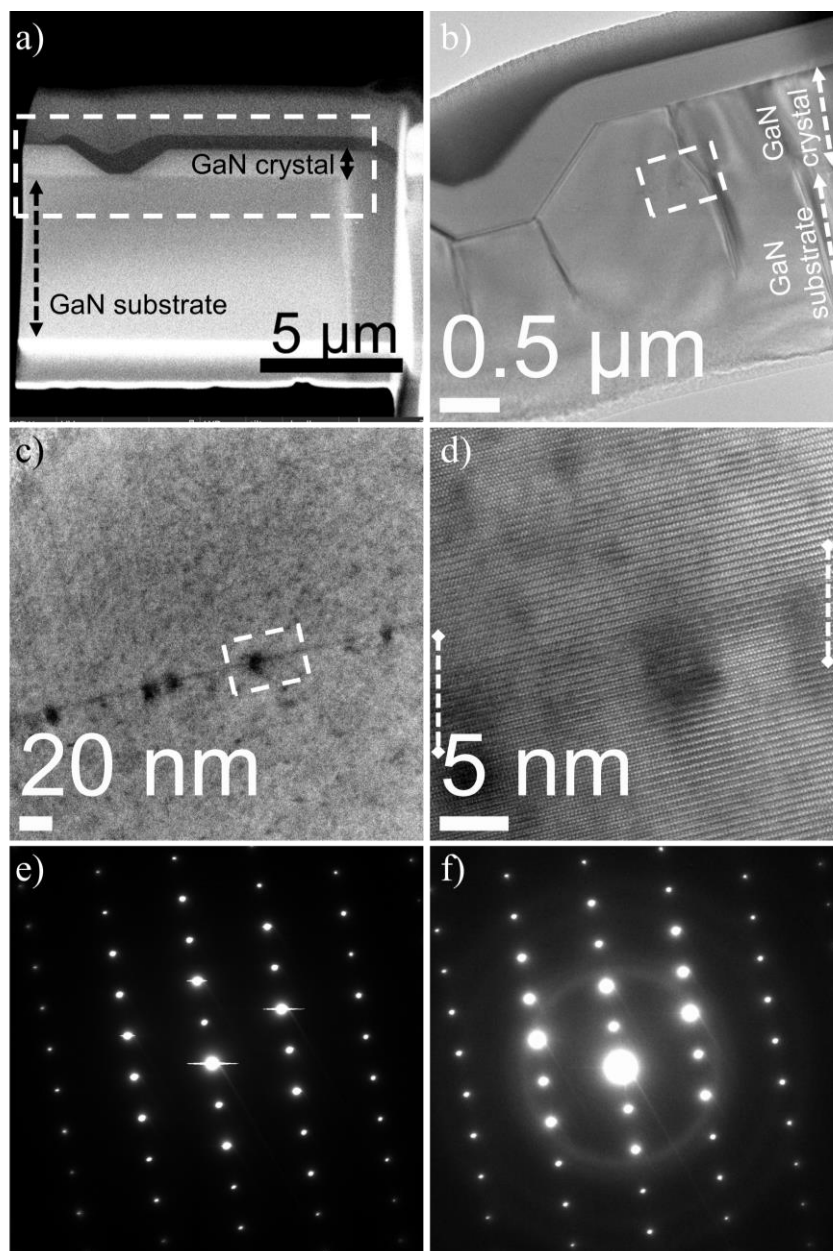


Figure 5.9 TEM characterization of the GaN crystals obtained in the thickest area of the Ga film. (a) SEM image of the TEM lamella used during characterization. White outlined area indicates the (b) area that was analyzed using TEM. (c) High resolution TEM image of the crystal. White outlined area indicates the interface between the grown layer and the substrate. (d) High-resolution TEM image of the interface. The area between the dashed lines indicates where the interface is. (e) Electron diffraction pattern of the substrate. (f) Electron diffraction pattern of the grown crystal.

The fact that three vastly different outcomes were obtained under the same experimental conditions indicates that the concentration of nitrogen in Ga at the surface of the substrate is different. Similar results were reported by Tanaka *et al.* who studied the LP-LPE of GaN under ammonia while utilizing a Ga film with varying thickness. From the results the researchers concluded that the nitrogen concentration inside the film varied according to the thickness of the film.<sup>138</sup> The results presented in this work suggest that the concentration of nitrogen inside the metal at the surface of the substrate is inversely proportional to the thickness of the film. This means that the concentration of nitrogen in the melt at the surface of the substrate is determined by the transport of nitrogen radicals from the surface of the Ga to the surface of the substrate. Due to the lack of a large thermal gradient along the z axis of the film it is assumed that there is no convection in the process. Therefore, the transport of nitrogen radicals to the surface of the substrate occurs through diffusion. The transport of radicals from the surface of the film to the surface of the substrate has two outcomes: (1) the concentration of nitrogen close to the substrate is increased, and (2) the concentration of nitrogen near the surface of the film is reduced. Thus, similar to the case of the recombination of radicals, the diffusion of radicals needs to be favored more than the dissolution of radicals in order to prevent the spontaneous nucleation of GaN. In the pulsed plasma-assisted LPE process this can be achieved by decreasing the on/off time ratio of the pulse sequence.

To improve the quality of the films a new set of experiments with a different pulse sequence was performed. The new sequences are explained as follows: first, the plasma was on for five minutes followed by five minutes in which the plasma was off; then a repetitive sequence in which the plasma was on for two minutes and then off for five

minutes was performed until the end of the experiment. The purpose of exposing the samples to plasma for five minutes in the first step was to rapidly increase the concentration of nitrogen. From previous experiments it was known that after five minutes of plasma exposure no GaN crust is formed. Thus, this step allows the initial nitrogen concentration of the melt into a growth regime to be set. On the other hand, the two-to-five on/off time ratio was intended to promote the transport of radicals to the surface of the substrate and to reduce the nitrogen concentration at the surface of the film. By doing this, a more uniform concentration of nitrogen along the Ga film is expected. The films obtained using this pulse configuration showed an improvement compared to films obtained previously. Figure 5.10 shows the growth of a GaN film under these conditions. The adherence of the film to the under-laying substrate is also good. As seen in the figure, the cleave marks, which are due to the breaking of the film, extend from the GaN layer grown via MOCVD to the GaN layer grown via pulsed plasma-assisted LPE. The quality of the film was maintained, and there was no polycrystalline growth on top, which indicates that the concentration of nitrogen was maintained in the Ostwald-Miers region during the entire length of the experiment. Further characterization of the sample was performed via TEM, Figure 5.11. High resolution TEM images at the interface between the GaN substrate and the GaN grown layer [Figure 5.11 (d)], and electron diffraction patterns of both the substrate and the GaN layer [Figure 5.11 (e)-(f)], indicate epitaxial growth of GaN. High-resolution TEM image of the film, Figure 5.11 (c), shows the presence of defects at the interface as well as a high concentration of basal stacking faults. The streaking of diffraction spots along the [0001] direction in the electron pattern of the GaN layer [Figure 5.11 (f)] confirms that the film contains a large number of basal stacking faults.<sup>190</sup> It is believed that

the defects at the interface between the substrate and the grown GaN layer are due to the presence of carbon and/or oxygen at the surface of the substrate. Different techniques including ultraviolet/ozone exposure and wet chemical treatments are used to remove surface carbon and to reduce the native oxide on the GaN surface.<sup>191</sup> The GaN-on-sapphire substrates used in this work were not subjected to any type of surface treatment, thus it is expected that the surface of the substrates contained carbon or oxygen. The growth rate of the of the film was  $\sim 0.5 \mu\text{m/h}$  which is similar to growth rates obtained in MOCVD processes. However, this growth rate is significantly faster than the growth rate obtained by Novikov *et al.* during their plasma-assisted electroepitaxy process.<sup>144</sup> The results obtained upon developing the pulsed plasma-assisted liquid phase epitaxy technique were found to be successful.

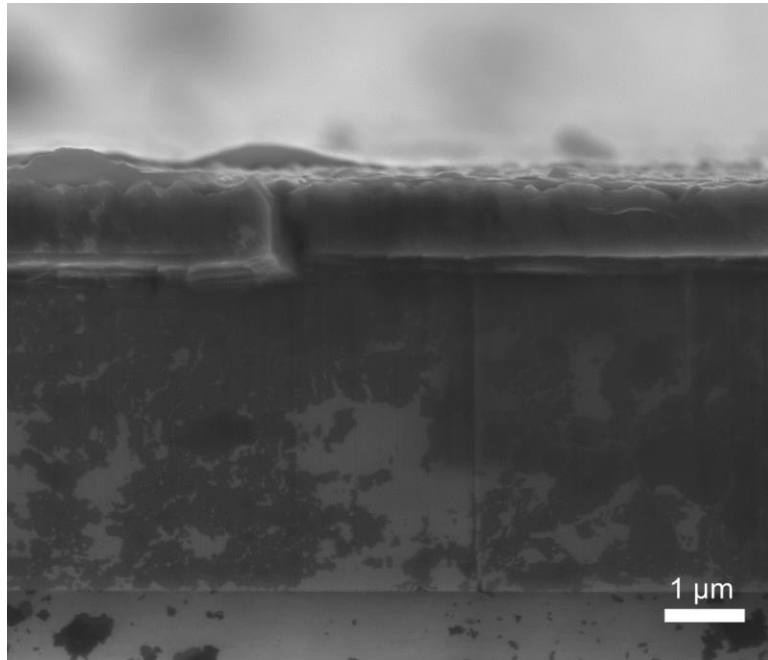


Figure 5.10 Pulsed plasma-assisted LPE of GaN utilizing a modified pulse sequence. In this experiment a two minutes-on, five-minutes off pulse was used.



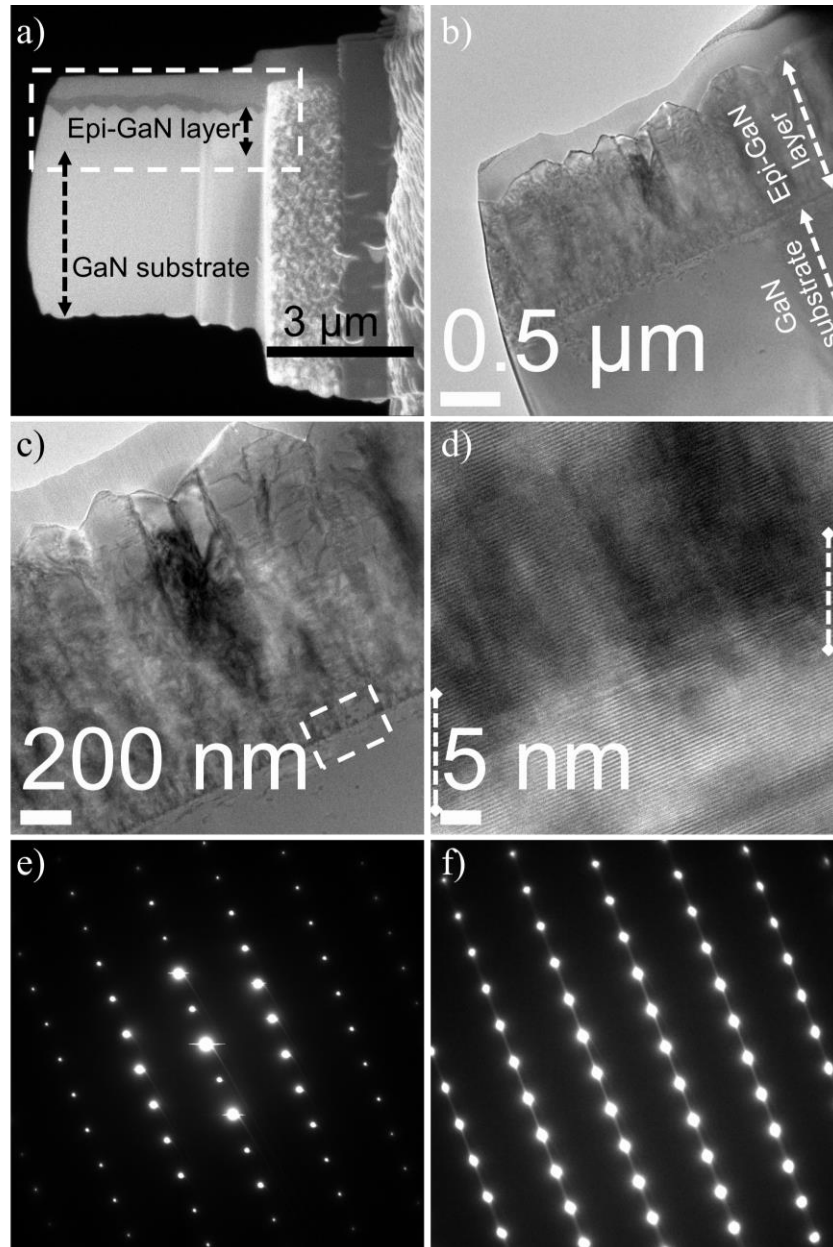


Figure 5.11 TEM characterization of the GaN film grown via the pulsed plasma-assisted LPE technique utilizing the modified pulse sequence. (a) SEM image of the TEM lamella used during characterization. White outlined area indicates the (b) area that was analyzed using TEM. (c) TEM image of the film. White outlined area indicates the interface between the grown layer and the substrate. (d) High-resolution TEM image of the interface. The area between the dashed lines indicates where the interface is. (e) Electron diffraction pattern of the substrate. (f) Electron diffraction pattern of the grown layer.

### 5.5. Parametric analysis of pulsed plasma-assisted liquid-phase epitaxy of GaN

As mentioned in chapter four, the concentration of nitrogen inside molten Ga that is exposed to nitrogen plasma is set by the interaction of five distinct processes, namely: surface adsorption, diffusion into the bulk, recombination inside the bulk, surface recombination, and desorption of species from the bulk. Mathematically, the concentration of nitrogen inside the melt can be related to these processes by developing a mass transport model. If a Ga film is exposed uniformly to a flux of nitrogen radicals, Figure 5.12, the model can be described as a one-dimensional version of Fick's second law with reaction, Equations 5.1- 5.3.

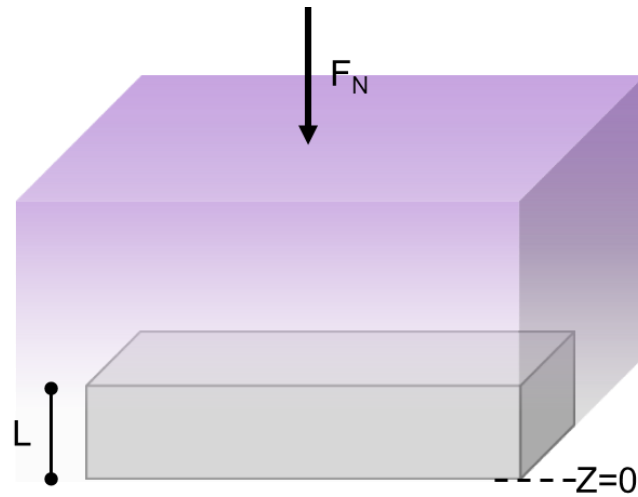


Figure 5.12. Time-dependent diffusion of nitrogen radicals from a plasma source into a molten Ga film.

$$\frac{D}{Dt} C_N = D_{NGa} \nabla^2 C_N + R_{N,bulk} \quad (5.1)$$

$$\frac{\partial C_N}{\partial t} + v \cdot \nabla C_N = D_{NGa} \nabla^2 C_N + R_{N,bulk} \quad (5.2)$$

$$\frac{\partial C_N}{\partial t} = D_{NGa} \frac{\partial^2 C_N}{\partial z^2} + R_{N,bulk} \quad (5.3)$$

Where  $R_{N,bulk}$  is the rate of N recombination in the bulk and is further described by the following equation,

$$R_{N,bulk} = -k_{BR} C_N^2 \quad (5.4)$$

Where  $k_{BR}$  is the nitrogen bulk recombination reaction constant.

Furthermore, the model assumes that prior to plasma exposure, no nitrogen radicals had dissolved into the Ga film. Therefore, the initial condition is defined as

$$C_N(z, t = 0) = 0 \quad (5.5)$$

The model also states that there is no transport of nitrogen radicals from the Ga film to the substrate and that the nitrogen radicals that stick on the surface of the film can either recombine or diffuse inside the film. The consequent boundary conditions are defined by

$$\left. \frac{\partial C_N}{\partial z} \right|_{z=0} = 0 \quad (5.6)$$

$$-D_{NGa} \left. \frac{\partial C_N}{\partial z} \right|_{z=L} = p(t) F_N S + R_{N,surf} \quad (5.7)$$

Where  $L$ ,  $R_{N,surf}$ ,  $F_N$ ,  $S$ , and  $p(t)$  are the thickness of the film, the rate of N recombination on the surface, the flux of N that strike the Ga surface, the sticking coefficient, and a pulse wave function, respectively. The recombination of N on the surface of Ga can be described by,

$$R_{N,surf} = -\gamma_N F_N \quad (5.8)$$

Where  $\gamma_N$  is the recombination coefficient of nitrogen and is defined as the fraction of atoms striking the surface which recombine. On the other hand, the pulse wave function includes the pulsing effect into the model. The mathematical expression of the pulse wave is presented in the following equation.

$$p(t) = \frac{\tau}{T} + \sum_{n=1}^{\infty} \frac{2}{n\pi} \sin\left(\frac{\pi n}{T} \tau\right) \cos\left(\frac{2\pi n}{T} (t - \tau/2)\right) \quad (5.9)$$

Where  $\tau$  and  $T$  are the pulse time and period, respectively. The pulse time determines the period in which the plasma is on ( $p(t)=1$ ), whereas  $\tau - T$  represents the period in which the plasma is off ( $p(t)=0$ ).

The solution of Equation 5.3, utilizing the initial and boundary conditions stated in Equations 5.5-5.7, provides the profile concentration of nitrogen inside the film as function of time,  $C_N(z, t)$ . Two assumptions were made to simplify the system: (1) the sticking coefficient is 1.0, and (2) the recombination on the surface is negligible. These two assumptions state that all radicals that strike the surface of the film are diffused into it. Argoitia *et al.* reported that because of the slow rate of recombination of nitrogen radicals on the surface of Ga, that nitrogen atoms diffuse into the bulk which leads to the formation of GaN crystals.<sup>139</sup> Furthermore, the small recombination coefficient of nitrogen on other metals suggests that the recombination of nitrogen radicals on the surface of Ga can be

neglected. The recombination coefficient of nitrogen on Fe, Ni, and Cu, was reported as  $2 \times 10^{-3}$ ,  $6.7 \times 10^{-5}$ , and  $6.8 \times 10^{-2}$ , respectively.<sup>168</sup> Finally, the values of the remaining three parameters i.e.  $k_{BR}$ ,  $D_{NGa}$ , and  $p(t)$  were set in order to obtain  $C_N(z, t)$ . The flux of species was set to  $5 \times 10^{-7} \text{ mol cm}^{-2} \text{ s}^{-1}$  as it is in good accordance with the flux of N radicals in a ECR nitrogen plasma reported by M. Meyyappan.<sup>192</sup> Neither the diffusion coefficient nor the recombination reaction constant is available in the literature. Inouye *et al.* studied the diffusion coefficient of nitrogen in molten iron. Further, the researchers developed an equation that relates the diffusion coefficient with temperature.<sup>193</sup> Utilizing this relationship at temperatures between 800 and 1000 °C (the temperatures that the growth of GaN takes place), it was found that the diffusion coefficient varies between as  $3 \times 10^{-6} \text{ cm}^2 \text{ s}^{-1}$  and  $1 \times 10^{-6} \text{ cm}^2 \text{ s}^{-1}$ . Assuming a middle point, the diffusion coefficient was set to  $5 \times 10^{-6} \text{ cm}^2 \text{ s}^{-1}$ . Finally, the recombination reaction constant was determined by a trial and error process in which the value was modified until the shape of the nitrogen concentration profile behave similarly to the pressure curve presented in Figure 4.4. The constant value was determined as  $1 \times 10^{-1} \text{ cm}^3 \text{ mol}^{-1} \text{ s}^{-1}$ .  $C_N(z, t)$ , and was obtained by solving numerically Equation 5.3 for  $z < 0 < 1 \text{ mm}$  and  $0 < t < 3000 \text{ s}$ . In order to complete this calculation, the pdepe solver included in Matlab was employed. In the pdepe solver the spatial derivatives are discretized according to finite-element discretization (FED), while the time derivatives are held continuous.<sup>194</sup>

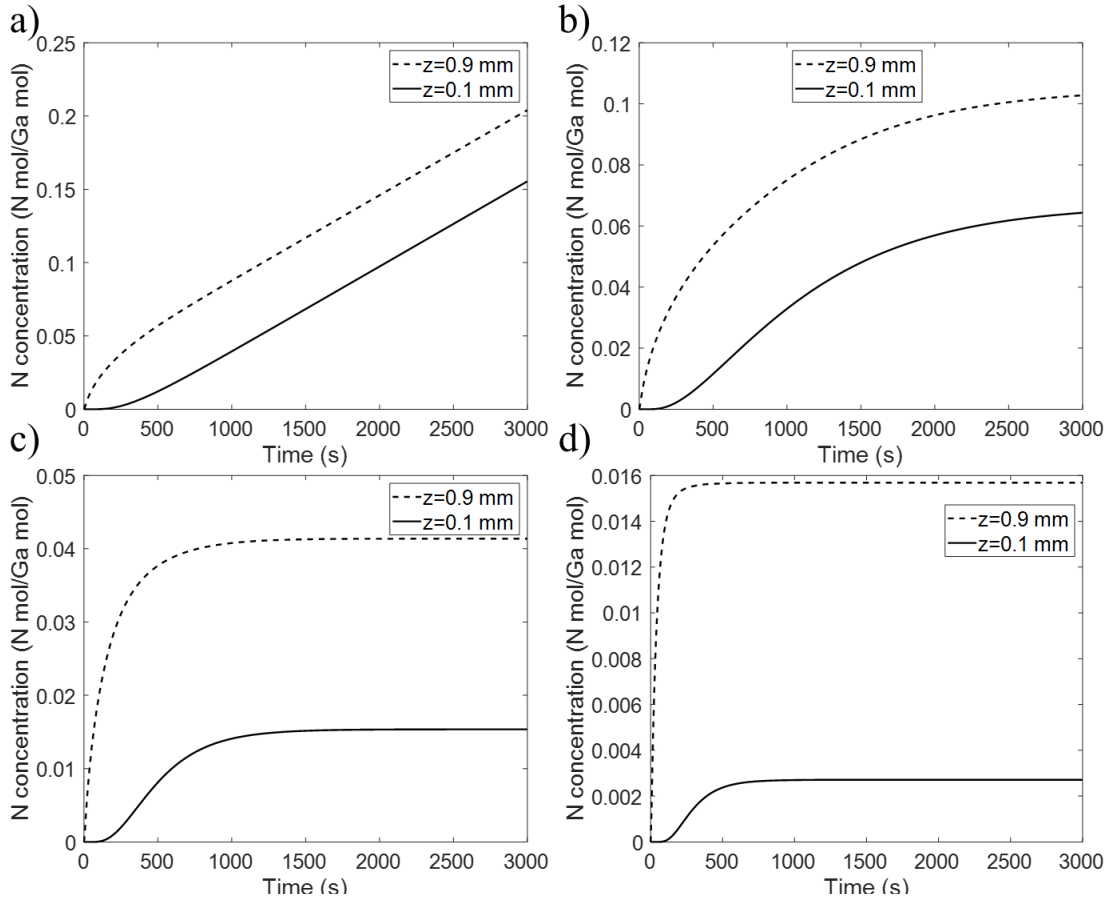


Figure 5.13 Effect of bulk recombination in the concentration of nitrogen inside a 1mm thick Ga film. Concentration profiles were calculated using  $D_{NGa} = 5 \times 10^{-6} \text{ cm}^2 \text{ s}^{-1}$ ,  $p(t) = 1$  and  $k_{BR} =$  (a) 0, (b)  $1 \times 10^{-1}$ , (c), 1, and (d) 10.

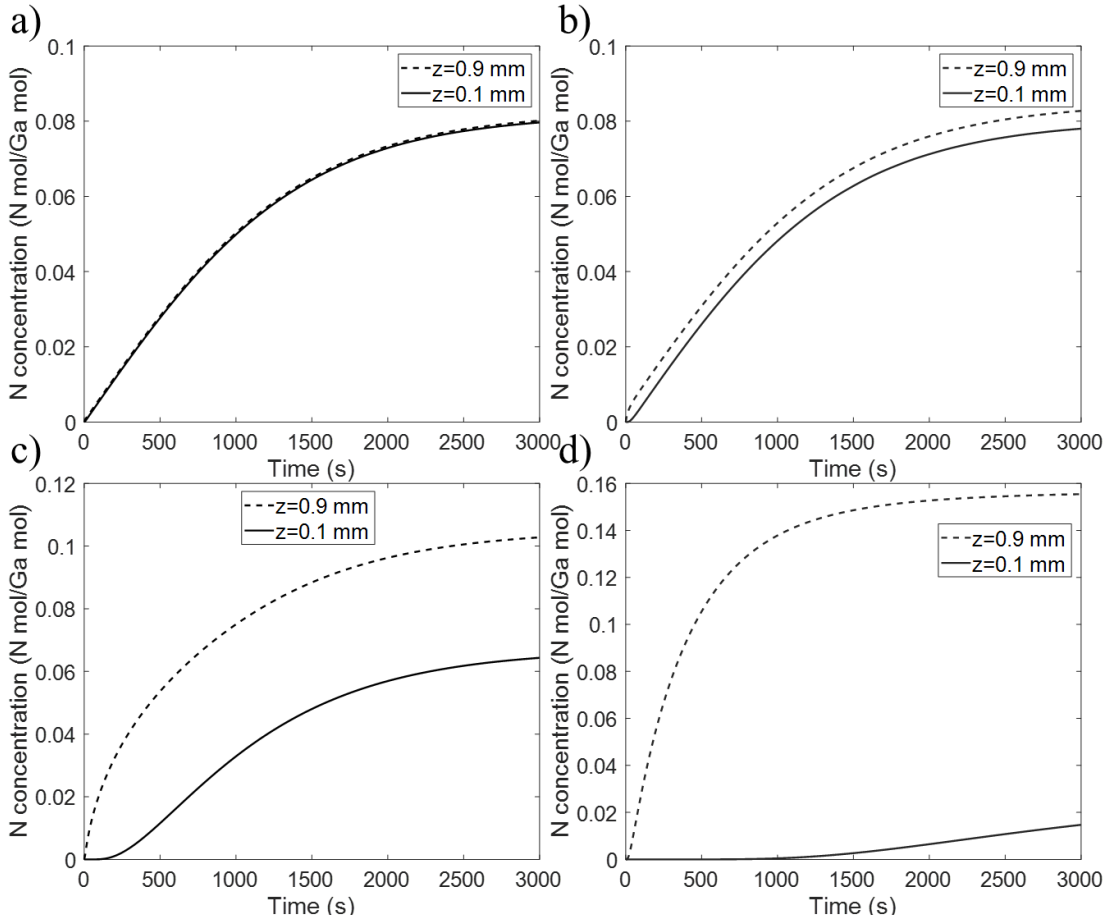


Figure 5.14 Effect of diffusion in the concentration of nitrogen inside a 1mm thick Ga film.

Concentration profiles were calculated using  $k_{BR} = 1 \times 10^{-1}$ ,  $p(t) = 1$  and  $D_{NGa} =$  (a)  $5 \times 10^{-4}$ , (b)  $5 \times 10^{-5}$ , (c)  $5 \times 10^{-6}$ , and (d)  $5 \times 10^{-7} \text{ cm}^2 \text{ s}^{-1}$ .

Bulk recombination, diffusion of radicals inside the melt, and pulsing are determined by these three parameters  $k_{BR}$ ,  $D_{NGa}$ , and  $p(t)$ , respectively. Further, the influence of diffusion, recombination in the bulk, and pulsing can be determined by modifying one of the parameters while maintaining the other two parameters constant. The influence of the bulk recombination was determined by obtaining  $C_N(z, t)$ , such that  $k_{BR}$  equals to 0,  $1 \times 10^{-1}$ , 1, and 10. Similarly, the effect of diffusion was determined by calculating  $C_N(z, t)$ , such that  $D_{NGa}$  equals to  $5 \times 10^{-4}$ ,  $5 \times 10^{-5} \text{ cm}^2$ ,  $5 \times 10^{-6} \text{ cm}^2$ , and  $5 \times$

$10^{-7} \text{ cm}^2 \text{ s}^{-1}$ . Finally, the influence of pulsing was determined by incorporating a five-to-five minutes on/off pulse. Figure 5.13, Figure 5.14, and Figure 5.15 depict the influence of bulk recombination, diffusion and pulsing, respectively by presenting the concentration of nitrogen at  $z$  equals to 0.1 and 0.9 mm under different conditions. Bulk recombination was found to be responsible for the maximum amount of nitrogen that can be dissolved into Ga. The larger the recombination rate was the sooner the maximum was reached and the smaller that value was. Additionally, it was found that the recombination affects the nitrogen concentration uniformity along the film. As the the bulk recombination becomes more dominant the concentration gradient becomes larger. From these results, it is observed that that diffusion of nitrogen radicals inside is responsible for the concentration uniformity along the film. The smaller the diffusion coefficient is, the larger the gradient is. Experimentally it was found that the concentration of nitrogen inside the melt was a function of the thickness of the film. Thus, it is assumed that this process is diffusion limited. Results regarding pulsing showed that the concentration in the pulsing case was lower than in the case when the plasma was on. This is explained by the fact that the film was exposed to plasma for twice as much time. To make a more fair comparison, a new concentration profile with  $p(t) = 0.5$  was calculated. By doing this, the total number of nitrogen radicals that strike the surface of Ga after 3000 seconds is the same for both the on/off pulse and when  $p(t) = 0.5$ . As seen from Figure 5.15, the average nitrogen concentration value of the pulsing experiment was lower at  $z = 0.9$  mm and higher at  $z = 0.1$  mm than when  $p(t) = 0.5$ . This means that that the use of pulsing allowed for more uniform nitrogen concentration distribution along the Ga film. However, the overall values are similar, which suggests that the reduction in the flux of nitrogen radicals can also



promote the epitaxial growth of GaN while decreasing homogeneous nucleation. To test this hypothesis a new growth experiment was performed. GaN on sapphire substrates with Ga on top were exposed continuously to a N<sub>2</sub>/Ar (1:9) plasma. By using a dilute nitrogen plasma, it was expected to reduce the total number of nitrogen radicals that strike the surface. As seen from Figure 5.16 (a), the resultant film was characterized by two distinct types of growth. On top of the substrate GaN was grown epitaxially, but as the layer became thicker, the growth became polycrystalline. The epitaxial layer, Figure 5.16 (b), was found to be similar to the epitaxial layer described in Section 5.4 (Figure 5.10). However, the growth rate was higher in this case. The growth rate of the epitaxial layer utilizing the dilute nitrogen plasma was ~1.6 μm/h. This rate was calculated utilizing the entire length of the experiment which means that the rate accounts for the time in which the polycrystalline growth took place. Therefore, the actual growth rate of the epitaxial layer could be even higher. The transition from epitaxial to polycrystalline growth indicates that the concentration of nitrogen inside the melt moved from the Ostwald-Miers region to the homogeneous nucleation region as the experiment was being performed. This phenomenon is a consequence of a continuous increment in the concentration of nitrogen. Over time, as seen in Figure 5.15 (a)-(b), the concentration inside the melt increases independently of the flux of nitrogen radicals. Nonetheless, by using a dilute nitrogen plasma, the nitrogen concentration was kept into the Ostwald-Miers region for longer time in comparison to the non-diluted nitrogen plasma resulting in a thicker GaN epitaxial layer.

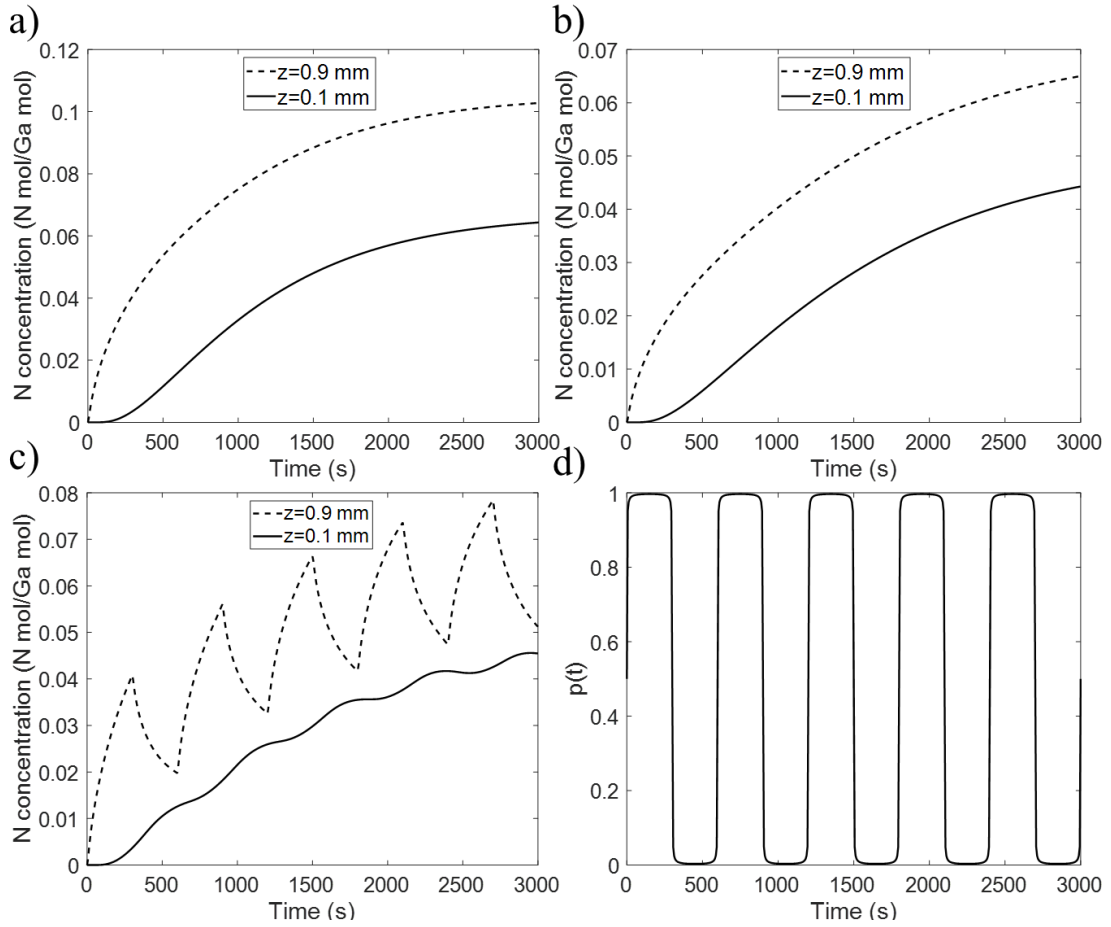


Figure 5.15 Effect of pulsing in the concentration of nitrogen inside a 1mm thick Ga film.

Concentration profiles were calculated using  $k_{BR} = 1 \times 10^{-1}$   $D_{NGa} = 5 \times 10^{-6}$   $\text{cm}^2 \text{s}^{-1}$ , and

$p(t) =$  (a) 1, (b) 0.5 and (c) five to five minutes on/off pulse. Pulse wave is shown in (d).

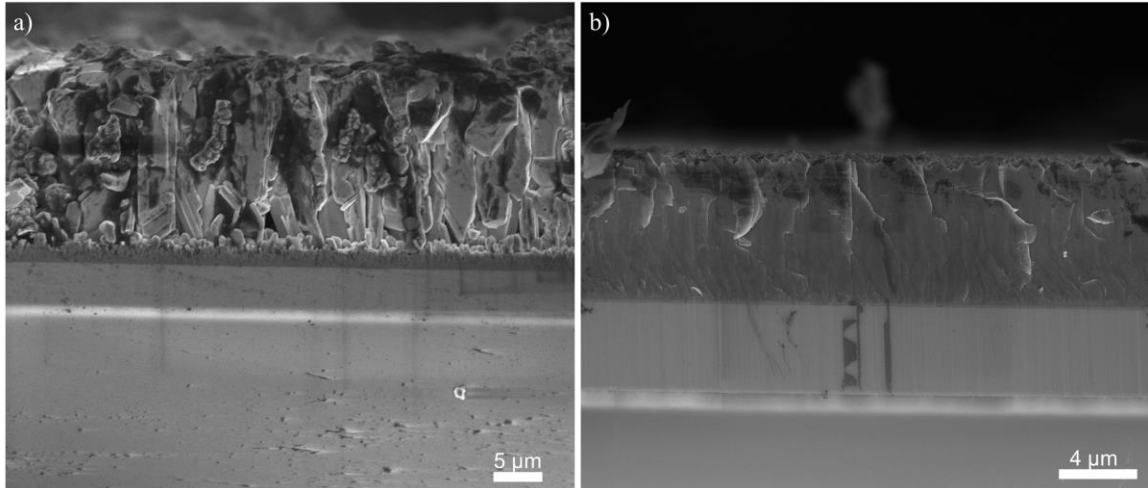


Figure 5.16. Liquid phase epitaxy of GaN utilizing a diluted nitrogen plasma. Nitrogen was diluted in argon in a 1:9 ratio in order to reduce the concentration of nitrogen radicals in the system. (a) Resultant film is characterized by having two distinct growths i.e., epitaxial and polycrystalline. (b) Zoom into the epitaxial GaN layer.

Finally, the concentration profile of the modified pulse sequence presented in Section 5.4, was calculated, Figure 5.17 (a). The sequence, Figure 5.17 (b) is described as five min on, then five min off, and then a two-to-five min on/off pulse, which is performed until the end of the experiment. Results showed that in the first five minutes of exposure to plasma the concentration of nitrogen inside the film increased rapidly; then when the two-to-five pulse sequence was started, the rate in which the concentration increases in time decreased. By changing the second part of the sequence to a one-to-five min pulse sequence it was found that the slope decreased even further, which resulted in the concentration remaining almost constant, Figure 5.17 (c). In addition to the change in slope, the second part of the pulse sequence was responsible for decreasing the concentration gradient. If the system is perfectly known, the initial plasma exposure time would be used to set the concentration of nitrogen inside the melt, whereas the proper on/off ratio in the consequent pulse would allow the concentration to be maintained constant while decreasing the

concentration gradient. As a proof of concept, a new experiment utilizing a modified pulse sequence was performed. The sequence was described as five minutes on, then thirty minutes off, followed by a one-to-thirty min on/off pulse. The results, Figure 5.18, showed the growth of an epitaxial GaN layer. The layer was  $\sim 13.5 \mu\text{m}$  thick and had only Ga on top even though the experiment was performed for 9 hours. This result indicates that the second part of the pulse allowed the concentration of nitrogen to be maintained within the Ostwald-Miers region for a longer time.

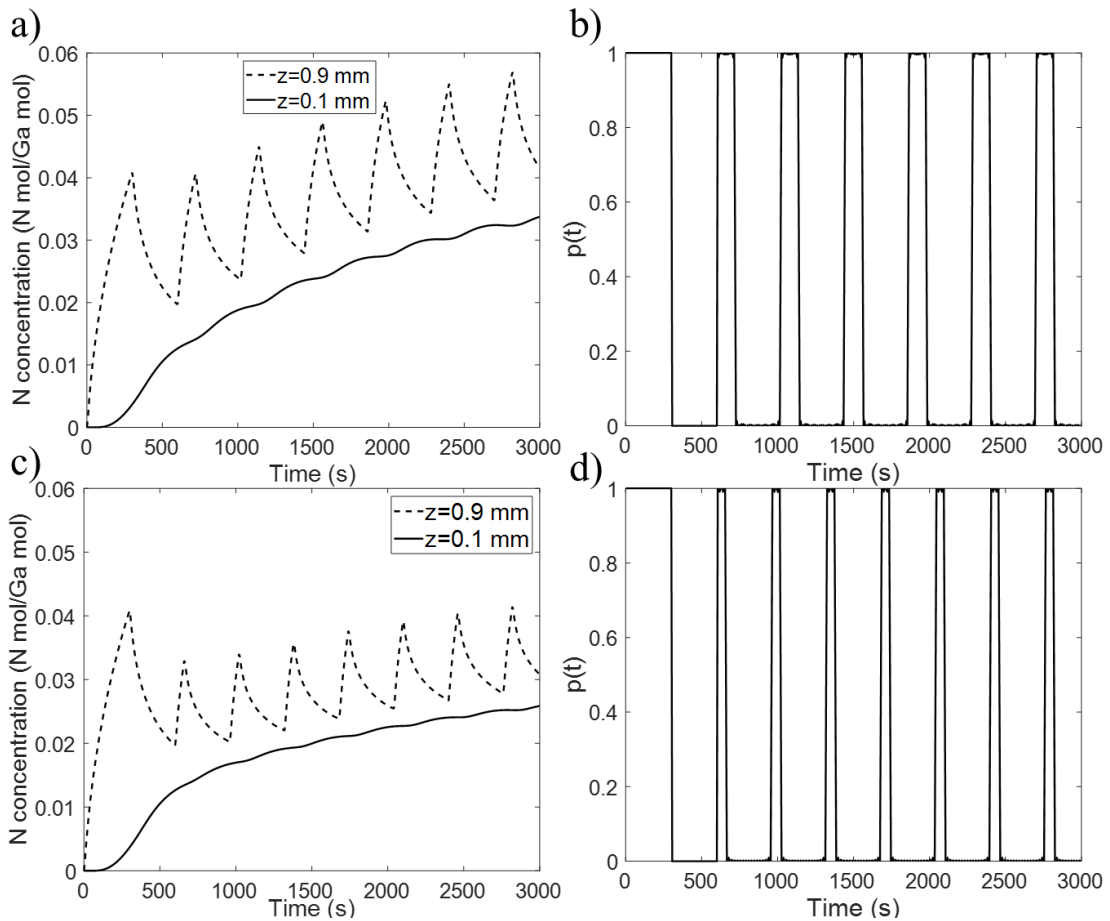


Figure 5.17 Concentration profile of modified pulsing sequence. Concentration profiles were calculated using  $k_{BR} = 1 \times 10^{-1}$   $D_{NGa} = 5 \times 10^{-6} \text{ cm}^2 \text{ s}^{-1}$  and a modified pulse sequence. Concentration profile in (a) corresponds to pulse sequence presented in (b), while concentration profile in (c) corresponds to pulse sequence presented in (d)

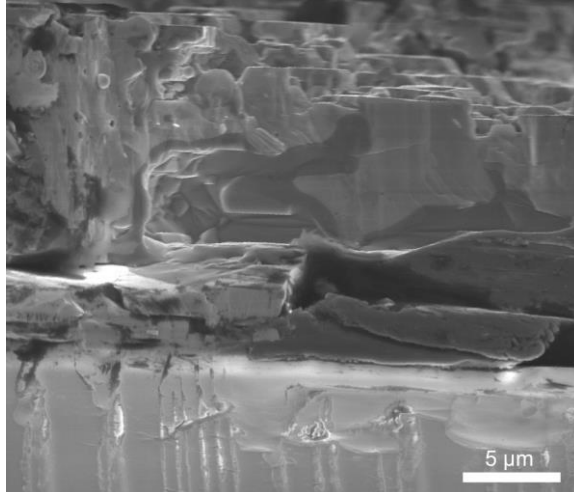


Figure 5.18 Pulsed plasma assisted LPE of GaN using a modified pulsing sequence. The sequence is described as five min on, then thirty min off, and then a one-to-thirty min on/off pulse, which is performed until the end of the experiment

#### 5.6. Summary

In this chapter pulsed plasma-assisted liquid phase epitaxy was presented as an alternative technique for growth of GaN. This novel technique hinders spontaneous nucleation while promoting the epitaxial growth of GaN. A parametric study was presented in order to discuss the effect of bulk recombination, diffusion, and pulsing in the concentration of nitrogen into the molten Ga. Results concerning the growth of seeds for both the film-based and crystal-based approaches were also presented. Highly oriented films were obtained based on the self-oriented growth concept. On the other hand, micron-sized wurtzite and zincblende GaN crystals were obtained by exposing a mixture of Ga and LiCl to nitrogen plasma.

## CHAPTER 6

### CONCLUSIONS

This work presents the development of a novel low-pressure technique for liquid-phase epitaxy of GaN based on the interaction between molten Ga and nitrogen plasma. As a first step in the development of the technique, the wetting properties of molten Ga, as well as the interaction between Ga and nitrogen were studied. The wetting properties of Ga were studied by a set of contact angle experiments in which some process variables were modified. The results from these experiments indicated that the surface on which the Ga sits on is not as influential as the temperature or the addition of other elements to the improvement of the wettability of Ga. It was found that both the temperature and the addition of other elements to Ga improved the wettability of Ga by reducing the surface tension of the metal. Among the different alloys, Ga<sub>0.95</sub>Bi<sub>0.05</sub> was the one that exhibited the lowest contact angle. The effect of nitrogen and hydrogen plasmas exposure to the wetting properties of Ga was also studied. Hydrogen plasma was found to be effective for the removal of the native oxide layer, but did not promote the wetting of Ga. On the other hand, the exposure of Ga to nitrogen plasma increased the wetting properties of Ga considerably. In fact, among the different variables that were evaluated N<sub>2</sub> plasma was found to be the most effective to promote the wetting behavior of Ga. The improvement in the wetting

properties of Ga is believed to be a consequence of the reduction of the surface tension due to nitrogen incorporation into the melt.

Absorption/desorption experiments were performed to study the interaction between molten Ga and nitrogen plasma. The existence of a synergism between gallium and nitrogen plasmas was observed. Results indicated a rapid adsorption/dissolution of the gas into the molten metal when gallium was exposed to plasma. However, the overall interaction of molecular nitrogen with molten gallium is composed of multiple simultaneous processes: surface adsorption, diffusion into the bulk, recombination inside the bulk, surface recombination, and desorption of species from the bulk. The concentration of radicals inside the metal is determined by the rate in which each process is completed. Absorption/desorption experiments utilizing hydrogen plasma showed similar results, indicating that the synergy between molten Ga and plasmas can be applied to a variety of applications, other than the growth of GaN.

Liquid phase epitaxy of GaN was performed by covering a substrate with molten Ga and then exposing the sample to nitrogen plasma. In these experiments single crystalline GaN crystals and MOCVD-grown GaN-on-sapphire wafers were used as substrates. Continuous exposure of Ga to nitrogen plasma resulted in the formation of a GaN crust that prevented further dissolution of nitrogen radicals. The formation of the GaN crust can be explained by the spinodal decomposition mechanism once the concentration of nitrogen inside the Ga has reached a limit. To control the concentration of nitrogen inside the melt, a unique concept of pulsed plasma was introduced. Results showed that pulsed plasma-assisted liquid phase epitaxy allowed the delay of spontaneous nucleation while promoting the epitaxial growth of GaN. Epitaxial GaN layers were obtained using this technique. The

dissolution of radicals takes place only when the plasma is on. Conversely, the recombination of radicals and the diffusion of species from the surface of Ga to the surface of the substrate can occur when the plasma is on or off. Thus, in the pulsed plasma-assisted LPE process, the recombination of radicals in the bulk and the diffusion of species into the metal are favored compared to the dissolution of radicals. This is reflected in a lower nitrogen concentration at the surface of the metal and a higher concentration of nitrogen at the surface of the substrate. A parametric study was presented to discuss the effect of bulk recombination, diffusion, and pulsing in the concentration of nitrogen into the molten Ga. Results showed that bulk recombination is responsible for the maximum amount of nitrogen that can be dissolved into Ga. The diffusion of radicals, on the other hand, determined the concentration gradient along the film. The results regarding the use of a pulse confirmed the hypothesis that pulsing reduces the concentration of nitrogen at the surface of the metal and increases the concentration of nitrogen at the surface of the substrate. Furthermore, by modifying the pulse sequence, it was observed that with the proper manipulation of the initial plasma exposure time and with the appropriate ratio of the consequent on/off pulse it is possible to maintain the concentration of nitrogen inside the molten metal constant. This means that the concentration of nitrogen in this type of process can be precisely controlled in such a way that the concentration will be optimal for epitaxial growth of GaN.

Results concerning the growth of seeds for both the film-based and crystal-based approaches were also presented. Highly oriented films were obtained based on the self-oriented growth concept. However, the process was found to depend on the ability of Ga to spread. XRD characterization showed that flat GaN films only presented reflections of



the (0002) and (0004) planes of the hexagonal GaN, whereas the non-flattened GaN films showed the presence of all the characteristic planes of the wurtzite GaN. On the other hand, micron-sized wurtzite and zincblende GaN crystals were obtained by exposing a mixture of Ga and LiCl to nitrogen plasma. It is believed that GaN crystals crystallized from a Li-Ga-N melt that were formed by the interaction between  $\text{Li}_3\text{N}$ , Li and Ga.

The growth of Si NWs on Cu foils was presented in this work to elucidate the potential of the synergism between molten Ga and plasma in other applications different than the growth of GaN. To prevent the formation of metal silicides, which is one of the main reasons why Si NWs have not been grown on Cu foils in a bottom-up fashion, a diffusion-blocking layer was used. Among the different materials that were tested as diffusion blocking layer,  $\text{Al}_2\text{O}_3$  had the best performance in terms of preventing the formation of metal silicides on the surface of the substrate. The better performance of alumina compared to other materials was attributed to its better stability under reducing conditions. Densely packed Si NWs ( $d \sim 100$  nm) were grown uniformly all over the surface of the alumina-coated substrates. The Si NWs arrays on  $\text{Al}_2\text{O}_3$ -coated Cu, which displayed good flexibility, were tested as an anode in Li-ion batteries showing a promising result. The anode exhibited a high reversible specific capacity in the first cycle of  $3083 \text{ mAhg}^{-1}$  with a capacity retention of 96.9 % after 13 cycles.

## CHAPTER 7

### RECOMMENDATIONS

The use of LiCl as part of the flux used to grow GaN crystals was found to be, to some extent, successful. Nonetheless, the role of Cl is not well understood. In fact, it is believed that the Cl present in the molten salt played a detrimental role in the process as it reduced the amount of Li available to react with the molten Ga. Furthermore, the growth of GaN crystals was concentrated on the surface of LiCl particles indicating that Ga and LiCl did not mix properly. In order to suppress the influence of elements that are not meant to participate in the process, it is suggested to use only compounds that are composed exclusively by nitrogen and alkali or semi alkali metals. Pure metals, azides, and nitrides are the only compounds that fulfill this requirement. Alkali and semi alkali metals react vigorously when they are exposed to oxygen or moisture, which limits their use in oxygen and moisture free environments. Azides decompose violently into the alkali metal and nitrogen at relatively low temperatures (275°C for  $\text{NaN}_3$  and 355°C for  $\text{KN}_3$ ). To develop a safe and controllable process, it is recommended to focus on the use of nitrides. Among these, lithium nitride ( $\text{Li}_3\text{N}$ ) and calcium nitride ( $\text{Ca}_2\text{N}_3$ ) are the most suitable for this task, as they are relatively, safe, easy to handle, and have been already used as reactants in the growth of bulk GaN via the flux method.<sup>113, 120</sup>

The suggested experiment using nitrides is explained as follows: a flux composed by Ga and  $\text{Li}_3\text{N}$  and/or  $\text{Ca}_2\text{N}_3$  is poured into a crucible, which is then placed into the reaction chamber. Once the base pressure has been reached and the purging cycles have been done, the crucible is exposed to nitrogen plasma and the temperature is increased until it reaches the process temperature. Once the desired growth time has elapsed, the plasma is shut down and the temperature is decreased slowly until it reaches room temperature. The content of the crucible is then poured into a beaker containing cold ethanol to remove any unreacted Li or Ca and later will be washed in a HCl solution to remove any unreacted Ga. The resultant GaN crystals can be characterized via SEM and XRD. SEM allows to obtain morphological information of the samples like crystal size, crystal shape, growing patterns, among others. Whereas XRD is used to determine the chemical composition of the intermediate and final products. This information can be used to understand the growth mechanisms and to demonstrate the crystalline quality and orientation of the crystals grown via this method.

Pulsed plasma-assisted liquid phase epitaxy experiments indicated that the thickness of the Ga film which sits on top of the substrate is critical on the quality of the resultant GaN film. Thin films resulted in the formation of a GaN crust due to a high nitrogen concentration in the melt, whereas thick films resulted in the nucleation of isolated crystals. In order to standardize the pulsed plasma-assisted liquid phase epitaxy process one must guarantee that a uniform thickness of the Ga film is maintained among all experiments. Preliminary experiments suggest that by placing the substrates vertically while constraining the area where the substrate is placed it is possible to obtain more uniform films. Additionally, it is recommended to perform the growth experiments at

higher temperature. S. Sunkara, who studied the growth of  $\text{GaSb}_x\text{N}_{1-x}$  via MOCVD, identified that the quality of the resultant film improved as the temperature was increased. At 900 °C the authors obtained highly textured  $\text{GaSb}_x\text{N}_{1-x}$  whereas at 1000 °C the author obtained epitaxial layers of GaN.<sup>195</sup> The concentration of nitrogen in the metal depends on the rates of dissolution, diffusion and recombination. It is possible that those rates change as a consequence of the rise in temperature, thus it is recommended to perform a tuning of the on/off ratio. Finally, characterization of these films via transmission electron microscopy (TEM) and XRD is recommended. TEM can provide information on threading dislocations, grain boundaries, and other extended defects as well as indicate proper epitaxial growth. On the other hand, XRD can provide information about the crystal plane spacing, in-plane orientation and density, and type of dislocations.

## REFERENCES

1. Flack, T. J.; Pushpakaran, B. N.; Bayne, S. B., GaN Technology for Power Electronic Applications: A Review. *JEMat* **2016**, *45* (6), 2673-2682.
2. Tamura, S.; Anda, Y.; Ishida, M.; Uemoto, Y.; Ueda, T.; Tanaka, T.; Ueda, D. In *Recent Advances in GaN Power Switching Devices*, 2010 IEEE Compound Semiconductor Integrated Circuit Symposium (CSICS), 3-6 Oct. 2010; 2010; pp 1-4.
3. Bose, B. K., Power Electronics in Smart Grid and Renewable Energy Systems [Scanning the Issue]. *Proceedings of the IEEE* **2017**, *105* (11), 2007-2010.
4. GaN Systems Inc Faq - Frequently Asked Questions. <https://gansystems.com/gan-transistors/faq/#toggle-id-1> (accessed 05/20/2018).
5. Zhang, A. P.; Ren, F.; Anderson, T. J.; Abernathy, C. R.; Singh, R. K.; Holloway, P. H.; Pearton, S. J.; Palmer, D.; McGuire, G. E., High-Power GaN Electronic Devices. *Crit. Rev. Solid State Mater. Sci.* **2002**, *27* (1), 1-71.
6. Schnauffer, D.; Peterson, B., *Gallium Nitride – a Critical Technology for 5g (White Paper)*. Qorvo: [www.qorvo.com](http://www.qorvo.com), 2016.
7. Mishra, U. K.; Shen, L.; Kazior, T. E.; Wu, Y. F., GaN-Based Rf Power Devices and Amplifiers. *Proceedings of the IEEE* **2008**, *96* (2), 287-305.
8. Steranka, F. M.; Bhat, J.; Collins, D.; Cook, L.; Craford, M. G.; Fletcher, R.; Gardner, N.; Grillot, P.; Goetz, W.; Keuper, M.; Khare, R.; Kim, A.; Krames, M.; Harbers, G.; Ludowise, M.; Martin, P. S.; Misra, M.; Mueller, G.; Mueller-Mach, R.; Rudaz, S.; Shen, Y. C.; Steigerwald, D.; Stockman, S.; Subramanya, S.; Trottier, T.; Wierer, J. J., High Power Leds – Technology Status and Market Applications. *physica status solidi (a)* **2002**, *194* (2), 380-388.
9. Hangleiter, A., Iii–V Nitrides: A New Age for Optoelectronics. *MRSBu* **2011**, *28* (5), 350-353.
10. Dwiliński, R.; Doradziński, R.; Sierzputowski, L.; Kucharski, R.; Zajac, M.; Krupka, J. In *Highly Resistive GaN Substrates for High Frequency Electronics*, 2013 European Microwave Conference, 6-10 Oct. 2013; 2013; pp 523-525.
11. Denis, A.; Goglio, G.; Demazeau, G., Gallium Nitride Bulk Crystal Growth Processes: A Review. *Materials Science and Engineering: R: Reports* **2006**, *50* (6), 167-194.
12. Dwiliński, R.; Doradziński, R.; Garczyński, J.; Sierzputowski, L.; Kucharski, R.; Zajac, M.; Rudziński, M.; Kudrawiec, R.; Strupiński, W.; Misiewicz, J., Ammonothermal GaN Substrates: Growth Accomplishments and Applications. *physica status solidi (a)* **2011**, *208* (7), 1489-1493.

13. Avrutin, V.; Silversmith, D. J.; Mori, Y.; Kawamura, F.; Kitaoka, Y.; Morkoc, H., Growth of Bulk GaN and AlN: Progress and Challenges. *Proceedings of the IEEE* **2010**, 98 (7), 1302-1315.
14. Chandrasekaran, H.; Sunkara, M. K., Growth of Gallium Nitride Textured Films and Nanowires on Polycrystalline Substrates at Sub-Atmospheric Pressures. *MRS Proceedings* **2001**, 693.
15. Li, H.; Sunkara, M. K., Growth of Oriented Gallium Nitride Films on Amorphous Substrates by Self Assembly. *MRS Proceedings* **2002**, 743.
16. Li, H.; Chandrasekaran, H.; Sunkara, M. K.; Collazo, R.; Sitar, Z.; Stukowski, M.; Rajan, K. In *Self-Oriented Growth of GaN Films on Molten Gallium*, MRS Proceedings, Cambridge Univ Press: 2004; p E11. 34.
17. Meissner, E.; Hussy, S.; Friedrich, J., Low Pressure Solution Growth of Gallium Nitride. In *Technology of Gallium Nitride Crystal Growth*, Ehrentraut, D.; Meissner, E.; Bockowski, M., Eds. Springer Berlin Heidelberg: Berlin, Heidelberg, 2010; pp 245-273.
18. Boćkowski, M.; Grzegory, I.; Krukowski, S.; Łuczniak, B.; Wróblewski, M.; Kamler, G.; Borysiuk, J.; Kwiatkowski, P.; Jasik, K.; Porowski, S., Gallium Nitride Growth on Sapphire/GaN Templates at High Pressure and High Temperatures. *Journal of Crystal Growth* **2005**, 274 (1), 55-64.
19. Nakamura, S.; Fasol, G., *The Blue Laser Diode : GaN Based Light Emitters and Lasers*. Springer: Berlin ; New York, 1997; p xvi, 343 p.
20. Bi, W. W.; Kuo, H. H.; Ku, P.; Shen, B., *Handbook of GaN Semiconductor Materials and Devices*. CRC Press: 2017.
21. Levinshtein, M. E.; Rumyantsev, S. L.; Shur, M. S., *Properties of Advanced Semiconductor Materials: GaN, AlN, InN, BN, SiC, SiGe*. John Wiley & Sons: 2001.
22. Ibach, H., *Physics of Surfaces and Interfaces*. Springer: 2006; Vol. 12.
23. Inaba, K., General Features of GaN-Related Materials. *Rigaku Journal* **2014**, 30 (1).
24. Liu, L.; Edgar, J. H., Substrates for Gallium Nitride Epitaxy. *Materials Science and Engineering: R: Reports* **2002**, 37 (3), 61-127.
25. Neumayer, D. A.; Ekerdt, J. G., Growth of Group III Nitrides. A Review of Precursors and Techniques. *Chemistry of Materials* **1996**, 8 (1), 9-25.
26. Nakamura, S.; Harada, Y.; Seno, M., Novel Metalorganic Chemical Vapor Deposition System for GaN Growth. *Appl. Phys. Lett.* **1991**, 58 (18), 2021-2023.
27. Wang, H. X.; Wang, T.; Mahanty, S.; Komatsu, F.; Inaoka, T.; Nishino, K.; Sakai, S., Growth of GaN Layer by Metal-Organic Chemical Vapor Deposition System with a Novel Three-Flow Reactor. *Journal of Crystal Growth* **2000**, 218 (2), 148-154.
28. Amano, H.; Sawaki, N.; Akasaki, I.; Toyoda, Y., Metalorganic Vapor Phase Epitaxial Growth of a High Quality GaN Film Using an AlN Buffer Layer. *Appl. Phys. Lett.* **1986**, 48 (5), 353-355.
29. Nakamura, S., GaN Growth Using GaN Buffer Layer. *Japanese Journal of Applied Physics* **1991**, 30 (Part 2, No. 10A), L1705-L1707.
30. Denbaars, S., *Gallium Nitride Materials Technology*. 2019.
31. Nakamura, S.; Mukai, T.; Senoh, M.; Iwasa, N., Thermal Annealing Effects on P-Type Mg-Doped GaN Films. *Japanese Journal of Applied Physics* **1992**, 31 (Part 2, No. 2B), L139-L142.
32. Cho, A. Y.; Arthur, J. R., Molecular Beam Epitaxy. *Prog. Solid State Chem.* **1975**, 10, 157-191.

33. Martín-Palma, R. J.; Lakhtakia, A., Chapter 15 - Vapor-Deposition Techniques. In *Engineered Biomimicry*, Lakhtakia, A.; Martín-Palma, R. J., Eds. Elsevier: Boston, 2013; pp 383-398.
34. Wang, C.; Davis, R. F., Deposition of Highly Resistive, Undoped, and P-Type, Magnesium-Doped Gallium Nitride Films by Modified Gas Source Molecular Beam Epitaxy. *Appl. Phys. Lett.* **1993**, *63* (7), 990-992.
35. Ng, H. M.; Doppalapudi, D.; Moustakas, T. D.; Weimann, N. G.; Eastman, L. F., The Role of Dislocation Scattering in N-Type Gan Films. *Appl. Phys. Lett.* **1998**, *73* (6), 821-823.
36. Gil, E.; André, Y.; Cadoret, R.; Trassoudaine, A., 2 - Hydride Vapor Phase Epitaxy For current Iii-V and Nitride Semiconductor Compound Issues. In *Handbook of Crystal Growth (Second Edition)*, Kuech, T. F., Ed. North-Holland: Boston, 2015; pp 51-93.
37. Hemmingsson, C.; Monemar, B.; Kumagai, Y.; Koukitu, A., Growth of Iii-Nitrides with Halide Vapor Phase Epitaxy (Hvpe). In *Springer Handbook of Crystal Growth*, Dhanaraj, G.; Byrappa, K.; Prasad, V.; Dudley, M., Eds. Springer Berlin Heidelberg: Berlin, Heidelberg, 2010; pp 869-896.
38. Maruska, H. P.; Tietjen, J. J., The Preparation and Properties of Vapor-Deposited Single-Crystal-Line Gan. *Appl. Phys. Lett.* **1969**, *15* (10), 327-329.
39. Koukitu, A.; Kumagai, Y., Hydride Vapor Phase Epitaxy of Gan. In *Technology of Gallium Nitride Crystal Growth*, Ehretraut, D.; Meissner, E.; Bockowski, M., Eds. Springer Berlin Heidelberg: Berlin, Heidelberg, 2010; pp 31-60.
40. Oshima, Y.; Yoshida, T.; Eri, T.; Watanabe, K.; Shibata, M.; Mishima, T., Freestanding Gan Wafers by Hydride Vapor Phase Epitaxy Using Void-Assisted Separation Technology. In *Technology of Gallium Nitride Crystal Growth*, Ehretraut, D.; Meissner, E.; Bockowski, M., Eds. Springer Berlin Heidelberg: Berlin, Heidelberg, 2010; pp 79-96.
41. Van Vechten, J. A., Quantum Dielectric Theory of Electronegativity in Covalent Systems. Iii. Pressure-Temperature Phase Diagrams, Heats of Mixing, and Distribution Coefficients. *Physical Review B* **1973**, *7* (4), 1479-1507.
42. Karpiński, J.; Jun, J.; Porowski, S., Equilibrium Pressure of N<sub>2</sub> over Gan and High Pressure Solution Growth of Gan. *Journal of Crystal Growth* **1984**, *66* (1), 1-10.
43. Boćkowski, M.; Strąk, P.; Grzegory, I.; Porowski, S., High Pressure Solution Growth of Gallium Nitride. In *Technology of Gallium Nitride Crystal Growth*, Ehretraut, D.; Meissner, E.; Bockowski, M., Eds. Springer Berlin Heidelberg: Berlin, Heidelberg, 2010; pp 207-234.
44. Bockowski, M., Growth and Doping of Gan and Aln Single Crystals under High Nitrogen Pressure. *Crystal Research and Technology* **2001**, *36* (8-10), 771-787.
45. Doradziński, R.; Dwiliński, R.; Garczyński, J.; Sierzputowski, L. P.; Kanbara, Y., Ammonothermal Growth of Gan under Ammono-Basic Conditions. In *Technology of Gallium Nitride Crystal Growth*, Ehretraut, D.; Meissner, E.; Bockowski, M., Eds. Springer Berlin Heidelberg: Berlin, Heidelberg, 2010; pp 137-160.
46. Hashimoto, T.; Nakamura, S., A Pathway toward Bulk Growth of Gan by the Ammonothermal Method. In *Technology of Gallium Nitride Crystal Growth*, Ehretraut, D.; Meissner, E.; Bockowski, M., Eds. Springer Berlin Heidelberg: Berlin, Heidelberg, 2010; pp 161-182.

47. Ehretraut, D.; Kagamitani, Y., Acidic Ammonothermal Growth Technology for Gan. In *Technology of Gallium Nitride Crystal Growth*, Ehretraut, D.; Meissner, E.; Bockowski, M., Eds. Springer Berlin Heidelberg: Berlin, Heidelberg, 2010; pp 183-203.
48. Ehretraut, D.; Meissner, E., A Brief Review on the Na-Flux Method toward Growth of Large-Size Gan Crystal. In *Technology of Gallium Nitride Crystal Growth*, Ehretraut, D.; Meissner, E.; Bockowski, M., Eds. Springer Berlin Heidelberg: Berlin, Heidelberg, 2010; pp 235-244.
49. Karpiński, J.; Porowski, S., High Pressure Thermodynamics of Gan. *Journal of Crystal Growth* **1984**, *66* (1), 11-20.
50. Bockowski, M., Bulk Growth of Gallium Nitride: Challenges and Difficulties. *Crystal Research and Technology* **2007**, *42* (12), 1162-1175.
51. Bockowski, M.; Strak, P.; Grzegory, I.; Lucznik, B.; Porowski, S., Gan Crystallization by the High-Pressure Solution Growth Method on Hype Bulk Seed. *Journal of Crystal Growth* **2008**, *310* (17), 3924-3933.
52. Porowski, S. In *High Pressure Crystallization of Ii-V Nitrides*, International School of Semiconducting Compounds, Jaszowiec, Jaszowiec, 1994.
53. Grzegory, I.; Jun, J.; Boćkowski, M.; Krukowski, S. T.; Wróblewski, M.; Łuczniak, B.; Porowski, S., Iii-V Nitrides—Thermodynamics and Crystal Growth at High N2 Pressure. *JPCS* **1995**, *56* (3), 639-647.
54. Porowski, S.; Grzegory, I., Thermodynamical Properties of Iii-V Nitrides and Crystal Growth of Gan at High N2 Pressure. *Journal of Crystal Growth* **1997**, *178* (1), 174-188.
55. Grzegory, I., High Pressure Growth of Bulk Gan from Solutions in Gallium. *Journal of Physics: Condensed Matter* **2001**, *13* (32), 6875.
56. Inoue, T.; Seki, Y.; Oda, O.; Kurai, S.; Yamada, Y.; Taguchi, T., Growth of Bulk Gan Single Crystals by the Pressure-Controlled Solution Growth Method. *Japanese Journal of Applied Physics* **2000**, *39* (Part 1, No. 4B), 2394-2398.
57. Krukowski, S.; Romanowski, Z.; Grzegory, I.; Porowski, S., Interaction of N2 Molecule with Liquid Ga Surface – Quantum Mechanical Calculations (Dft). *Journal of Crystal Growth* **1998**, *189-190*, 159-162.
58. Porowski, S., High Pressure Growth of Gan — New Prospects for Blue Lasers. *Journal of Crystal Growth* **1996**, *166* (1), 583-589.
59. Grzegory, I.; Boćkowski, M.; Łuczniak, B.; Wróblewski, M.; Teisseyre, H.; Borysiuk, J.; Porowski, S., Seeded Growth of Gan at High N2 Pressure on (0001) Polar Surfaces of Gan Single Crystalline Substrates. *Mater. Sci. Semicond. Process.* **2001**, *4* (6), 535-541.
60. Grzegory, I., High-Pressure Crystallization of Gan for Electronic Applications. *Journal of Physics: Condensed Matter* **2002**, *14* (44), 11055-11067.
61. Grzegory, I.; Boćkowski, M.; Łuczniak, B.; Krukowski, S.; Romanowski, Z.; Wróblewski, M.; Porowski, S., Mechanisms of Crystallization of Bulk Gan from the Solution under High N2 Pressure. *Journal of Crystal Growth* **2002**, *246* (3), 177-186.
62. Boćkowski, M.; Grzegory, I.; Krukowski, S.; Łuczniak, B.; Romanowski, Z.; Wróblewski, M.; Borysiuk, J.; Weyher, J.; Hageman, P.; Porowski, S., Directional Crystallization of Gan on High-Pressure Solution Grown Substrates by Growth from Solution and Hype. *Journal of Crystal Growth* **2002**, *246* (3), 194-206.



63. Boćkowski, M.; Grzegory, I.; Krukowski, S.; Łuczniak, B.; Wróblewski, M.; Kamler, G.; Borysiuk, J.; Kwiatkowski, P.; Jasik, K.; Porowski, S., Deposition of Bulk GaN from Solution in Gallium under High N<sub>2</sub> Pressure on Silicon Carbide and Sapphire Substrates. *Journal of Crystal Growth* **2004**, *270* (3), 409-419.
64. Boćkowski, M.; Grzegory, I.; Łuczniak, B.; Sochacki, T.; Kryśko, M.; Strąk, P.; Dzięcielowski, I.; Litwin-Staszewska, E.; Porowski, S., High Nitrogen Pressure Solution Growth of Bulk GaN in “Feed-Seed” Configuration. *physica status solidi (a)* **2011**, *208* (7), 1507-1510.
65. Bockowski, M.; Grzegory, I.; Lucznik, B.; Sochacki, T.; Nowak, G.; Sadovyi, B.; Strak, P.; Kamler, G.; Litwin-Staszewska, E.; Porowski, S., Multi Feed Seed (Mfs) High Pressure Crystallization of 1–2in GaN. *Journal of Crystal Growth* **2012**, *350* (1), 5-10.
66. Tassaing, T.; Soetens, J.-C.; Vyalov, I.; Kiselev, M.; Idrissi, A., Supercritical Ammonia: A Molecular Dynamics Simulation and Vibrational Spectroscopic Investigation. *The Journal of Chemical Physics* **2010**, *133* (21), 214505.
67. Jacobs, H.; Stüve, C., Hochdrucksynthese Der H-Phase Im System Mn-N: Mn<sub>3</sub>N<sub>2</sub>. *Journal of the Less Common Metals* **1984**, *96*, 323-329.
68. Dwiliński, R.; Wyszomolek, A.; Baranowski, J.; Kamińska, M.; Doradziński, R.; Garczyński, J.; Sierzputowski, L.; Jacobs, H., GaN Synthesis by Ammonothermal Method. *AcPPA* **1995**, *88* (5), 833-836.
69. Dwiliński, R.; Baranowski, J.; Kamińska, M.; Doradziński, R.; Garczyński, J.; Sierzputowski, L., On GaN Crystallization by Ammonothermal Method. *Acta Phys Pol A* **1996**, *90* (4), 763-766.
70. Dwiliński, R.; Doradziński, R.; Garczyński, J.; Sierzputowski, L.; Baranowski, J. M.; Kamińska, M., Exciton Photo-Luminescence of GaN Bulk Crystals Grown by the Ammono Method. *Materials Science and Engineering: B* **1997**, *50* (1–3), 46-49.
71. Dwiliński, R.; Doradziński, R.; Garczyński, J.; Sierzputowski, L.; Baranowski, J. M.; Kamińska, M., Ammono Method of GaN and AlN Production. *Diamond and Related Materials* **1998**, *7* (9), 1348-1350.
72. Purdy, A. P., Ammonothermal Synthesis of Cubic Gallium Nitride. *Chemistry of Materials* **1999**, *11* (7), 1648-1651.
73. Purdy, A. P.; Jouet, R. J.; George, C. F., Ammonothermal Recrystallization of Gallium Nitride with Acidic Mineralizers. *Crystal Growth & Design* **2002**, *2* (2), 141-145.
74. Dwiliński, R.; Doradziński, R.; Garczyński, J.; Sierzputowski, L.; Kanbara, Y. Method of and Apparatus for Obtaining Voluminous, Gallium Containing, Monocrystalline Nitride. Polish Application No. PL207400B1, 2001.
75. Dwilinski, R.; Doradzinski, R.; Garczynski, J.; Sierzputowski, L.; Kanbara, Y. Epitaxial Layer Substrate. Polish Application No. PL350375A1, 2001.
76. Dwilinski, R.; Doradzinski, R.; Garczynski, J.; Sierzputowski, L.; Kanbara, Y. Bulk Single Crystal Production Facility Employing Supercritical Ammonia. International Application No. WO2003097906A1, 2002.
77. Dwilinski, R.; Doradzinski, R.; Garczynski, J.; Sierzputowski, L. P.; Kanbara, Y. Process for Obtaining of Bulk Monocrystalline Gallium-Containing Nitride. US Application No. US10/519,141, 2003.
78. Dwiliński, R.; Doradziński, R.; Garczyński, J.; Sierzputowski, L. P.; Puchalski, A.; Kanbara, Y.; Yagi, K.; Minakuchi, H.; Hayashi, H., Excellent Crystallinity of Truly Bulk Ammonothermal GaN. *Journal of Crystal Growth* **2008**, *310* (17), 3911-3916.

79. Dwiliński, R.; Doradziński, R.; Garczyński, J.; Sierzputowski, L. P.; Puchalski, A.; Kanbara, Y.; Yagi, K.; Minakuchi, H.; Hayashi, H., Bulk Ammonothermal Gan. *Journal of Crystal Growth* **2009**, *311* (10), 3015-3018.
80. Kucharski, R.; Rudziński, M.; Zajac, M.; Doradziński, R.; Garczyński, J.; Sierzputowski, L.; Kudrawiec, R.; Serafińczuk, J.; Strupiński, W.; Dwiliński, R., Nonpolar Gan Substrates Grown by Ammonothermal Method. *Appl. Phys. Lett.* **2009**, *95* (13), 131119.
81. Kucharski, R.; Zajac, M.; Doradzinski, R.; Garczynski, J.; Sierzputowski, L.; Kudrawiec, R.; Serafinczuk, J.; Misiewicz, J.; Dwilinski, R., Structural and Optical Properties of Semipolar Gan Substrates Obtained by Ammonothermal Method. *Applied Physics Express* **2010**, *3* (10), 101001.
82. Kucharski, R.; Zajac, M.; Doradziński, R.; Rudziński, M.; Kudrawiec, R.; Dwiliński, R., Non-Polar and Semi-Polar Ammonothermal Gan Substrates. *Semicond. Sci. Technol.* **2012**, *27* (2), 024007.
83. Zajac, M.; Kucharski, R.; Grabianska, K.; Gwardys-Bak, A.; Puchalski, A.; Wasik, D.; Litwin-Staszewska, E.; Piotrkowski, R.; Z Domagala, J.; Bockowski, M., Basic Ammonothermal Growth of Gallium Nitride – State of the Art, Challenges, Perspectives. *Prog. Cryst. Growth Charact. Mater.* **2018**, *64* (3), 63-74.
84. Hashimoto, T.; Fujito, K.; Saito, M.; Speck, J. S.; Nakamura, S., Ammonothermal Growth of Gan on an over-1-Inch Seed Crystal. *Japanese Journal of Applied Physics* **2005**, *44* (No. 52), L1570-L1572.
85. Hashimoto, T.; Wu, F.; Speck, J. S.; Nakamura, S., A Gan Bulk Crystal with Improved Structural quality Grown by the Ammonothermal method. *Nature Materials* **2007**, *6*, 568.
86. Hashimoto, T.; Wu, F.; Speck, J. S.; Nakamura, S., Ammonothermal Growth of Bulk Gan. *Journal of Crystal Growth* **2008**, *310* (17), 3907-3910.
87. Wang, B.; Callahan, M. J.; Rakes, K. D.; Bouthillette, L. O.; Wang, S. Q.; Bliss, D. F.; Kolis, J. W., Ammonothermal Growth of Gan Crystals in Alkaline Solutions. *Journal of Crystal Growth* **2006**, *287* (2), 376-380.
88. Yamane, H.; Shimada, M.; Clarke, S. J.; DiSalvo, F. J., Preparation of Gan Single Crystals Using a Na Flux. *Chemistry of Materials* **1997**, *9* (2), 413-416.
89. Yano, M.; Okamoto, M.; Yap, Y. K.; Yoshimura, M.; Mori, Y.; Sasaki, T., Growth of Nitride Crystals, Bn, Aln and Gan by Using a Na Flux. *Diamond and Related Materials* **2000**, *9* (3), 512-515.
90. Yamane, H.; Shimada, M.; Sekiguchi, T.; DiSalvo, F. J., Morphology and Characterization of Gan Single Crystals Grown in a Na Flux. *Journal of Crystal Growth* **1998**, *186* (1), 8-12.
91. Yamane, H.; Kinno, D.; Shimada, M.; Sekiguchi, T.; Disalvo, F. J., Gan Single Crystal Growth from a Na-Ga Melt. *Journal of Materials Science* **2000**, *35* (4), 801-808.
92. Aoki, M.; Yamane, H.; Shimada, M.; Sarayama, S.; DiSalvo, F. J., Growth of 5 Mm Gan Single Crystals at 750 °C from an Na–Ga Melt. *Crystal Growth & Design* **2001**, *1* (2), 119-122.
93. Aoki, M.; Yamane, H.; Shimada, M.; Sarayama, S.; DiSalvo, F. J., Gan Single Crystal Growth Using High-Purity Na as a Flux. *Journal of Crystal Growth* **2002**, *242* (1), 70-76.

94. Kawamura, F.; Morishita, M.; Tanpo, M.; Imade, M.; Yoshimura, M.; Kitaoka, Y.; Mori, Y.; Sasaki, T., Effect of Carbon Additive on Increases in the Growth Rate of 2 in Gan Single Crystals in the Na Flux Method. *Journal of Crystal Growth* **2008**, *310* (17), 3946-3949.
95. Mori, Y.; Kitaoka, Y.; Imade, M.; Miyoshi, N.; Yoshimura, M.; Sasaki, T., Growth of Bulk Gan Crystals by Na Flux Method. *physica status solidi c* **2011**, *8* (5), 1445-1449.
96. Aoki, M.; Yamane, H.; Shimada, M.; Sarayama, S.; DiSalvo, F. J., Conditions for Seeded Growth of Gan Crystals by the Na Flux Method. *Materials Letters* **2002**, *56* (5), 660-664.
97. Kawamura, F.; Umeda, H.; Morishita, M.; Kawahara, M.; Yoshimura, M.; Mori, Y.; Sasaki, T.; Kitaoka, Y., Growth of a Two-Inch Gan Single Crystal Substrate Using the Na Flux Method. *Japanese Journal of Applied Physics* **2006**, *45* (No. 43), L1136-L1138.
98. Kawamura, F.; Tanpo, M.; Miyoshi, N.; Imade, M.; Yoshimura, M.; Mori, Y.; Kitaoka, Y.; Sasaki, T., Growth of Gan Single Crystals with Extremely Low Dislocation Density by Two-Step Dislocation Reduction. *Journal of Crystal Growth* **2009**, *311* (10), 3019-3024.
99. Imade, M.; Murakami, K.; Matsuo, D.; Imabayashi, H.; Takazawa, H.; Todoroki, Y.; Kitamoto, A.; Maruyama, M.; Yoshimura, M.; Mori, Y., Centimeter-Sized Bulk Gan Single Crystals Grown by the Na-Flux Method with a Necking Technique. *Crystal Growth & Design* **2012**, *12* (7), 3799-3805.
100. Imanishi, M.; Todoroki, Y.; Murakami, K.; Matsuo, D.; Imabayashi, H.; Takazawa, H.; Maruyama, M.; Imade, M.; Yoshimura, M.; Mori, Y., Dramatic Reduction of Dislocations on a Gan Point Seed Crystal by Coalescence of Bunched Steps During Na-Flux Growth. *Journal of Crystal Growth* **2015**, *427*, 87-93.
101. Imade, M.; Hirabayashi, Y.; Konishi, Y.; Ukegawa, H.; Miyoshi, N.; Yoshimura, M.; Sasaki, T.; Kitaoka, Y.; Mori, Y., Growth of Large Gan Single Crystals on High-Quality Gan Seed by Carbon-Added Na Flux Method. *Applied Physics Express* **2010**, *3* (7), 075501.
102. Mori, Y.; Imade, M.; Murakami, K.; Takazawa, H.; Imabayashi, H.; Todoroki, Y.; Kitamoto, K.; Maruyama, M.; Yoshimura, M.; Kitaoka, Y.; Sasaki, T., Growth of Bulk Gan Crystal by Na Flux Method under Various Conditions. *Journal of Crystal Growth* **2012**, *350* (1), 72-74.
103. Imanishi, M.; Murakami, K.; Imabayashi, H.; Takazawa, H.; Todoroki, Y.; Matsuo, D.; Maruyama, M.; Imade, M.; Yoshimura, M.; Mori, Y., Coalescence Growth of Dislocation-Free Gan Crystals by the Na-Flux Method. *Applied Physics Express* **2012**, *5* (9), 095501.
104. Mori, Y.; Imade, M.; Maruyama, M.; Yoshimura, M., Growth of Gan Crystals by Na Flux Method. *ECS Journal of Solid State Science and Technology* **2013**, *2* (8), N3068-N3071.
105. Hayashi, M.; Imanishi, M.; Yamada, T.; Matsuo, D.; Murakami, K.; Maruyama, M.; Imade, M.; Yoshimura, M.; Mori, Y., Enhancement of Lateral Growth of the Gan Crystal with Extremely Low Dislocation Density During the Na-Flux Growth on a Point Seed. *Journal of Crystal Growth* **2017**, *468*, 827-830.
106. Morishita, M.; Kawamura, F.; Kawahara, M.; Yoshimura, M.; Mori, Y.; Sasaki, T., Promoted Nitrogen Dissolution Due to the Addition of Li or Ca to Ga-Na Melt; Some

- Effects of Additives on the Growth of Gan Single Crystals Using the Sodium Flux Method. *Journal of Crystal Growth* **2005**, 284 (1), 91-99.
107. Kawamura, F.; Iwahashi, T.; Morishita, M.; Omae, K.; Yoshimura, M.; Mori, Y.; Sasaki, T., Growth of Transparent, Large Size Gan Single Crystal with Low Dislocations Using Ca-Na Flux System. *Japanese Journal of Applied Physics* **2003**, 42 (7A), L729.
108. Kawamura, F.; Morishita, M.; Iwahashi, T.; Yoshimura, M.; Mori, Y.; Sasaki, T., Synthesis of Bulk Gan Single Crystals Using Na-Ca Flux. *Japanese Journal of Applied Physics* **2002**, 41 (12B), L1440.
109. Morishita, M.; Kawamura, F.; Iwahashi, T.; Yoshimura, M.; Mori, Y.; Sasaki, T., Growth of Bulk Gan Single Crystals Using Li-Na Mixed Flux System. *Japanese Journal of Applied Physics* **2003**, 42 (6A), L565.
110. Feigelson, B. N.; Henry, R. L., Growth of Gan Crystals from Molten Solution with Ga Free Solvent Using a Temperature Gradient. *Journal of Crystal Growth* **2005**, 281 (1), 5-10.
111. Yamane, H.; Kajiwara, T.; Sekiguchi, T.; Shimada, M., Zinc-Blende-Type Cubic Gan Single Crystals Prepared in a Potassium Flux. *Japanese Journal of Applied Physics* **2000**, 39 (2B), L146.
112. Hanser, A. D.; Evans, K. R., Development of the Bulk Gan Substrate Market. In *Technology of Gallium Nitride Crystal Growth*, Ehretraut, D.; Meissner, E.; Bockowski, M., Eds. Springer Berlin Heidelberg: Berlin, Heidelberg, 2010; pp 3-27.
113. Song, Y.; Wang, W.; Yuan, W.; Wu, X.; Chen, X., Bulk Gan Single Crystals: Growth Conditions by Flux Method. *Journal of Crystal Growth* **2003**, 247 (3), 275-278.
114. Song, Y. T.; Chen, X. L.; Wang, W. J.; Yuan, W. X.; Cao, Y. G.; Wu, X., Preparation and Characterizations of Bulk Gan Crystals. *Journal of Crystal Growth* **2004**, 260 (3), 327-330.
115. Wang, W. J.; Chen, X. L.; Song, Y. T.; Yuan, W. X.; Cao, Y. G.; Wu, X., Assessment of Li-Ga-N Ternary System and Gan Single Crystal Growth. *Journal of Crystal Growth* **2004**, 264 (1), 13-16.
116. Chen, X. L., Growth of Bulk Gan Single Crystals by Flux Method. *Science and Technology of Advanced Materials* **2005**, 6 (7), 766.
117. Schönherr, E.; Müller, G.; Winckler, E., Czochralski Growth of Li<sub>3</sub>n Crystals. *Journal of Crystal Growth* **1978**, 43 (4), 469-472.
118. Yonco, R. M.; Veleckis, E.; Maroni, V. A., Solubility of Nitrogen in Liquid Lithium and Thermal Decomposition of Solid Li<sub>3</sub>n. *Journal of Nuclear Materials* **1975**, 57 (3), 317-324.
119. Wang, G.; Jian, J.; Yuan, W.; Chen, X., Growth of Gan Single Crystals Using Ca-Li<sub>3</sub>n Composite Flux. *Crystal Growth & Design* **2006**, 6 (5), 1157-1160.
120. Jian, J. K.; Wang, G.; Wang, C.; Yuan, W. X.; Chen, X. L., Gan Single Crystals Grown under Moderate Nitrogen Pressure by a New Flux: Ca<sub>3</sub>n<sub>2</sub>. *Journal of Crystal Growth* **2006**, 291 (1), 72-76.
121. Blair, R. C.; Munir, Z. A., Vapor Pressure and Heats of Sublimation of Calcium Nitride. *The Journal of Physical Chemistry* **1968**, 72 (7), 2434-2437.
122. Bao, H. Q.; Li, H.; Wang, G.; Song, B.; Wang, W. J.; Chen, X. L., Exploration of Ba<sub>3</sub>n<sub>2</sub> Flux for Gan Single-Crystal Growth. *Journal of Crystal Growth* **2008**, 310 (12), 2955-2959.

123. Ivantsov, V. A.; Sukhoveev, V. A.; Nikolaev, V. I.; Nikitina, I. P.; Dmitriev, V. A., Physical Properties of Bulk Single-Crystal Wafers of Gallium Nitride. *PhSS* **1997**, 39 (5), 763-765.
124. Ivantsov, V. A.; Sukhoveev, V. A.; Dmitriev, V. A., Gan Crystals Grown from a Liquid Phase at Reduced Pressure. *MRS Proceedings* **1997**, 468, 143.
125. Sukhoveyev, V. A.; Ivantsov, V. A.; Nikitina, I. P.; Babanin, A. I.; Polyakov, A. Y.; Govorkov, A. V.; Smirnov, N. B.; Mil'vidskii, M. G.; Dmitriev, V. A., Gan 20-Mm Diameter Ingots Grown from Melt-Solution by Seeded Technique. *MRS Proceedings* **1999**, 595, F99W6.6.
126. Soukhoveev, V.; Ivantsov, V.; Melnik, Y.; Davydov, A.; Tsvetkov, D.; Tsvetkova, K.; Nikitina, I.; Zubrilov, A.; Lavrentiev, A.; Dmitriev, V., Characterization of 2.5-Inch Diameter Bulk Gan Grown from Melt-Solution. *physica status solidi (a)* **2001**, 188 (1), 411-414.
127. Johnson, W. C.; Parson, J. B.; Crew, M. C., Nitrogen Compounds of Gallium. Iii. *The Journal of Physical Chemistry* **1931**, 36 (10), 2651-2654.
128. Ejder, E., Growth and Morphology of Gan. *Journal of Crystal Growth* **1974**, 22 (1), 44-46.
129. Thurmond, C. D.; Logan, R. A., The Equilibrium Pressure of N<sub>2</sub> over Gan. *Journal of The Electrochemical Society* **1972**, 119 (5), 622-626.
130. Logan, R. A.; Thurmond, C. D., Heteroepitaxial Thermal Gradient Solution Growth of Gan. *Journal of The Electrochemical Society* **1972**, 119 (12), 1727-1735.
131. Elwell, D.; Feigelson, R. S.; Simkins, M. M.; Tiller, W. A., Crystal Growth of Gan by the Reaction between Gallium and Ammonia. *Journal of Crystal Growth* **1984**, 66 (1), 45-54.
132. Shibata, M.; Furuya, T.; Sakaguchi, H.; Kuma, S., Synthesis of Gallium Nitride by Ammonia Injection into Gallium Melt. *Journal of Crystal Growth* **1999**, 196 (1), 47-52.
133. Meissner, E.; Birkmann, B.; Hussy, S.; Sun, G.; Friedrich, J.; Mueller, G., Characterisation of Gan Crystals and Epilayers Grown from a Solution at Room Pressure. *physica status solidi (c)* **2005**, 2 (7), 2040-2043.
134. Klemenz, C.; Scheel, H. J., Crystal Growth and Liquid-Phase Epitaxy of Gallium Nitride. *Journal of Crystal Growth* **2000**, 211 (1), 62-67.
135. Sun, G.; Meissner, E.; Berwian, P.; Müller, G.; Friedrich, J., Study on the Kinetics of the Formation Reaction of Gan from Ga-Solutions under Ammonia Atmosphere. *Journal of Crystal Growth* **2007**, 305 (2), 326-334.
136. Hussy, S.; Meissner, E.; Berwian, P.; Friedrich, J.; Müller, G., Low-Pressure Solution Growth (Lpsg) of Gan Templates with Diameters up to 3 Inch. *Journal of Crystal Growth* **2008**, 310 (4), 738-747.
137. Hussy, S.; Berwian, P.; Meissner, E.; Friedrich, J.; Müller, G., On the Influence of Solution Density on the Formation of Macroscopic Defects in the Liquid Phase Epitaxy of Gan. *Journal of Crystal Growth* **2008**, 311 (1), 62-65.
138. Tanaka, A.; Funayama, Y.; Murakami, T.; Katsuno, H., Gan Crystal Growth on an Sic Substrate from Ga Wetting Solution Reacting with Nh<sub>3</sub>. *Journal of Crystal Growth* **2003**, 249 (1), 59-64.
139. Argoitia, A.; Hayman, C. C.; Angus, J. C.; Wang, L.; Dyck, J. S.; Kash, K., Low Pressure Synthesis of Bulk, Polycrystalline Gallium Nitride. *Appl. Phys. Lett.* **1997**, 70 (2), 179-181.

140. Dyck, J. S. Indium Nitride and Gallium Nitride Grown From the Melt at Subatmospheric Pressures Case Western Reserve University, 2000.
141. Dyck, J. S.; Kash, K.; Grossner, M. T.; Hayman, C. C.; Argoitia, A.; Yang, N.; Hong, M.-H.; Kordesch, M. E.; Angus, J. C., Growth of Oriented Thick Films of Gallium Nitride from the Melt. *MRS Internet J. Nitride Semicond. Res.* **1999**, *4* (S1), 227-232.
142. Novikov, S. V.; Staddon, C. R.; Kent, A. J.; Foxon, C. T., Plasma-Assisted Electroepitaxy as a Method for the Growth of Gan Layers. *Journal of Crystal Growth* **2011**, *316* (1), 51-55.
143. Novikov, S. V.; Staddon, C. R.; Powell, R. E. L.; Akimov, A. V.; Kent, A. J.; Foxon, C. T., Plasma-Assisted Electroepitaxy as a Novel Method for the Growth of Gan Layers. *physica status solidi c* **2012**, *9* (3-4), 538-541.
144. Novikov, S.; Foxon, C., Plasma-Assisted Electroepitaxy of Gan Layers from the Liquid Ga Melt. *Journal of Crystal Growth* **2012**, *354* (1), 44-48.
145. Tiller, W. A.; Feigelson, R. S.; Elwell, D., A Feasibility Study on the Growth of Bulk Gan Single Crystals. Defense, U. S. D. o., Ed. Center for Materials Research, Stanford University: Stanford, Ca, 1980.
146. Peshek, T. J. Studies in the Growth and Properties of ZnGe<sub>2</sub> and the Thermochemistry of Gan. Case Western Reserve University, 2008.
147. Li, H. Novel Processes for Large Area Gallium Nitride Single Crystal and Nanowire Growth. University of Louisville, 2005.
148. Dogan, A.; Arslan, H., Calculation of the Surface Tension of Liquid Ga-Based Alloys. *PMag* **2018**, *98* (13), 1170-1185.
149. Kleinbaum, E.; Kash, K., Plasma Assisted Liquid Phase Epitaxial Growth of Gan. Case Western University: 2011.
150. Dickey, M. D., Emerging Applications of Liquid Metals Featuring Surface Oxides. *ACS Applied Materials & Interfaces* **2014**, *6* (21), 18369-18379.
151. The Editors of Encyclopaedia Britannica Nucleation. (accessed March 12/2019).
152. Gurrutxaga-Lerma, B.; Balint, D. S.; Dini, D.; Eakins, D. E.; Sutton, A. P., Chapter Two - Dynamic Discrete Dislocation Plasticity. In *Adv. Appl. Mech.*, Bordas, S. P. A., Ed. Elsevier: 2014; Vol. 47, pp 93-224.
153. Chandrasekaran, H.; Sumanasekara, G. U.; Sunkara, M. K., Rationalization of Nanowire Synthesis Using Low-Melting Point Metals. *The Journal of Physical Chemistry B* **2006**, *110* (37), 18351-18357.
154. Favvas, E. P.; Mitropoulos, A. C., What Is Spinodal Decomposition? *J Eng Sci Technol Rev* **2008**, (1), 25-27.
155. Cahn, J. W.; Hilliard, J. E., Free Energy of a Nonuniform System. I. Interfacial Free Energy. *The Journal of Chemical Physics* **1958**, *28* (2), 258-267.
156. MKS, Model Ax4500 Ecr Plasma Source - Operation Manual.
157. Chatterjee, A. K., 8 - X-Ray Diffraction. In *Handbook of Analytical Techniques in Concrete Science and Technology*, Ramachandran, V. S.; Beaudoin, J. J., Eds. William Andrew Publishing: Norwich, NY, 2001; pp 275-332.
158. Budowle, B., *Microbial Forensics*. 2nd ed.; Elsevier/Academic Press: Burlington, MA, 2011; p xxii, 722 p.
159. Tostmann, H.; DiMasi, E.; Shpyrko, O.; Pershan, P. S.; Ocko, B.; Deutsch, M., Microscopic Structure of the Wetting Film at the Surface of Liquid Ga-Bi Alloys. *Physical review letters* **2000**, *84* (19), 4385.

160. Zisman, W. A., Relation of the Equilibrium Contact Angle to Liquid and Solid Constitution. In *Contact Angle, Wettability, and Adhesion*, AMERICAN CHEMICAL SOCIETY: 1964; Vol. 43, pp 1-51.
161. Aqra, F.; Ayyad, A.; Takrori, F., Model Calculation of the Surface Tension of Liquid Ga–Bi Alloy. *Applied Surface Science* **2011**, *257* (8), 3577-3580.
162. Carreon, M., Plasma Catalysis Using Low Melting Point Metals. **2015**.
163. Carreon, M. L.; Jaramillo-Cabanzo, D. F.; Chaudhuri, I.; Menon, M.; Sunkara, M. K., Synergistic Interactions of H<sub>2</sub> and N<sub>2</sub> with Molten Gallium in the Presence of Plasma. *J. Vac. Sci. Technol. A* **2018**, *36* (2), 021303.
164. Luo, Y.-r.; Kerr, J., Bond Dissociation Energies. *CRC Handbook of Chemistry and Physics* **2012**, 89.
165. Nord, J.; Albe, K.; Erhart, P.; Nordlund, K., Modelling of Compound Semiconductors: Analytical Bond-Order Potential for Gallium, Nitrogen and Gallium Nitride. *Journal of Physics: Condensed Matter* **2003**, *15* (32), 5649.
166. Brutti, S.; Balducci, G.; Gigli, G., A Gas-Inlet System Coupled with a Knudsen Cell Mass Spectrometer for High-Temperature Studies. *Rapid Communications in Mass Spectrometry* **2007**, *21* (2), 89-98.
167. Rahman, M. L.; Linnett, J. W., Recombination of Atoms at Surfaces. Part 10.- Nitrogen Atoms at Pyrex Surfaces. *Trans. Faraday Society* **1971**, *67* (0), 170-178.
168. Rahman, M. L.; Linnett, J. W., Recombination of Atoms at Surfaces. Part 12.- Nitrogen Atoms at Some Metal and Alloy Surfaces. *Trans. Faraday Society* **1971**, *67* (0), 183-190.
169. Wood, B. J.; Wise, H., The Kinetics of Hydrogen Atom Recombination on Pyrex Glass and Fused Quartz<sup>1</sup>. *The Journal of Physical Chemistry* **1962**, *66* (6), 1049-1053.
170. Gat, R.; Angus, J. C., Hydrogen Atom Recombination on Tungsten and Diamond in Hot Filament Assisted Deposition of Diamond. *J. Appl. Phys.* **1993**, *74* (10), 5981-5989.
171. Melin, G. A.; Madix, R. J., Energy Accommodation During Hydrogen Atom Recombination on Metal Surfaces. *Trans. Faraday Society* **1971**, *67* (0), 2711-2719.
172. Beaulieu, L. Y.; Eberman, K. W.; Turner, R. L.; Krause, L. J.; Dahn, J. R., Colossal Reversible Volume Changes in Lithium Alloys. *Electrochemical and Solid-State Letters* **2001**, *4* (9), A137-A140.
173. Ohara, S.; Suzuki, J.; Sekine, K.; Takamura, T., A Thin Film Silicon Anode for Li-Ion Batteries Having a Very Large Specific Capacity and Long Cycle Life. *Journal of Power Sources* **2004**, *136* (2), 303-306.
174. Cho, J., Porous Si Anode Materials for Lithium Rechargeable Batteries. *Journal of Materials Chemistry* **2010**, *20* (20), 4009-4014.
175. Magasinski, A.; Dixon, P.; Hertzberg, B.; Kvit, A.; Ayala, J.; Yushin, G., High-Performance Lithium-Ion Anodes Using a Hierarchical Bottom-up Approach. *Nat Mater* **2010**, *9* (4), 353-358.
176. Liu, N.; Wu, H.; McDowell, M. T.; Yao, Y.; Wang, C. M.; Cui, Y., A Yolk-Shell Design for Stabilized and Scalable Li-Ion Battery Alloy Anodes. *Nano Letters* **2012**, *12* (6), 3315-3321.
177. Ma, H.; Cheng, F. Y.; Chen, J.; Zhao, J. Z.; Li, C. S.; Tao, Z. L.; Liang, J., Nest-Like Silicon Nanospheres for High-Capacity Lithium Storage. *Advanced Materials* **2007**, *19* (22), 4067-+.

178. Chan, C. K.; Peng, H.; Liu, G.; McIlwrath, K.; Zhang, X. F.; Huggins, R. A.; Cui, Y., High-Performance Lithium Battery Anodes Using Silicon Nanowires. *Nat Nano* **2008**, 3 (1), 31-35.
179. Peng, K. Q.; Jie, J. S.; Zhang, W. J.; Lee, S. T., Silicon Nanowires for Rechargeable Lithium-Ion Battery Anodes. *Appl. Phys. Lett.* **2008**, 93 (3), 3.
180. Park, M.-H.; Kim, M. G.; Joo, J.; Kim, K.; Kim, J.; Ahn, S.; Cui, Y.; Cho, J., Silicon Nanotube Battery Anodes. *Nano Letters* **2009**, 9 (11), 3844-3847.
181. Du, N.; Zhang, H.; Fan, X.; Yu, J.; Yang, D., Large-Scale Synthesis of Silicon Arrays of Nanowire on Titanium Substrate as High-Performance Anode of Li-Ion Batteries. *Journal of Alloys and Compounds* **2012**, 526 (Supplement C), 53-58.
182. Peng, K.; Jie, J.; Zhang, W.; Lee, S.-T., Silicon Nanowires for Rechargeable Lithium-Ion Battery Anodes. *Appl. Phys. Lett.* **2008**, 93 (3), 033105.
183. Hieu, N. S.; Lim, J. C.; Lee, J. K., Free-Standing Silicon Nanorods on Copper Foil as Anode for Lithium-Ion Batteries. *Microelectronic Engineering* **2012**, 89 (Supplement C), 138-140.
184. Nguyen, S. H.; Lim, J. C.; Lee, J. K., Electrochemical Characteristics of Bundle-Type Silicon Nanorods as an Anode Material for Lithium Ion Batteries. *Electrochimica Acta* **2012**, 74 (Supplement C), 53-58.
185. Cho, J.-H.; Picraux, S. T., Enhanced Lithium Ion Battery Cycling of Silicon Nanowire Anodes by Template Growth to Eliminate Silicon Underlayer Islands. *Nano Letters* **2013**, 13 (11), 5740-5747.
186. Memarzadeh, E. L.; Kalisvaart, W. P.; Kohandehghan, A.; Zahiri, B.; Holt, C. M. B.; Mitlin, D., Silicon Nanowire Core Aluminum Shell Coaxial Nanocomposites for Lithium Ion Battery Anodes Grown with and without a Tin Interlayer. *Journal of Materials Chemistry* **2012**, 22 (14), 6655-6668.
187. Carreon, M. L.; Jasinski, J.; Sunkara, M., Low Temperature Synthesis of Silicon Nanowire Arrays. *Materials Research Express* **2014**, 1 (4), 045006.
188. Jaramillo-Cabanzo, D. F.; Willing, G. A.; Sunkara, M. K., Plasma Etching Chemistry for Smoothing of Ultrananocrystalline Diamond Films. *ECS Solid State Letters* **2015**, 4 (10), P80-P84.
189. Howard, S. M., Ellingham Diagrams. *SD School of Mines and Technology: Rapid City, SD, USA* **2006**.
190. Zakharov, D. N.; Liliental-Weber, Z.; Wagner, B.; Reitmeier, Z. J.; Preble, E. A.; Davis, R. F., Structural Tem Study of Nonpolar a-Plane Gallium Nitride Grown on (11  $\bar{2}$  0) 4 H-Sic by Organometallic Vapor Phase Epitaxy. *Physical Review B* **2005**, 71 (23), 235334.
191. Lee, K. N.; Donovan, S. M.; Gila, B.; Overberg, M.; Mackenzie, J. D.; Abernathy, C. R.; Wilson, R. G., Surface Chemical Treatment for the Cleaning of Aln and Gan Surfaces. *Journal of The Electrochemical Society* **2000**, 147 (8), 3087-3090.
192. Meyyappan, M., Characteristics of an Electron Cyclotron Resonance Plasma Source for the Production of Active Nitrogen Species in Iii-V Nitride Epitaxy. *Materials Research Society Internet Journal of Nitride Semiconductor Research* **1997**, 2.
193. Inouye, M.; Kojima, Y.; Choh, T.; Uekawa, S.; Yamada, Y., On the Measurements of Diffusion Coefficients of Nitrogen in the Liquid Iron. *Tetsu-to-Hagane* **1973**, 59 (2), 205-213.



194. Skeel, R. D.; Berzins, M., A Method for the Spatial Discretization of Parabolic Equations in One Space Variable. *SIAM journal on scientific and statistical computing* **1990**, *11* (1), 1-32.
195. Sunkara, S., New Visible Light Absorber for Solar Fuels: Ga (Sbx) N1-X Alloys. **2015**.

## APPENDIX I

### AIP PUBLISHING LICENSE TERMS AND CONDITIONS

Apr 23, 2019

---

This Agreement between University of Louisville - Conn Center for Renewable Energy Research -- Daniel Jaramillo-Cabanzo ("You") and AIP Publishing ("AIP Publishing") consists of your license details and the terms and conditions provided by AIP Publishing and Copyright Clearance Center.

License Number	4574861353342
License date	Apr 23, 2019
Licensed Content Publisher	AIP Publishing
Licensed Content Publication	Journal of Vacuum Science & Technology A
Licensed Content Title	Synergistic interactions of H2 and N2 with molten gallium in the presence of plasma
Licensed Content Author	Maria L. Carreon, Daniel F. Jaramillo-Cabanzo, Indira Chaudhuri, et al
Licensed Content Date	Mar 1, 2018
Licensed Content Volume	36
Licensed Content Issue	2
Type of Use	Thesis/Dissertation
Requestor type	Author (original article)
Format	Print and electronic
Portion	Excerpt (> 800 words)
Will you be translating?	No
Title of your thesis / dissertation	Plasma-assisted liquid phase epitaxy of gallium nitride using molten gallium
Expected completion date	May 2019
Estimated size (number of pages)	165
Requestor Location	University of Louisville - Conn Center for Renewable Energy Research 216 Eastern Parkway Phoenix House  LOUISVILLE, KY 40208 United States Attn: University of Louisville - Conn Center for Renewable Energy Research
Total	0.00 USD

## CURRICULUM VITAE

Daniel Felipe Jaramillo Cabanzo

### **Education**

Doctor of Philosophy in Chemical Engineering, University of Louisville  
Thesis Title: Plasma-assisted liquid phase epitaxy using molten gallium  
Aug. 2013-May 2019  
Louisville, KY

Master of Science in Chemical Engineering, Universidad de los Andes  
Thesis Title: Growth of WO<sub>x</sub> films on Si and glass substrates via Hot Filament CVD (HFCVD): Study of the microstructure, composition, and mechanical properties.  
Jan. 2011-Dec. 2011  
Bogotá, Colombia

Bachelor of Science in Chemical Engineering, Universidad de los Andes  
Thesis title: Influence of temperature and O<sub>2</sub> concentration in the deposition of WO<sub>x</sub> films via HFCVD  
Jan. 2007-Dec. 2010  
Bogotá, Colombia

### **Research and Work Experience**

Conn Center for Renewable Energy Research - University of Louisville  
Graduate Research Assistant  
Aug. 2013-May 2019  
Louisville, KY

Productos Ramo S.A.  
Project Analyst  
May 2012-Apr. 2013  
Bogotá, Colombia

Universidad de los Andes  
Graduate Research Assistant  
Jan. 2011-Jan. 2012  
Bogotá, Colombia

## Patents

M.K. Sunkara, B.P. Ajayi, **D. Jaramillo-Cabanzo**, A. Nambo (2016) *Production of Mixed Metal Oxide Nanostructured Compounds* U.S. Patent Application No. 15,342,048

## Publications

- **D.F. Jaramillo-Cabanzo** & M.K. Sunkara et al. *Plasma-Enhanced Liquid Phase Epitaxy of GaN*, Manuscript in Preparation (2019)
- **D.F. Jaramillo-Cabanzo** & M.K. Sunkara et al., *Growth of Si Nanowire Arrays on Cu foils as Anode Material for Li-ion Batteries*, Manuscript in Preparation (2019)
- **D.F. Jaramillo-Cabanzo\***, B.P. Ajayi\* and M.K. Sunkara, *1D Nanomaterials for Li-ion Batteries*, J. Phys D: Appl. Phys., Invited Review (Submitted) (**\*Authors contributed equally to this work**)
- M.L. Carreon\*, **D.F. Jaramillo-Cabanzo\***, I. Chaudhuri, M. Menon and M.K. Sunkara, *Synergistic Interactions of H<sub>2</sub> and N<sub>2</sub> with Molten Gallium in the Presence of Plasma*, J. Vac. Sci. Technol. A, 2018. **36**(2): p. 021303 (**\*Authors contributed equally to this work**)
- B.P. Ajayi, S. Kumari, **D. Jaramillo-Cabanzo**, J. Spurgeon, J. Jasinski and M. Sunkara, *A rapid and scalable method for making mixed metal oxide alloys for enabling accelerated materials discovery*, Journal of Materials Research, 2016. **31**(11): p. 1596-1607.
- **D.F. Jaramillo-Cabanzo**, G.A. Willing and M.K. Sunkara, *Plasma Etching Chemistry for Smoothing of Ultrananocrystalline Diamond Films*, ECS Solid State Letters, 2015. 4(10): p. P80-P84

## Selected Presentations

- D.F. Jaramillo-Cabanzo et al., *Low pressure plasma Interactions with molten metals for materials processing*, iPlasmaNano-IX Conference, New Buffalo Mi, Aug. 2018
- D.F. Jaramillo-Cabanzo et al., *The Synergetic Catalytic Effect of Molten Gallium in the Presence of Hydrogen and Nitrogen Plasmas: Study and Applications*, ECS Prime Meeting, Honolulu HI, Oct. 2016
- D.F. Jaramillo-Cabanzo et al., *Plasma Etching Chemistry for Smoothing of Ultrananocrystalline Diamond Films*, ECS Meeting, San Diego Ca, May 2016

- D.F. Jaramillo-Cabanzo et al., *Effect of Process Variables on Microstructure and Composition of HWCVD Tungsten Oxides Thin Films*, AIChE Meeting, Minneapolis MN, Oct. 2011

### **Honors and Awards**

- Grosscurth Fellowship, J.B Speed School of Engineering, University of Louisville, 2013-2015
- Universidad de los Andes Graduate Fellowship, 2011
- Excelencia Semestral Scholarship – Granted for achieving the highest GPA of the School of Engineering in the spring semester of 2010, Universidad de los Andes, Bogotá, Colombia, 2010
- Quiero Estudiar Scholarship – Granted to promising students who score exceptionally in the ICFES exam (Colombian standardized test), Universidad de los Andes, Bogotá, Colombia, 2007-2010
- Placa del Bello Carácter, Gimnasio Moderno, Bogotá, Colombia, 2006

### **Leadership Activities, Campus Involvement, and volunteer work**

President of the Chemical Engineering Graduate Student Association (2017-2019).  
Served as advisor/mentor for high-school students in research summer camps, and science fair projects